CENTENNIAL VARIABILITY IN SOUTHEAST PACIFIC HYDROGRAPHY AND ITS LINK TO THE BIPOLAR SEESAW AND ICE SHEET DYNAMICS

BY

THALE DAMM-JOHNSEN

MASTER THESIS IN MARINE GEOLOGY

Department of Earth science

University of Bergen

November 2019

Abstract

Ocean upwelling along the Chilean coast supplies nutrients crucial for sustaining major fisheries and food resources. Atmospheric wind systems are facilitating this upwelling and consequently, a better understanding of climatic shifts and underlying dynamics that drive this upwelling will be of major interest when predicting a warmer future.

This study reports new high resolution foraminiferal and Ice rafted debris (IRD) census counts on multi-decadal timescales (~36 years) spanning Antarctic Warming Event 1 (A1) (40-34 kyr BP) from ODP Site 1233 (41°0.005'S, 74°26.992'W, 838 m.b.s.l) in the Southeast Pacific. This core site is ideally located to reconstruct changes in near surface water masses, understand the effect of the major ocean-atmosphere dynamics intersecting this region, as well as unraveling variations in the Patagonian Ice Sheet. This pilot study shows that during A1, there were large- scale shifts in the upwelling along the coast of central Chile. These changes indicate a poleward shift of Southern Westerly Wind (SWW)-belt, facilitating a northward coastal wind driving offshore Ekman flow and upwelling. As upwelling primarily occurs north of ODP Site 1233 today, our new faunal counts indicate an even more southward displaced SWW during warm intervals of Marine Isotope Stage 3. We suggest that extensive Northern Hemisphere glaciations during A1 drove the SWW and the Intertropical Convergent Zone further south. This demonstrates the importance of the atmospheric component of the rapid ocean-atmosphere climate linkage of the two hemispheres through the bipolar seesaw. The relative abundance of planktic foraminifera *Neogloboquadrina pachyderma* and *Neogloboquadrina incompta* reveal both rapid and long-term variability in the sea surface properties, interpreted as fluctuation in temperature, salinity, and nutrients tied to shifts in the Subtropical Front (STF), which ultimately controls the extent of the Patagonian Ice Sheet. The Antarctic timing of A1 is evident and superimposed on the observed centennial climate variability—suggesting previously unidentified rapid changes in the SWW-belt during MIS 3 in the study region. The Northern limb of the Patagonian Ice Sheet was positioned right onshore of the study site during the last glacial cycle and the lithic counts of IRD provide new insight regarding the timing and dynamics of this climatically important marine terminating ice sheet.

Acknowledgements

A sincere thank-you goes to the super-team Kikki Kleiven, Nil Irvali and Ulysses Ninnemann, for their marvellous guidance and supervising, introducing paleoclimatology in such a holistic way, which facilitatedI would never have achieved without you.

A special thanks goes to Kikki Kleiven for interesting discussions, amazing, thorough feedback on the thesis and for always being accessible and welcoming at the office (and for an amazing Trude Drevland-imitation), I have really appreciated it all. Also, a huge thank you to Nil Irvali, for the foraminifera training and for being so patient and encouraging in the whole process (and for putting all my "*N. pachyderma"* into Italic a numerous times).

I would also like to express my gratitude to Stephen Barker for sending over the TNO57-21 *N. pachyderma* data and commenting on my results, Jo Brendyren for solving the mysterious Corel draw-problem, and Joachim Schönfeld and Elisabeth Alve for assessing the results from the relative abundance of *Uvigerina peregrina*.

Finally, I would like to express my gratitude to Louise and Alex for housing me in Fusa, in times of great need for some rest, proper food and mental guidance. Also, to my family for pretending to care, when I kept going on and on about the thesis, and last but not least, a huge thank-you to Jenny Marie, Daniel, Hedda and Henning for keeping me sane, accompanied and encouraged during late nights at the study hall. You are the best.

Thale Damm-Johnsen

TABLE OF CONTENTS

1. INTRODUCTION

1.1 Project

This study utilises material from the International Ocean Discovery Program (IODP), which is a scientific ocean drilling program. This international research platform has for several decades monitored and sampled seafloor environments and provided geology researchers from its 23 member nations with marine sediment cores from ocean basins in all latitudes to enhance our understanding of the oceans and their role in Earth's climate systems. The material for this thesis is from a legacy core from an expedition that was part of the prior Ocean Drilling Program (ODP). Drilled during expedition 202, ODP Site 1233 is located in the Southeast Pacific, and provides a 135-meter-long high-resolution sediment archive that can be used to assess variations in the climatic and oceanic conditions in the Southern Hemisphere over the last 75 kyr.

In this thesis, new high-resolution foraminiferal and lithic counts from ODP Site 1233 are presented. The high productivity at the study site facilitates the use of foraminiferal census counts as a method for resolving past climate change. This method adds new perspectives in constraining and interpreting sea surface variability and climate dynamics in this region. The use of Ice rafted debris (IRD) counts also provides new insight to the dynamics of the North Patagonian Ice sheet (NPIS), which previously only has been reconstructed using terrestrial archives. The aim of this thesis is to use the foraminiferal faunal assemblages to assess how the variability of sea surface properties and the dynamics of the NPIS has developed over Antarctic Warming Event 1 (Antarctic Isotopic Maximum (AIM) 8 following the new nomenclature from the European Project of Ice Coring in Antarctica (EPICA) project). A1 is a warm stadial event during Marine Isotope Stage (MIS) 3, inherent in the interval studied, which spans from 40-34 kyr BP. This project was supervised by associate professor Kikki Kleiven, researcher Nil Irvali and professor Ulysses Ninnemann at the department of Earth Science and the Bjerknes Centre for Climate Research at the University of Bergen.

1.2 Aim of study

- To resolve the variability of Southeast Pacific hydrography over A1.
- Monitor changes in marine calving intensity of the Patagonian Ice Sheet.
- Resolve the connection between local hydrography and ice sheet change and their relationship to ocean-atmosphere dynamics of the bipolar seesaw.

2. BACKGROUND

To reconstruct and interpret past climate variability has over the recent years, not only been a subject of pure research curiosity, but also a matter of necessity. Due to rising atmospheric carbon dioxide emissions and consequently an increasingly warmer Earth, the need to constrain the drivers of our climate system on both long and short timescales has become a case of urgency: How are we going to predict the future, if we don't know the trends and behaviors of the past? And on what scale and rate does natural climate variability occur? Changes in the climate system that leads to warming (El Niño) will amplify man-made warming, whereas change that leads to cooling (volcanoes) will dampen these changes. Hence, to be able to better constrain the natural variability of the past, will aid us in predicting our future climate.

Marine sediment cores, along with lacustrine cores, ice cores and speleothems (amongst other) provide important and detailed insight into our climatic past. These archives are used to reconstruct various proxy records depicting Earth´s climate. For instance, the variation in the pressure gradient between equator to the poles gives rise to ocean and wind circulation, which are altered by continents, bathymetry and the Coriolis effect. The interaction between the atmosphere, ocean, land and ice sheets will alter the chemistry of the ocean, and traces of this change are archived in the marine sediments, where they can be extracted and interpreted.

One of the key elements to obtain these records is found in the calcareous shells of small planktic and benthic marine calcareous protists, the foraminifera. The foraminifera are among the most abundant shelled organisms in many marine environments, and when they die and sink to the ocean floor, they accumulate to become a part of the vast pelagic ooze of the ocean seafloor. The foraminifera shells provide information about the seawater in which it grew, both through the chemistry of the shell and the faunal assemblage (Kucera, 2007). Because different species of foraminifera are found in different environments, marine geologists can use the fossils to determine environments in the past. For example the ratio of stable oxygen isotopes in foraminifera have been used to track global ocean temperature changes during the ice ages (CLIMAP, 1976). The faunal assemblage is a direct representation of the water in which they lived, because the organisms respond to variable temperatures and variable amounts of nutrients, oxygen, etc. Consequently, detailed knowledge about the individual foraminifera

species when interpreting the climate signal is crucial. If a sample of fossil foraminifera contains many existing species, the present-day distribution of those species can be used to infer the environment at that site when the fossils were alive. Due to the outstanding preservation of the marine sediments, the fossilized foraminifera are a common source for palaeoceanographic research and crucial when reconstructing frontal movements.

Marine climate reconstructions have been heavily focused towards the last glacial-interglacial cycle. One of the reasons is that age models can be obtained relatively easy with the AMS ^{14}C-method, ash chronology, biostratigraphy and correlation of paleomagnetism over this time span. Another reason is that most conventional coring techniques use gravity and piston cores with a limited depth range and hence recovery. IODP coring provides high-quality sediment cores that go beyond the reach of piston cores (ocean drilling can recover several 100-meters of marine sediments) and is especially known for recovering thick high-resolution sediment packages. ODP Site 1233 spans 135 meters of marine mud (Shipboard Scientific Party, Leg 202, Chapter 4, 2003) of which 110 meters spans the glacial MIS 2-3 (25-75 kyr). This period is also the time interval studied in this thesis, more precisely 34-40 kyr BP. These seven millennia, spans Antarctic Isotopic Maximum (AIM) 1, which in the Antarctic ice cores represents an interstadial, with prominent millennial-scale climate oscillations (Grootes et al., 1993, Orsi et al., 2014).

The benthic oxygen isotope archive from marine cores in the Northern Hemisphere (NH), which mirrors the isotopic signals in ice cores from Greenland, reveal a glacial climate, associated with both long-term (100 kyr) and short-term (decadal) variations (Imbrie et al., 1992, Lisiecki and Raymo, 2005). The most characteristic features are repeated, sudden increases in temperature of up to 12-15ºC in the atmosphere over Greenland (Johnsen et al., 2001). These increases in temperature occurs over a few decades, followed by a more gradual cooling. The ice cores show that the increases vary in length, but after approximately 1000 years the temperature cease more gradual down to the initial level. These abrupt climate change events are called Dansgaard-Oeschger (D-O) events, and occurred recurrently (approximately every 1500 years) over the last glacial cycle (Dansgaard et al., 1993). There is currently increasing evidence suggesting that the D-O events had a global footprint, evidence which is preserved in a variety of global paleoclimate archives, from marine cores (Voelker, 2002,

Buiron et al., 2012) to lake cores (Melles et al., 2012) and speleothems (Southon et al., 2012, Cheng et al., 2016). During cold phases in the North Atlantic, large regions of North America and Eurasia became colder and drier (Allen et al., 1999, Asmerom et al., 2010, Wagner et al., 2010). A southward shift in the tropical rain belt caused drier conditions in the northern hemisphere, and wetter conditions in many regions in the Southern Hemisphere (SH) (Wang et al., 2001, Kanner et al., 2012, Deplazes et al., 2013). Antarctic ice cores exhibit warming, consistent with a reduction of northward heat transport from the SH (Brook et al., 2005, EPICA community members, 2006). The D-O events in Greenland are observed as a more muted and gradual signal in the Antarctic ice cores, called Antarctic Isotope Maxima (AIM) occurring 200 years after Greenland(EPICA community members, 2006, Buizert et al., 2018). The warming

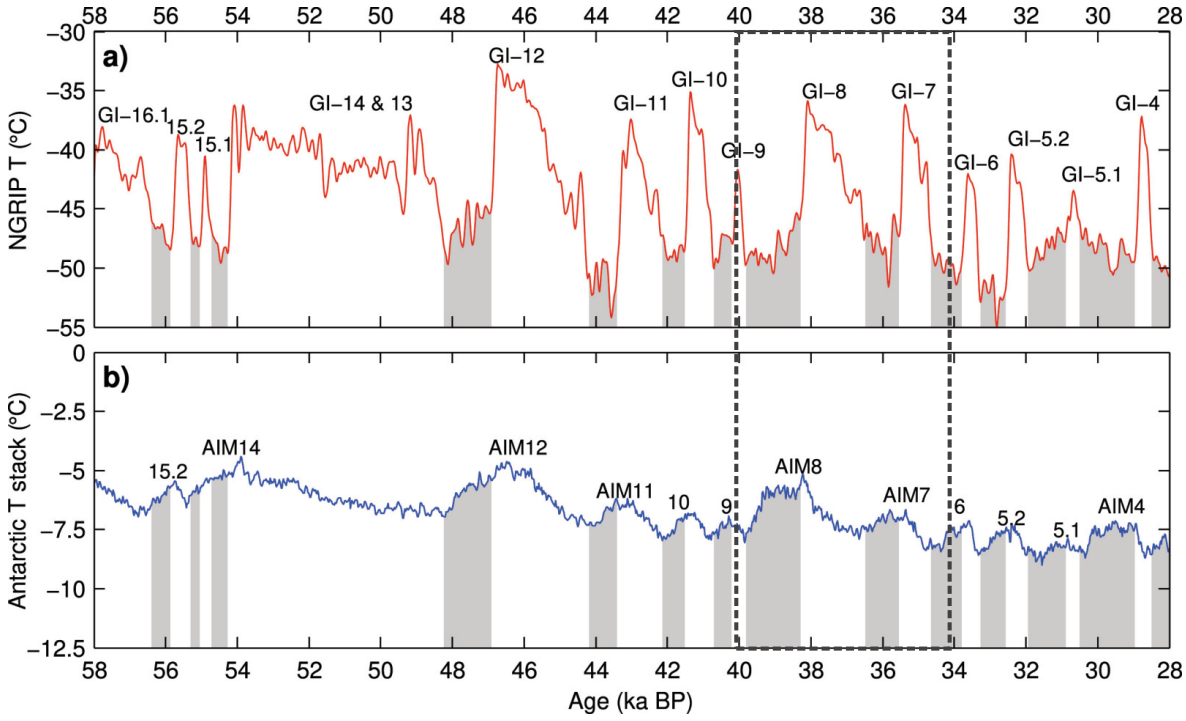

Figure 2.1. Temperature reconstructions of Greenland and Antarctica spanning MIS 3. A) North Greenland Ice core project (NGRIP) b) Stacked temperature records from EDML, Talos Dome, Dome Fuji, Vostok and WAIS divide. Grey shading represents Greenland stadial. Note that warm periods of Antarctica (AIM), coincide with Greenland stadials (GI). Modified after Pedro et al. (2018).

phases of AIM correspond to Greenland stadials and the cooling of AIMs correspond to Greenland interstadials (Figure 2.1). The climate anomalies are consistent with a slowdown of the thermohaline circulation and subsequent reduced ocean heat transport into the northern high latitudes. The lag in the signal is halted by the Southern Ocean (SO) and its atmospheric

counterpart the Southern Westerly Wind belt (SWW)(Stocker and Johnsen, 2003). The north to south oceanic signal propagation is suggested to be driven by the Atlantic Meridional Overturning Circulation (AMOC), controlled by the fine balance between temperature and salt (McManus et al., 2004, Barker et al., 2009). The phenomenon that temperature changes in the Northern and Southern hemisphere may be out of phase is called the bipolar seesaw and was first proposed by Broecker (1998) and Stocker and Johnsen (2003). When it is cooling over Greenland, it is warming over Antarctica, and vice versa.

An immediate atmospheric counterpart to the bipolar seesaw has been suggested; a temperature propagation from north to south, through latitudinal shifts in the Intertropical convergence zone (ITCZ) and the SWW. Consequently, the changes in Greenland and SH mid-latitude temperature occurs more or less simultaneously, due to changes in the atmospheric process which links the Hadley cells and mid-latitude storm tracks in both hemispheres and once again enfacing the importance of SH climate dynamics (Moreno et al., 2001, Lamy et al., 2004, Lee et al., 2011, Montade et al., 2015, Markle et al., 2017, Buizert et al., 2018). The new studies reveal that the mid-latitude SH play a crucial role in driving the global climate, consequently, is it important to study the Southern Ocean and understand more of the changing ocean-atmosphere dynamics tied to wind, ocean currents and fronts in the Southern Hemisphere (Figure 2.2) (Pahnke et al., 2003).

The SO is a global climate regulator on both long and short time scales. Firstly, the SO represent the place where all the major deep-to-intermediate ocean currents meet, are mixed and re-distributed back into the world oceans, at differentiated depths (Figure 2.2). This mixing is driven by the strong wind driven surface current; the Atlantic Circumpolar Current (ACC)(Rintoul et al., 2001). Secondly, the stratification between the surface and the deeper water masses depicts how much heat and CO_2 that are stored in the deep ocean and consequently kept away from the atmosphere, through the biological pump (Anderson et al., 2009, Skinner et al., 2010, Basak et al., 2018). It is also suggested that rapid climate alterations associated with changes in the thermohaline circulation are induced by long-term gradual changes at high southern latitudes (Knorr and Lohmann, 2003).

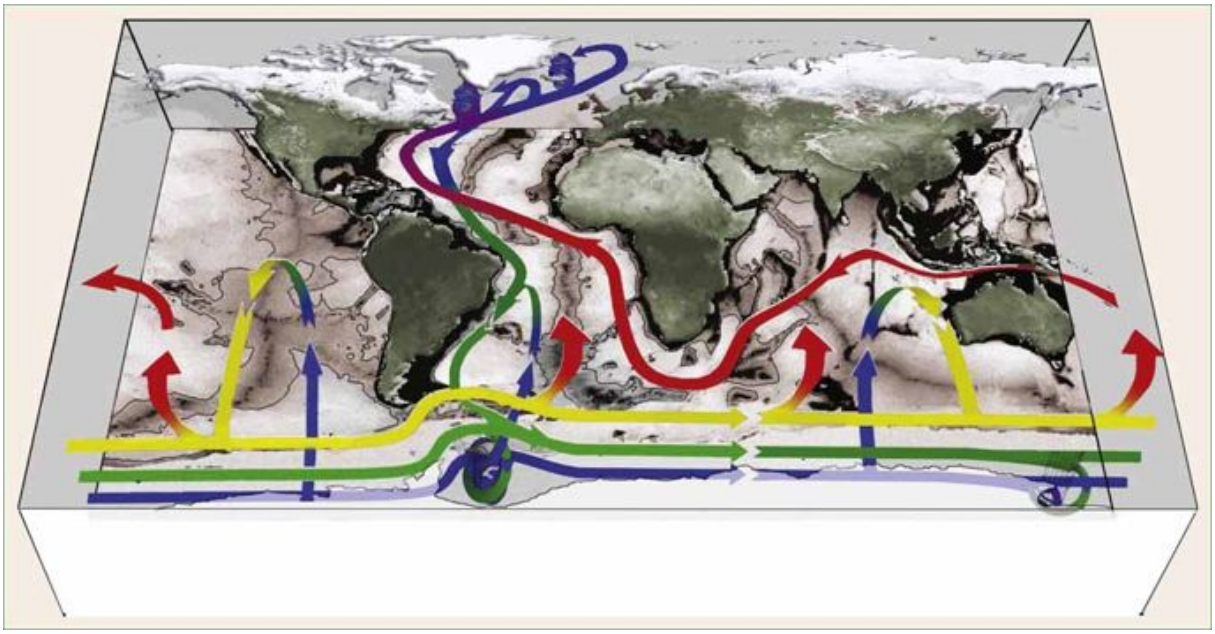

Figure 2.2 depicts the global meridional overturning circulation. The importance of the Southern Ocean upwelling (red arrows) and sinks (blue arrows) are emphasized. Yellow arrows represent the Antarctic circumpolar current with its contributors. After Marshall and Speer (2012).

Incorporated into the climate signals observed from records are natural climate variability on orbital (tens to hundreds of thousands of years) and centennial to millennial (hundreds to thousands of years) timescales. The natural variability will likely enhance and/or diminish human induced global warming. The West Antarctic Peninsula and the southern part of Patagonia in Chile are some of the fastest warming areas on Earth with only some areas of the Arctic Circle experiencing faster raising temperatures (IPCC, 2019). The coast of Chile and Peru are influenced by nutrient-rich upwelling driven by southerly winds providing high productive marine ecosystems that are crucial for sustaining the human population with food.

A natural variability disturbing this upwelling is El Niño years, where huge masses of warm water move east across the Pacific Ocean toward South America and form a warm lid over the normal currents of cold, deep water that typically rise to the surface off the coast of Chile and Peru (Philander, 1983). Reduced upwelling means reduced phytoplankton leading to a drop in the fish population and the fishing industries that many coastal regions depend upon can collapse. Recent studies have found that global warming is intensifying El Niño events, hence

making the otherwise natural cycles of weather more powerful (Fasullo et al., 2018). Other societal impacts in this region from ENSO (El Niño – Southern Oscillation) changes in a warmer climate are wildfires, rainfall fluctuations and temperature extremes (Berg et al., 2016).

Especially, reconstructing past natural variability in the South East (SE) Pacific region, over a range of timescales, is important to better understand how both natural and man-made climate variability will affect human civilization locally and all over the globe. ODP Site 1233 provides a temporal resolution that will provide for instance mathematical climate models with new insight into SO climate and ocean variability on decadal timescales. To further contextualize this study, a review of the major studies done on ODP Site 1233 will follow.

2.1 Previous studies from ODP Site 1233

There are few other marine core locations in the world, which yields marine sediment sequences with a resolution as high as ODP Site 1233. The record extends 75 kyr back in time with sedimentation rates as high as 220cm/1000yr spanning MIS 3 (H. Kleiven, pers.comm). This allows a high-resolution approach, when resolving the scale and rate of climate fluctuations in the SE Pacific, providing insight into climate variability on decadal timescales spanning glacial, de-glacial and interglacial intervals (Shipboard Scientific Party, Leg 202, Chapter 4, 2003).

The sediment recovery as Site 1233 has allowed a multi-proxy approach and over the last 15 years the core has been studied, by using XRF, planktic and benthic isotope analysis, alkenones, radiolara, pollen and X-ray Flourescence (XRF) scanning to reconstruct oceanic variables in an glacial and interglacial climate through MIS 1-4 (Pisias et al., 2001, Lamy et al., 2004, Kaiser et al., 2005, Heusser et al., 2006, Euler and Ninnemann, 2010). The early results demonstrated that climate variability at Site 1233 are in sync with the Antarctic signal on millennial timescales and clearly monitor SWW variability. These results provide strong indications of a consistent SH atmospheric-ocean climate linkage. For instance Lamy et al. (2007) showed the interhemispheric relevance of Site 1233, with a two-step Alkenone-based Sea Surface Temperature reconstruction that could be directly tied to the bipolar seesaw and AMOC, through changes in the SWW-belt during the last deglaciation.

Euler and Ninnemann (2010), Førde (2008) and Soltvedt (2014) constrained the covariance between Site 1233 and the Antarctic signal with decadal resolution. On these timescales, the properties of the near surface ocean exhibited temperature variability of as much as 3ºC in just 50 years for the Holocene and a 4ºC change per decade in MIS 3. Hence, the decadal variability is a robust feature in both warm and cold climate states in this region. In addition, these studies demonstrate a co-variance on centennial time scales between the $\delta^{18}O$-signal of the near surface water at Site 1233 and in the core of Antarctic Intermediate Water (AAIW), both during the Holocene and during MIS 3. This underscores the rapid mixing and transmission of physical (temperature and salinity) and chemical (nutrients) properties through the water column and along the flow path from high to low latitudes of major intermediate and surface water masses. The XRF Fe-values have been used as a proxy for the relative Patagonian Ice Sheet (PIS)

extent/run off (Lamy et al., 2004). The Fe- and Alkenone-based SST-signal covaries and exhibits a millennial variability of 2-3ºC. The Fe-signal lags the SST signal 400-700 years (Figure 1.3). This lag was also observed by Soltvedt (2014) who found a lag of 500-600 years between the Fe-signal and the planktic δ^{18}O-signal at Site 1233. This demonstrates the sensitivity of Northern Patagonian Ice Sheet (NPIS) to offshore oceanographic changes.

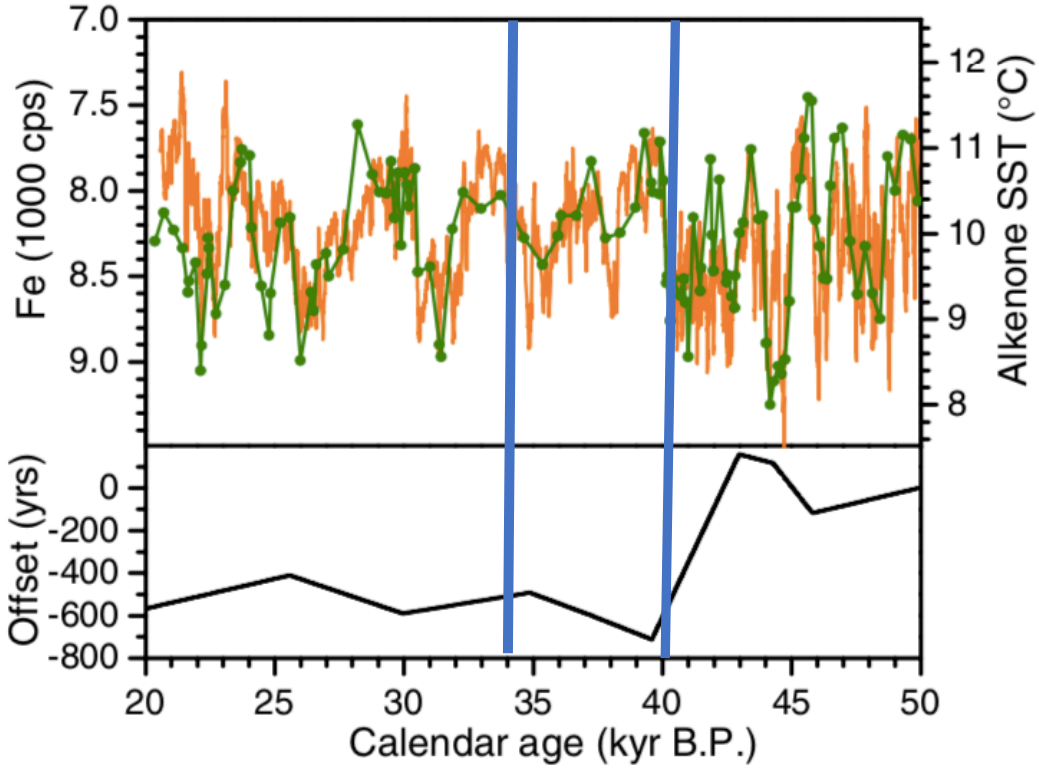

Figure 2.3 demonstraes the covariance between alkenone SST (Green) and the XRF Fe-signal (Orange) of ODP Site 1233 during MIS3-2. The graph represents the offset in years between the two, with the SST leading with 500-600 years during the time period 34-40 kyr BP. Blue bars constrain the study interval in this thesis. Figure modified after Lamy et al. (2004).

The coastal regions of Chile represent a unique area where terrestrial, atmospheric and oceanic interactions create an area of high marine productivity. The result is a thick hemipelagic sequence containing abundant and well preserved calcareous nannofossils, foraminifera and diatoms (Shipboard Scientific Party, Leg 202, Chapter 4, 2003). This thesis utilizes this diverse and rich faunal assemblage of ODP Site 1233 to reconstruct the first past climate variability record based on foraminiferal assemblages, spanning MIS3 from the coastal Chile. Furthermore, using lithic counts (IRD) to reconstruct the extent and the variability of the PIS, have so far only been done in a site further south along the Chilean margin (Caniupán et al.

(2011). In their study, they used samples from core MD07-3128 (at 53ºS) to reconstruct a low-resolution record of ice sheet calving from the southern part of PIS during MIS1-4. Previous paleoceanographic studies from the region has assumed that the southern and northern parts of the Patagonian ice sheet fluctuated in sync, something this thesis will be able to shed new light on.

In this multi proxy study we use both marine and terrestrial record along with the new planktic foraminiferal planktic and lithic counts to resolve the variability of the hydrography at the study site over A1 and monitor the changes in the frequency of marine calving from the PIS. Combined, will this thesis provide new insight into the atmospheric and oceanic connection at the ODP Site 1233.

2.2 Geographical setting

ODP Site 1233 is located in the Southeast Pacific, along the continental shelf of central Chile on the South American plate, close to the Nazca subduction zone (41°0.005′ S, 74°26.992′ W, at 838 m.b.s.l). The subduction zone gives rise to a prominent geographical feature; the magmatic Andean Cordilleran mountain range, positioned to the east (Figure 2.4). Westward, from the Andean mountain chain, lies the Coastal range, separated by the Chilean longitudinal valley (Borsdorf and Stadel, 2015). The longitudinally valley is a north-south oriented tectonic depression, filled with 4000 m of sediments. The Chilean Lake District (39º to 43º S) are positioned in this valley, an area with numerous glacially derived lakes (Thornburg and Kulm, 1987). The Andean Cordillera with an elevation of 2000 to 3000 meter above sea level (m.a.s.l) has a mafic magmatic origin, and consequently a high Fe-content. At this latitude, along an east-west transect, the glaciers have a median elevation of 1900 to 2250 m.a.s.l (Porter, 1981). The orogeny and glaciers are drained by rivers (Rio Maulin and Rio Bueno) that flow into the ocean north and south of ODP Site 1233. At 41ºS it is only 170 km from the highest peaks of the Andean Mountains to sea level, which creates a steep gradient, which give rivers a high erosional capacity. This, together with the exceptionally high precipitation rates along with periods of glaciation, have led to high sedimentation rates in the region throughout the Pleistocene (Lamy et al., 2001), that has consequently built out the continental shelf. A sequence of fjords and glacially eroded valleys stretch perpendicular to the coast

from 38ºS to 56ºS. These erosional structures, follows a strike-slip fault, related to the subduction zone (Glasser and Ghiglione, 2009). The oldest till found in Patagonia is dated to late Miocene indicating a long glacial history in the region (Wenzens, 2006).

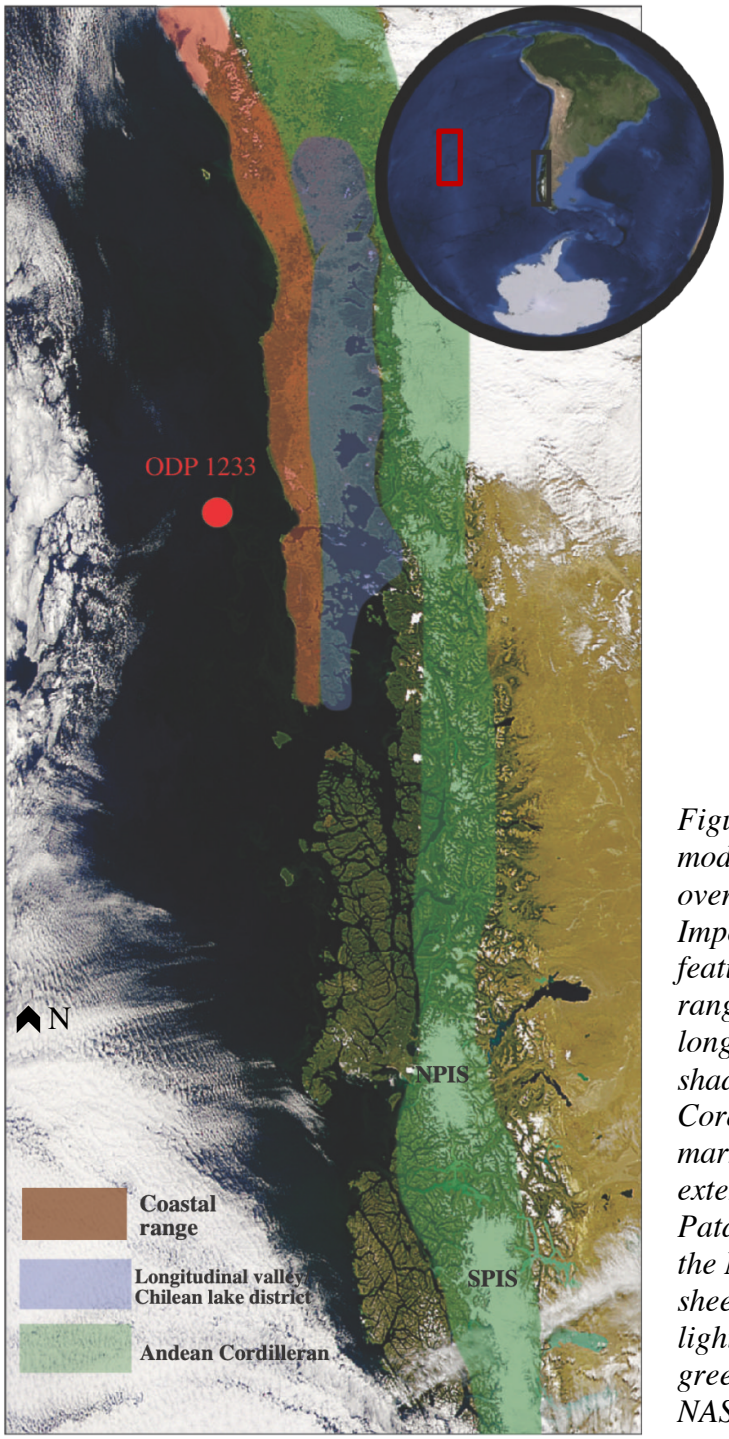

Figure 2.4. Satellite photo modified to depict a regional overview of the study area. Important geographical features such as the Coastal range (orange shading), the longitudinal valley (blue shading) and the Andean Cordillera (green shading) are marked. The present-day extents of the Southern Patagonia ice sheet (SPIS) and the Northern Patagonia ice sheet (NPIS) are indicated in lighter green, indicated in the green shading. Modified from NASA (2014).

2.3 The Patagonian Ice Sheet

The modern day PIS are separated into three big glacier systems; the northern Patagonian ice sheet (NPIS), the southern Patagonian ice sheet (SPIS) and the Cordillera Darwin icefield (Figure 2.5). Combined, they are the biggest temperate extrapolar ice sheets on the planet, with dynamic and fast flowing calving outlet glaciers (Meier and Post, 1987, Warren and Sugden, 1993, Warren and Aniya, 1999, Glasser and Jansson, 2005). These ice sheets are unique for their latitudinal outreach, and are preserved due to atmospheric and oceanographic circulation patterns (Pickard, 1971). Recent evidence from SH ice sheets, suggested that large scale climate changes are more important to the glaciation, than alterations in the regional climate (Boex et al., 2013). For instance, synchronization between alpine glacier variability in New Zealand and SST from the SO on millennial time scales suggests a broad SH mid-latitude climate connection through the SWW (Moreno et al., 2015, García et al., 2018).

New studies find the role of SWW in the interhemispheric climate signal propagation to be crucial (Buizert et al., 2015, Moreno et al., 2015, Smedley et al., 2016, García et al., 2018). The PIS is the largest icefield that are transected by the mid-latitude SWW-belt and have consequently gained increased research focus because it is an important paleoclimatic recorder. The timing of advances and retreats of the PIS provides insight into the past variations in the SWW as they deliver snow and rain to the western coast of the southern South America, sustaining the PIS (Garreaud et al., 2009). Marine and terrestrial studies spanning the LGM confirm a close coupling between the PIS variability and the SWW (Figure 2.5). After LGM, the sub-tropical front along with the SWW-belt shifted rapidly southwards (Lamy et al., 2007). Some terrestrial reconstructions from moraine fields have been carried out (Denton et al., 1999a, Hulton et al., 2002, García et al., 2018) and confirms rapid retreat of glacier outlets around the same time as the latitudinal shifts of the oceanic and atmospheric fronts, around 18 kyr ago (Boex et al., 2013, Moreno et al., 2015). This indicates that a pole-ward shifting SWW leads to a decrease in transportation of moisture and subsequently thinning of the Patagonian ice sheet. The southward displacement of the front induced warmer surface waters around Patagonia, facilitating further retreat of the ice sheet margin (Lamy et al., 2007).

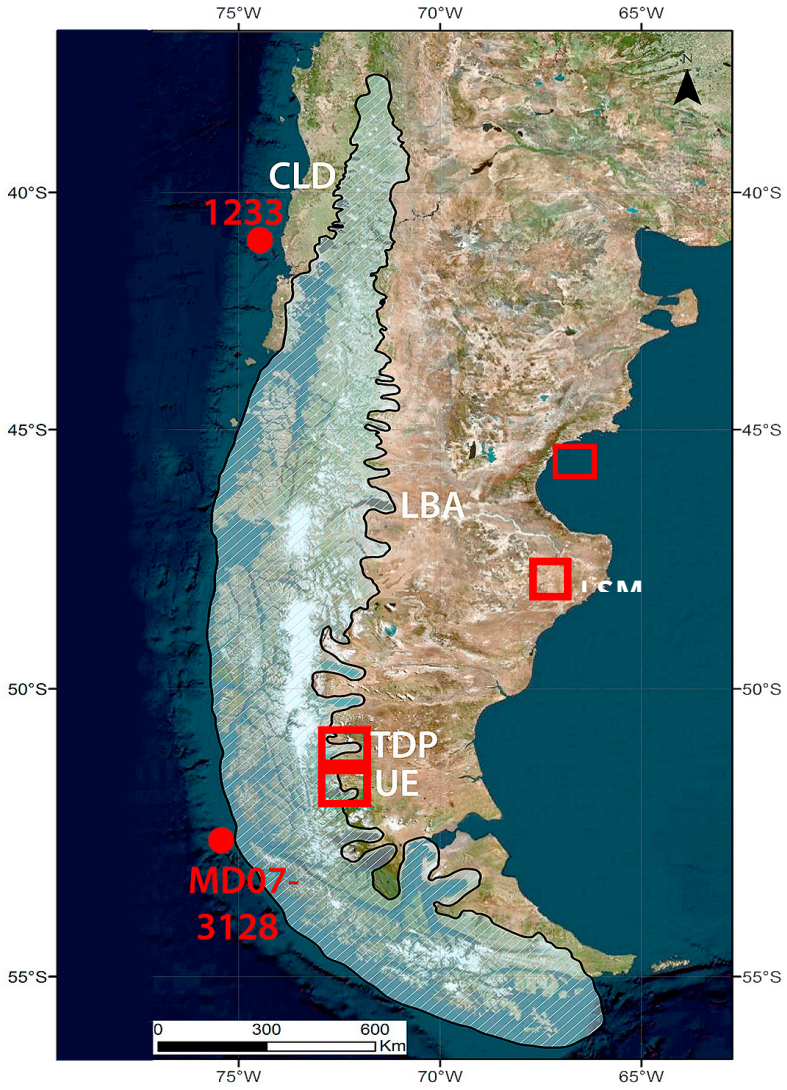

Figure 2.5 Shaded blue area represent the Patagonian ice sheet limits during the LGM.Note the moderns extents below blue shading. Red dots mark marine sediment cores taken in the region, suited to monitor changes in the PIS. ODP Site 1233 monitors change in the northern Patagonia ice sheet, while MD07-3128 monitor the southern parts. The modern extents of the Patagonia ice fields is outlined and shaded in white. Lagos Buenos Aires (LBA), Lago San Martin (LSM), Torres del Paine (TDP), Ultima Esperanza (UE), CLD (Chilean lake district) are areas where the extent of the PIS have been reconstructed and will be discussed in the subsequent chapter. The figure is modified after García et al. (2018).

An atmospheric mean annual temperature increase of 0,5ºC over the last 50 years has caused acceleration in the negative mass balance of the glacier outlets, facilitating a rapid retreat of both the northern and southern ice fields (IPCC, 2019). The warming causes melting in the summer, and the precipitation to fall as rain in the winter (Rasmussen et al., 2007) Together with a declining amount of precipitation and wind stress brought to the area by the Antarctic polar front zone, the Patagonia glaciers are shrinking (Rivera et al., 2002). In the period between 1995-2000 the PIS contributed with 0,105 mm to the global sea level rise (Rignot et al., 2003).

Marine records have only sparsely been used for PIS reconstruction. Caniupán et al. (2011) demonstrated that IRD fluctuated in sync with terrestrial dated advances of the SPIS on the eastern side of the ice divide over MIS 3, and that the alkenone derived SST reconstructions followed a clear Antarctic timing, consistent with the records from ODP Site 1233. At Site 1233 the Fe-content have also been used to depict variability of the Northwestern PIS. These records demonstrate a lagged coupling between the PIS variability (Fe), the alkenone based SST reconstructions and the planktic and benthic δ^{18}O-signal (Lamy et al., 2004, Soltvedt, 2014).

During glacial intervals of the Pleistocene epoch, the current ice fields were coalescent into one big ice field, which extended 1800 km from 38ºS to 56ºS (figure 2.5). Little is known about the PIS terminus towards the west, but it is assumed that the ice sheet advanced onto the but Pacific (figure 2.5). Further north, the ice sheet terminated on land, in 13 piedmont lobes (Denton et al., 1999b, Hulton et al., 2002, Glasser et al., 2008). The main spillway of the NPIS was through Canal de Chacao, draining the Golfo de Ancud ice lobe (Figure 2.6). Glacimarine sediments facies in the Golfo de Ancud reveal two main types of depositional processes; sediments deposited proximate to temperate tidewater glaciers, and deposited by meltwater of a retreating glacier (DaSilva et al., 1997). During MIS 3 the global sea level were approximately 70-80 meters below the present sea level, exposing much of the continental shelf for glacial erosion (Siddall et al., 2008).

Darvill et al. (2015b) and García et al. (2018) argue that the SPIS reached its maximum at 48 kyr BP, during MIS 3. SPIS are sensitive to latitudinal precipitation changes, caused by southward shifts in the SWW. These changes occurred frequent during MIS 3, due to large scale alterations in the global climate (Kerr and Sugden, 1994, Darvill et al., 2015a, Zhang et al., 2015, García et al., 2018). In the SH, the duration of the local summer season is assumed to be the dominant factor controlling climate on orbital timescales (Huybers and Denton, 2008). The MIS 3 interval were dominated by long summers and short winters, due to maritime conditions for the western part of the PIS, this might have played much less of a role for the glacial expansions (García et al., 2018). On the contrary, the NPIS reached its maximum from 18-26 kyr BP (Kaplan et al., 2008). Modeling of SH climate during LGM by Rojas et al. (2009) suggests a wetter climate over NW-Patagonia during the LGM, with a drier climate southward.

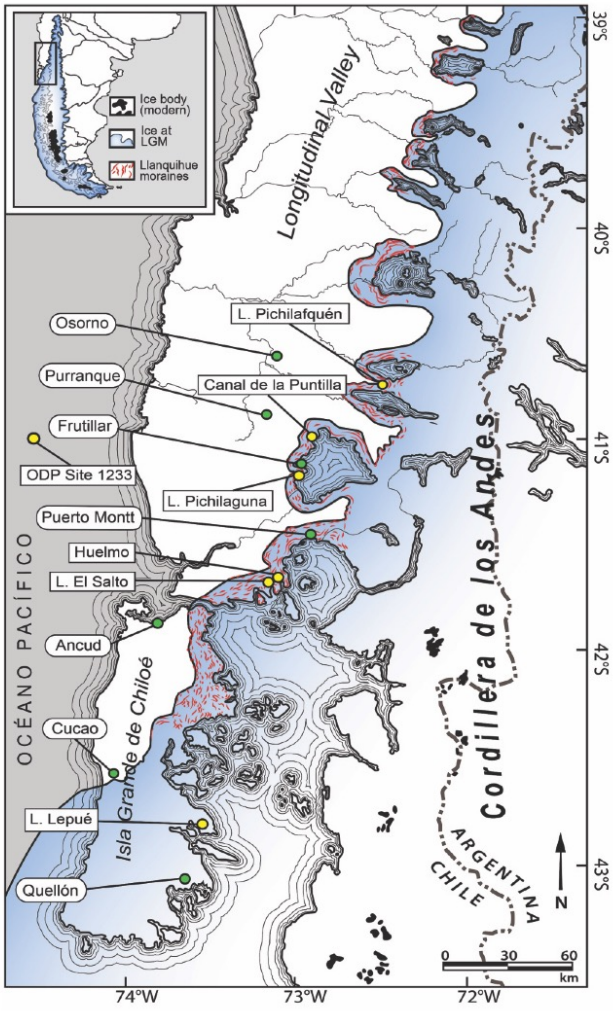

Figure 2.6 The north western part of Patagonia reconstruction from Last glacial maximum. Note the characteristic piedemont ice lobes of Northwestern Patagonia. Modified after Moreno et al. (2015).

This is also supported by the XRF records from ODP Site 1233 (Lamy et al. (1999), (Lamy et al., 2001)) and pollen reconstruction from Heusser (2003). These evidences of difference in local climate forcing could explain the substantial difference and asynchrony between the glacial dynamics of the SPIS and NPIS.

2.3.1 PIS advances during 34-40 kyr BP.

Southern Patagonia Ice Sheet

Two glacial advances have been detected in the seven millennia spanning 34 to 39 kyr BP. At 34 and 39 kyr BP, luminescence dating from Lagos Buenos Aires and exposure dating (^{10}Be) from Ultima Esperansa, Lago san Martin (LSM) and Torres del paine (TDP) all point to a glacial advance (Glasser et al., 2011, Smedley et al., 2016, García et al., 2018). A lithic study

on millennial time scales from 53ºS detected a small IRD peak at 33 kyr BP, closely matching the data from the terrestrial domain (Caniupán et al., 2011) In the valley of UE, a ^{10}Be-dating of a moraine boulders suggests a glacial advance also around 38 kyr BP (Sagredo et al., 2011), but lack of corroborating dates makes this advance less constrained.

Northern Patagonia Ice Sheet

In the north western part of the PIS in the Chilean Lake District (Figure 2.6), an glacial advance was dated to 33,8 kyr BP in connection to the work presented by Moreno et al. (2015)(pers.comm, 2019). Denton et al. (1999b) date a piedmont glacier advance close to the Lake Llanquihue in the Chilean lake district dated at >34 kyr BP.

2.4 General climatic setting

The dominating climate factor in the Southern Hemisphere is the Antarctic ice-sheet, with its massive marine ice shelves and its surrounding sea ice belt. The ice covering land-ocean nearly doubles in size due to sea ice formation up to 1000 km off the Antarctic coast line (Anderson, 1999). The seasonal fluctuating sea ice, are of great significance to the world climate on all time scales (Toggweiler and Samuels, 1993, Ferrari et al., 2014). Antarctica is surrounded by the circumpolar Southern Ocean (SO), which boarders the Pacific, the Atlantic and the Indian Oceans (Figure 2.7). Here water masses, originating in the Northern Hemisphere, are pushed up to the surface by topography and wind, and new cold and dense water masses are created, which sink down and fills all major ocean basins with oxygenated and nutritious water. The polar front (PF) and the sub Antarctic front (SAF) is the atmospheric counterpart to the SO.

Because Chile is situated at the fringes of the SO, it is a unique place for detecting and reconstructing ocean and climate variability and associated frontal changes driven by the Antarctic ice sheet, the ACC and SWW. The South American continent is the only landmass, which directly intersects the ACC/SWW, providing a unique opportunity to unravel latitudinal changes in the coupled climate mechanism both on land and in the ocean. Due to adiabatic

cooling of the moist air brought to the region by the SWW-belt, precipitation on the west coast fall in rates of up to 8 000 mm per year (Schneider et al., 2003, Mouginot and Rignot, 2015).

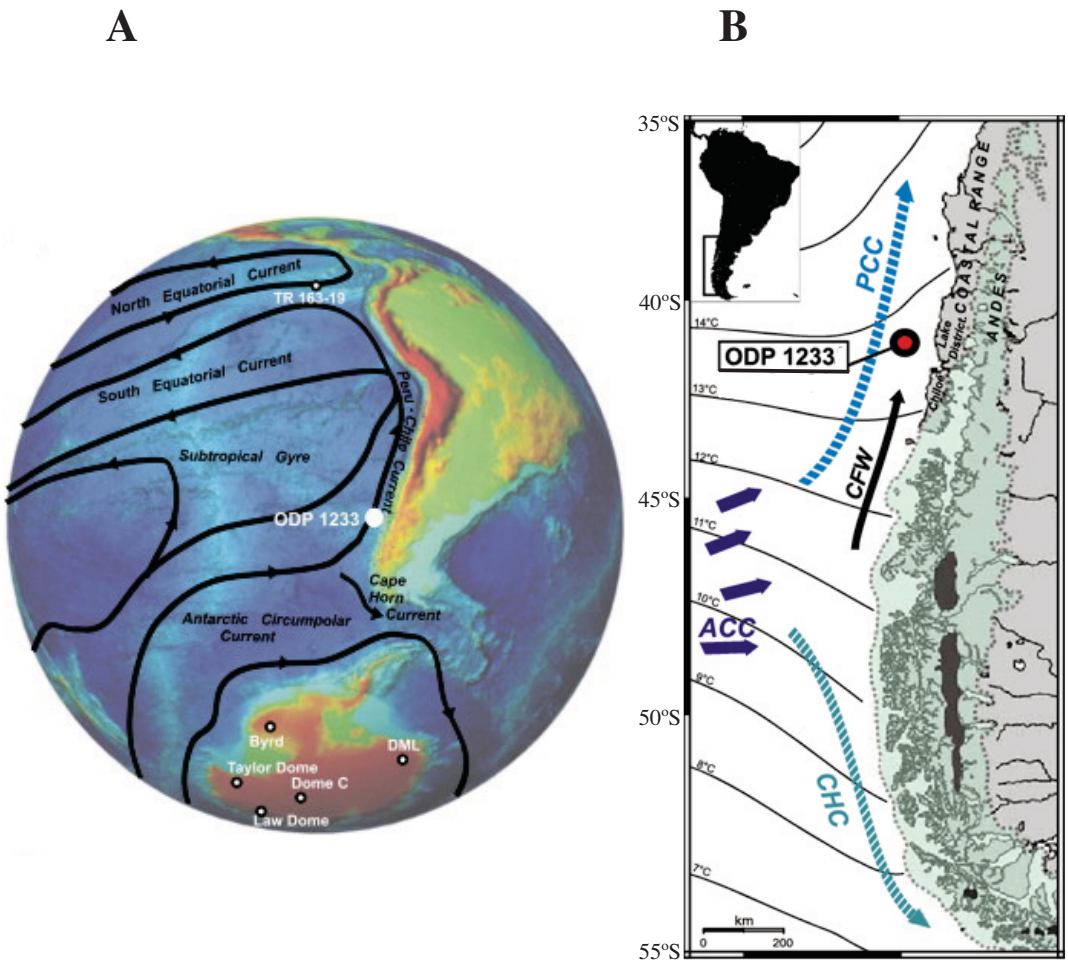

Figure 2.7. The oceanic region and local setting of ODP Site 1233 A)The position of ODP Site 1233 relative to important ocean currents and gyres, represented by black lines. Topography and bathymetry are represented in the shading from blue (low), through green to red (high). B) Important water masses intersecting the ODP Site 1233 (red dot). The ACC (purple arrow), with the branching of the PCC (blue) and CHC (turquoise). Black arrow represents Chileans fjord waters originating in the fjord region south of the core site. Black lines show the modern isotherms of the ocean. Green shadings represent the PIS during LGM, with the modern extents in dark grey. The figure is modified after Lamy and Kaiser (2009) and Lamy et al. (2007).

The core site is heavily influenced by the strong annual variability of the subtropical anticyclone (Figure 2.7). This annual fluctuation also facilitates a strong N-S precipitation gradient, tied to the latitudinal position of the SWW, which is dynamically tied to its oceanic counterpart, the ACC. The westerly winds are strongest during the austral summer and the northward blowing wind facilitates an enhanced upwelling in cells between 20 - 39ºS (Strub, 1998). However, the

upwelling regions are concentrated in zones, controlled by variation in topography, precipitation and wind stress (Djurfeldt, 1989, Figueroa and Moffat, 2000). This results in elevated nutrients to the euphotic zone, facilitating high biological productivity and affecting chemical and physical properties (temperature, salinity, nitrogen) of the surface ocean (Talley, 2011).

2.4.1 Frontal movements

An oceanic front is characterized as a zone which coincides with the maximum gradient within temperature, salinity and density(Fedorov, 1986). The abundance and species assemblage of planktic foraminifera are sensitive to changes in these properties and will consequently reflect changes in frontal positions that controls upwelling intensity (Imbrie et al., 1971, Rutherford et al., 1999). The frontal positions are being altered by the waxing and waning of the Antarctic ice sheet (Figure 2.8)(Gersonde and Zielinski, 2000).

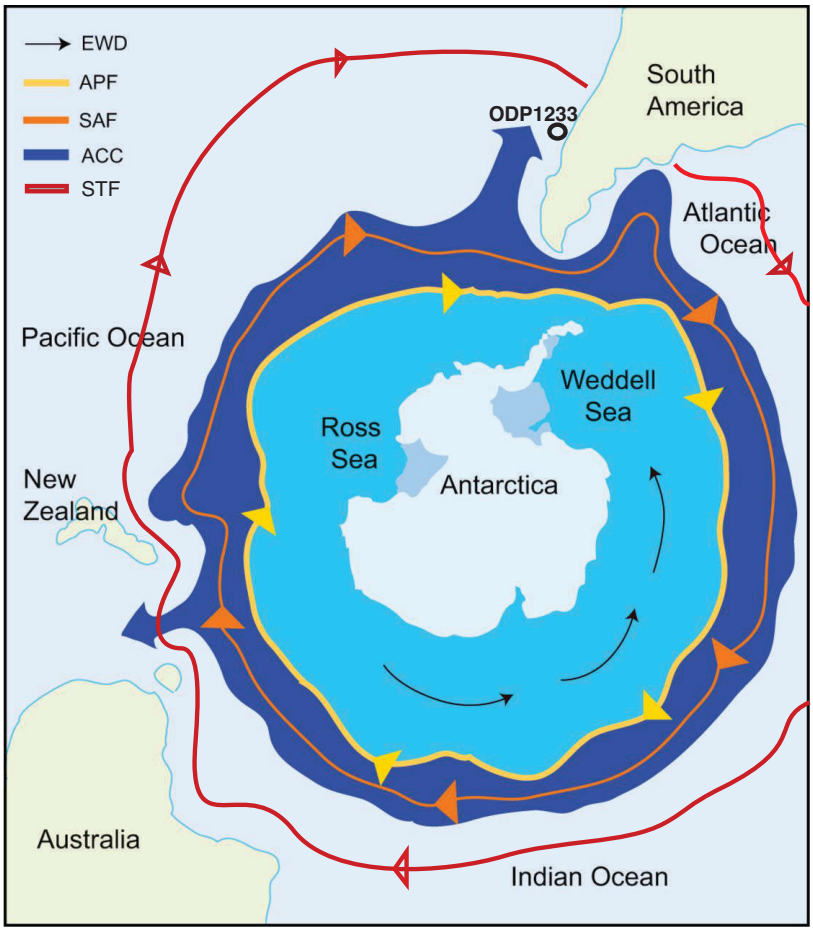

Figure 2.8 illustrates the most important oceanic and atmospheric fronts around Antarctica, that affects ODP Site 1233. The core site is positioned in the latitudinal middle of the subtropical high pressure and circum-Antarctic low-pressure zones. The main drift of the Antarctic Circumpolar Current (ACC) is positioned between 50-60°S. (Subtropical front (STF), Sub Antarctic front (SAF), Antarctic Polar front (APF), East wind drift (EWD)). Modified after Beers and Jayasundara (2015).

The Subtropical front (STF) intersects Chile between 42º and 38ºS, in winter and summer respectively - hence ODP Site 1233 at 41ºS an ideally located to monitor alterations in this front zone (Strub, 1998)(Figure 2.8). The (STF) is controlled by winds, created by the difference between the subtropical high-pressure and the sub Antarctic low-pressure domains. The STF marks the boundary between the (warmer and saltier) subtropical water and the (nutrient-rich, colder and fresher) subpolar waters, and is the northern most reach of the ACC and the SO. With a steep temperature gradient of 4ºC over 0,5º of latitude, and with an interannual variation of 4º latitude, this front position represent a major climate boundary in the SH (Rintoul et al., 1997). STF changes are also reflected by the seasonally shifts in the latitudinal span of SWW, along with the velocity and position of the PCC (Heusser et al., 2006)(Figure 2.7). During glacial intervals, with a global mean temperature drop of 3ºC, studies demonstrate that the STF moved 7º north of its interglacial position (at 33ºS), and possibly played a crucial role in the buoyancy distribution of the AMOC (Bard and Rickaby, 2009).

The sub Antarctic front marks the southernmost reach of the subtropical gyre, and the combination of warm water and nutrient content creates high marine productivity. Consequently, the highest abundance of planktic foraminifera are found in the subtropical gyres. Bathymetry also plays an important part altering frontal positions, along with the waxing and waning of the Antarctic ice sheet (Figure 2.8) (Sikes et al., 2009). However, unlike the Antarctic Polar front (APF) the STF are only slightly steered by bathymetry (Matsumoto et al., 2001, Wilson et al., 2005).

2.5 Atmospheric Setting

2.5.1 The Southern Westerly Wind belt

ODP Site 1233 are situated in the midlatitudes and in close proximity to the vast South Pacific ocean, and are under the influence of the SWW belt throughout the year (Garreaud, 2007). The position and strength of the SWW changes seasonally and interannual between 40-60ºS, due to shifting position of the storm tracks, but most importantly the position and the strength are driven by latitudinal position of the subtropical high-pressure and circum-Antarctic low pressure belt (Trenberth, 1991, Garreaud et al., 2013) (Figure 2.9). An equatorward movement of the SWW are coherent with a weakening of the SE Pacific anticyclone, and are related to

austral winters (Veit, 1996). The Andean Cordilleran and the strength of the SWW influence the spatial distribution of the precipitation in the southern South America. The seasonal changes in wind strength creates a large variability in runoff and accumulation of snow during winter (Figure 2.9).

The SWW-SO coupled system are regarded as a key-component in climate change on both short and long time scales, due to its ability to alter the rate of upwelling of deep water, and consequently alter the interior ocean heat distribution(Hodell et al., 2003, Anderson et al., 2009). Toggweiler et al. (2006) and Imbrie et al. (1992) argue that when the SWW intensifies and contracts around Antarctica, the interior heat and CO_2 of the deep ocean are drawn up to the surface through Ekman pumping, and from here blends into the atmosphere. This

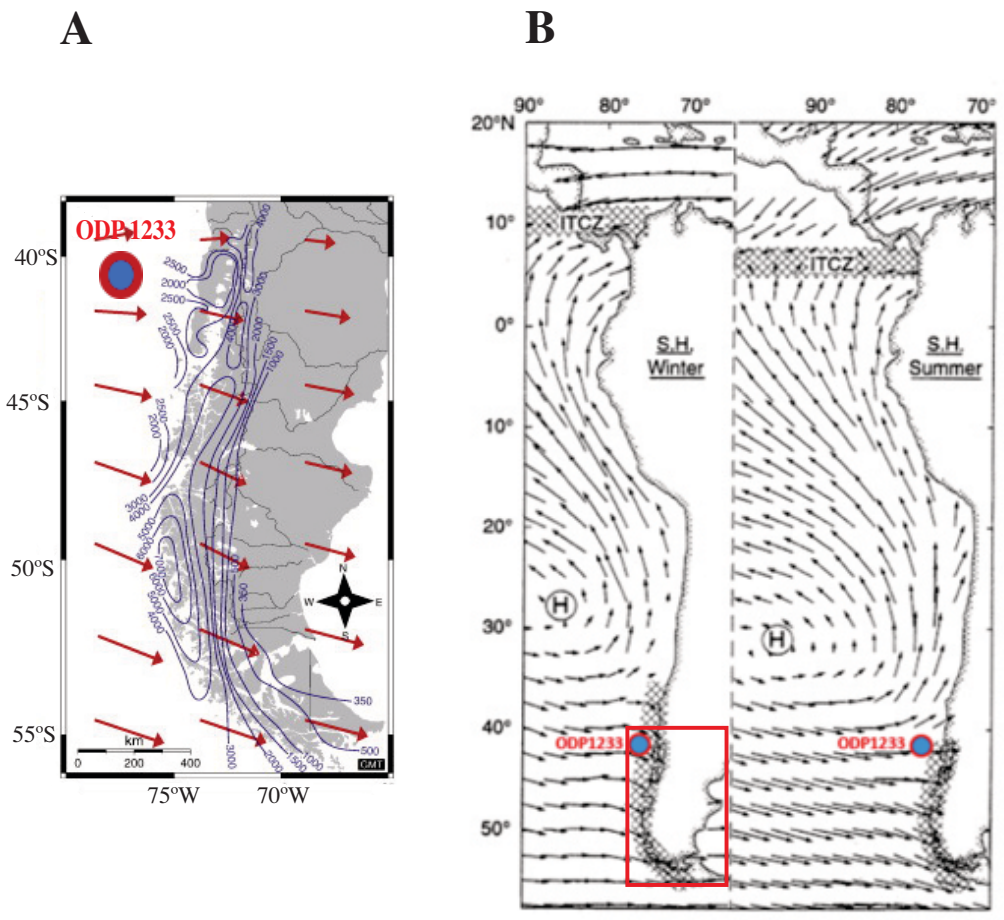

Figure 2.9 A) The annual precipitation and wind over Patagonia. B) The seasonal latitudinal prevailing winds affecting ODP Site 1233. A clear northward movement of the wind-belt during austral summers, with a coastal movement of the tropical high-pressure regions. Precipitation is shown by hatched area. Modified after Montade et al. (2011) and Strub (1998).

mechanism controls the atmospheric CO_2-level, contributing to a climate transition from a glacial to interglacial stage (Hodell et al., 2003).

The strengthening and weakening of the SWW plays an important role both on long time scales, and on shorter time scales. Buizert et al. (2018) shows that the rapid transition into an interstadial directly move the position of the SH westerlies equatorward, through an instantaneous atmospheric teleconnection. This signal reduces the Ekman transport and slows down the upwelling of CO_2 and heat from the deep SO, and hence cools the Antarctic. The opposite occurs during a stadial; a near instantaneous atmospheric response forces the SWW-belt poleward. This enhances the zonal wind speed of the SWW, increasing the Ekman transport and consequently brings more CO_2 from the deep ocean into the surface ocean, warming Antarctica. This link explains a number of results from studies in the adjacent SH, and from ODP site 1233, observing sudden alterations in SWW-induced proxy changes, prior to changes in the $\delta^{18}O$-signal in the Antarctic ice sheet (Moreno et al., 2001, Lamy et al., 2007).

During the LGM the tropospheric equator-to-pole gradient in pressure and temperature were weaker, facilitating a decrease in the SWW (Rojas et al., 2009). Studies suggests a northward latitudinal displacement of 5-6º of the SWW during LGM, resulting in a significant decrease in precipitation south of 40ºS, as observed from the Patagonian glacial reconstructions (Lamy et al., 1999, Moreno et al., 1999, Rojas et al., 2009). Changes in the position and strength of the SWW have significant implications for ocean circulation and the global carbon cycle, also during the Holocene. An observed a poleward shift in the SWW during the 20th century, facilitates increased mixing in the SO, enhancing the surface Ekman transport and thus strengthening the upwelling of the SO (Toggweiler et al., 2006, Toggweiler, 2009). The SWW have proven sensitive to temperature gradients in the middle of the atmosphere and has subsequently the last decades increased in speed as well (Moy et al., 2008, Toggweiler, 2009, Moreno et al., 2010, Swart and Fyfe, 2012, Voigt et al., 2015, IPCC, 2019).

2.6 Oceanographic setting

2.6.1 Surface water masses

The Antarctic circumpolar current (ACC) is the most dominant eastward flow of the Southern Ocean. It has a mean transport of 130-140 Sv, all of the ocean basins (2.10). The absence of large land barriers below 56ºS creates a circumpolar current facilitating a huge thermal inertia, which has a profound influence of the world's climate (Broecker, 1982, Rintoul et al., 2001). At approximately 43ºS the ACC impinge on the continent and splits into the poleward flowing Cape Horn current and the equator flowing Peru-Chile current (figure 2.10). One of its many mechanisms is that it brings macronutrients, such as phosphate and nitrate to the coast of Chile, facilitating, together with the upwelling regime and high continental run off, one of the most productive coasts in the world (Conkright et al., 1994).

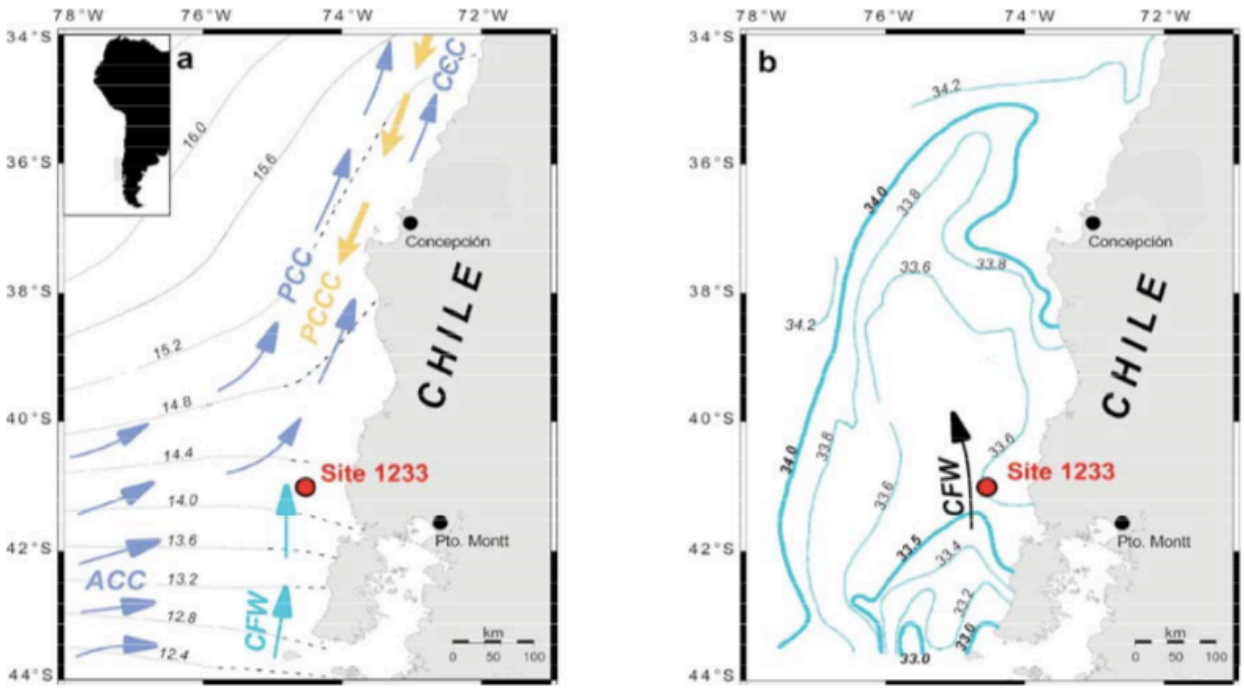

Fig. 2.10. The surface oceanography of ODP Site 1233. A) The ACC, flowing north as the Peru Chile Current (PCC) and the Peru Chile counter current (PCCC) with the Chilean fjord water marked by a blue arrow. The grey lines depict the changing surface temperature along the coast B) The surface salinity bars close to ODP Site 1233, with the low salinity Chilean fjord water ((CFW). From Førde (2008), modified after Mix et al. (2003).

The Peru-Chile current is an eastern boundary current that flows northwards along the coast of South America, transporting cold nutrient rich water to the tropics (Talley, 2011)(Figure 2.10). The northward transport is today approximately 15 Sv, however over the last glacial-interglacial cycle the PCC have been significantly colder and more intense, contributing to cooling the tropics during glacial periods (Wijffels et al., 2001, Feldberg and Mix, 2003, Kucera et al., 2005b). Below the surface currents are the poleward Gunther Undercurrent, at 100-400 meters depth, while the AAIW fills the water column down to 1000 m.b.s.l (Ingle Jr et al., 1980, Shaffer et al., 1995).

2.6.2 Chilean fjord water

The annual melting of the PIS and the high amounts of precipitation leads to high run off into the fjords resulting in a stratified water column south of 39ºS, with variable amount of suspended sediments(Mohtadi et al., 2005, González et al., 2013). This results in a low salinity tongue affecting the surface water of the core site. This tongue of low salinity water is brought into the warm saline subtropical water, creating a salinity of approximately 34,2‰(Mix et al., 2003) (Figure 2.10). During glacial times, with expanded PIS, this layer would consequently be a more dominant feature of the SE Pacific water column. The southern Patagonian ice field contribute today with melting of 3000m^3/s freshwater leaking into the ocean (Pantoja et al., 2011). The rate of glacier melting is expected to continue, and maybe even increase, in coming decades, contributing to global sea level rise (IPCC, 2019).

2.6.3 Upwelling

When the SWW impinge the Andean mountain Range, the wind continues northward. As a joint effect of the equatorward wind stress and the Coriolis effect, the surface water will flow to the west, a process called the Ekman transport (Price et al., 1987). Subsequently, deep resting water masses are drawn upwards in the water column, due to the vacuum that emerges as a result of the westward advected surface water. Whether it is the Gunther Undercurrent or the AAIW that are the source of the upwelling water, and consequently giving the water mass a northerly or southerly imprint, is still debated (Mohtadi et al., 2008, Muratli et al., 2010). However, $\delta^{15}N$ from ODP Site 1233, closely mirror the Alkenone derived SST, favoring a southerly sourced water mass (Martinez et al., 2006) The present upwelling along the Chilean

coast leads to a well-mixed and deep thermocline, at <38ºS, north of the subtropical front (Figure 2.11). Southwards is it a stratified water column and a more shallow thermocline that dominates (Mohtadi et al., 2005). However, there are interannual variability in the upwelling regimes, due to shifting position and strength of the SWW, which leads to upwelling all the way south to 42ºS during the austral summer (Pinochet et al., 2019)(Figure 2.11). The upwelling water masses consists of nutrients that sustains a highly productive surface water, where the planktic foraminiferal fauna are dominated by *Neogloboquadrina pachyderma* and *Globigerina bulloides* (Hebbeln et al., 2000). However, at the modern-day core site, the upwelling is so weak that these species are not present further south than 39ºS (Mohtadi et al., 2005). The zones of maximum upwelling have been known to shift during the last glacial cycle. Hence—during the LGM, Site 1233 experienced a minimum of upwelling due to the direct

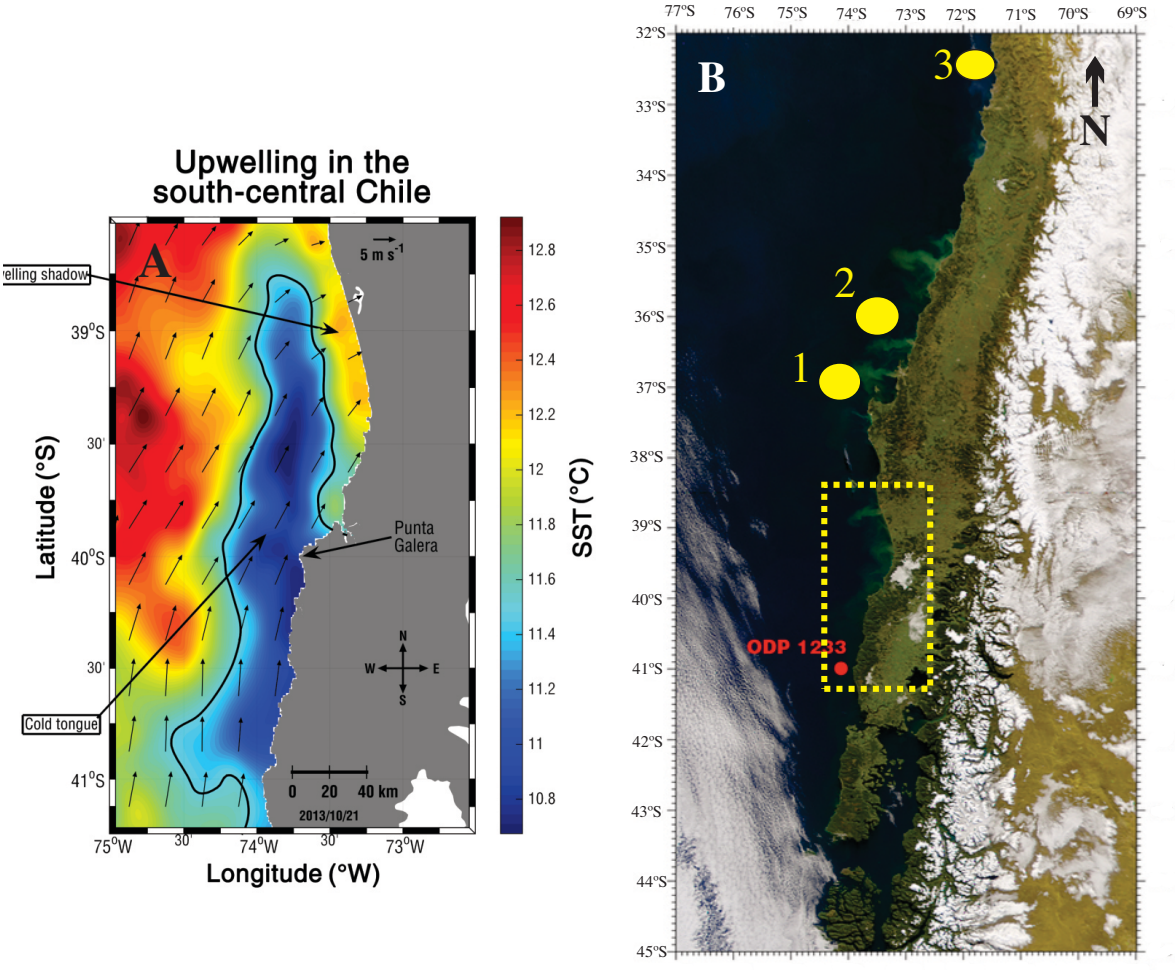

Figure 2.11 Modern day upwelling regimes of the central Chile. A.) upwelling that occur close Site 1233 during Austral summer, because of southward shifted westerlies. B.) Overview of the upwelling cells that dominates throughout the year due to Ekman pumping. Marked by yellow dots are the cells of Golfo Arauco (1), Concepción (2) and Punta Curaumilla (3). Note also the high run off visible along the coast, due to heavy rainfall. Modified after Pinochet et al. (2019) and photo from U. Ninnemann (printed with permission).

onshore blowing SWW (Romero et al., 2006, Mohtadi et al., 2008). Recent observations indicate that anthropogenic warming leads to south shifting winds, which results in a deepening in the mixed layer between 35 and 42ºS, indicating favorable conditions for coastal upwelling in further south (Aguirre et al., 2018).

2.6.4 Antarctic Intermediate Water

The Southern Ocean forms a number of deep and intermediate water masses, contributing to fill the world ocean basins with water of different properties (Figure 2.12). One of these water masses is the Antarctic Intermediate Water (AAIW), which contributes with ventilation of water to the subtropical gyres, and in addition distributes heat, freshwater and carbon from the SH (Talley, 1999, Hanawa and Talley, 2001, Sijp and England, 2009). The AAIW is important because its fills most of the Southern Hemisphere and the tropical oceans from about 800 to 1000 m depth. Variations in the SO surface properties are communicated throughout the subtropical SH and into the tropics through the AAIW, acting as an oceanic tunnel into all the ocean basins (Liu and Alexander, 2007).

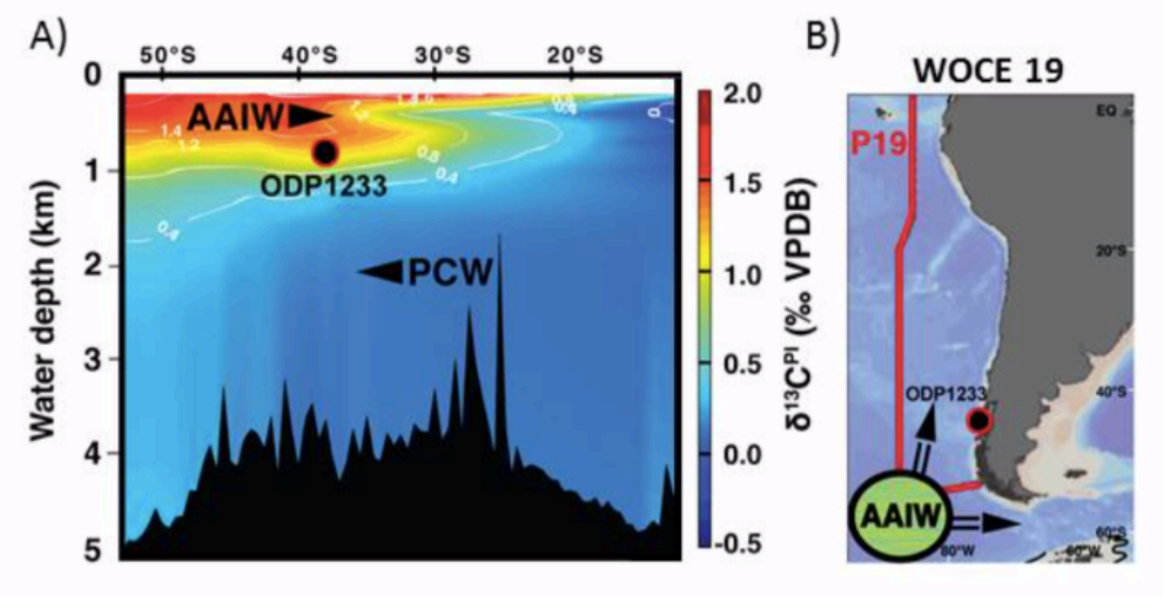

Figure 2.12. The location of ODP Site 1233, with relation to the AAIW. A) The modern position of the ODP Site 1233, relative to the position of AAIW and Pacific Central Water (PCW). B) Green circle represents the formation area of AAIW, and black arrows represent how the water mass flow into the subtropical gyres. The red line P19 in B, represent the profile shown in figure A (Soltvedt, 2014).

AAIW forms in the SE Pacific and intersects ODP Site 1233 with a core depth of 838 m.b.s.l, before it continues equatorward (Sloyan and Rintoul, 2001) (Figure 2.13). The AAIW is a distinct salinity minimum layer, with a high level of oxygen and nutrients located near the base of the pycnocline (Figure 2.13) (Talley, 2011, Bostock et al., 2013).

The variability of AAIW during glacial times is not yet fully constrained, but sediment cores indicate that the water masse has played a crucial role in interglacial/glacial climate change (Ninnemann and Charles, 1997, Spero and Lea, 2002, Loubere et al., 2007). A 970-kyr record from the coast of northern Chile reveals high AAIW variability. Maximum AAIW contribution occurs during glacial periods, whereas AAIW is completely absent during warm interglacial. This is explained by sea level changes, latitudinal migration of the AAIW formation site and intensified formation of the AAIW during cold periods (Martínez-Méndez et al., 2013). The same has been observed for the LGM, where the peak in oxygenation of the sediments coincide with maximum cold (Liu et al., 2002, Muratli et al., 2010). Euler and Ninnemann (2010) showed that the AAIW variability were significant over the last millennium, underscoring the unstable variability of the AAIW during warmer periods.

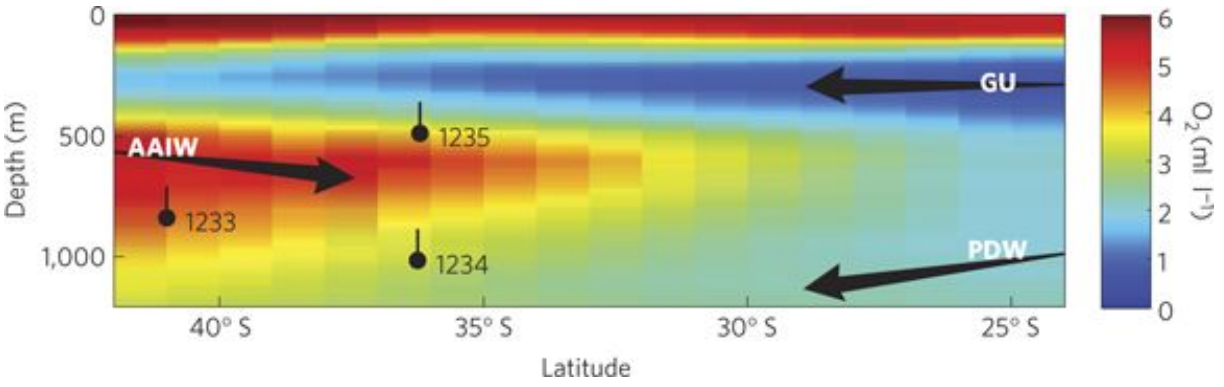

Figure 2.13 The oxygen concentration of the water masses adjacent to ODP Site 1233. AAIW which intersects the core site, holds a high oxygen concentration (red). The bars from the black dot, representing the core, represents the position after a 130 m sea level drop, representative for LGM. The dark blue water masses represent the Gunther Undercurrent (GU) and the light blue are Pacific deep water(PDW), both flowing polewards (Muratli et al., 2010).

3. CORE SELECTION AND SETTING

3.1 Core setting

Ocean Drilling Program (ODP) Site 1233 was drilled during ODP Leg 202, at 41º00`S; 74º27`W, about 38 km off the coast along the central Chile margin. This site was chosen as a drill target due to its high sedimentation rate (Lamy et al., 1999) and its position within the northern most latitudinal span of the ACC/SWW, consequently being sensitive to frontal change. The core was drilled in a small forearc basin at 838m, away from major turbidite currents, in the path of the northward flowing AAIW (Figure 3.1). The Peru-Chile current branches off from the ACC and flows equator-ward over the site location, along with the AAIW at 838 meters depth. Because of the coastal proximity, lithic counts in the core will reflect changes in the calving intensity from northern PIS.

The extent of the ice sheet is highly dependent on the moisture from the Pacific brought to the region by the SWW (Boex et al., 2013). The SWW bring heavy rainfall to the coastal mountains and the Andes, resulting in high sedimentation fluxes to the ocean (Shipboard Scientific Party, Leg 202, Chapter 4, 2003, (Lamy et al., 2001). The faunal assemblages will reflect variability of the STF, being the northernmost reach of the SO (Shipboard Scientific Party, Leg 202, Chapter 4, 2003).

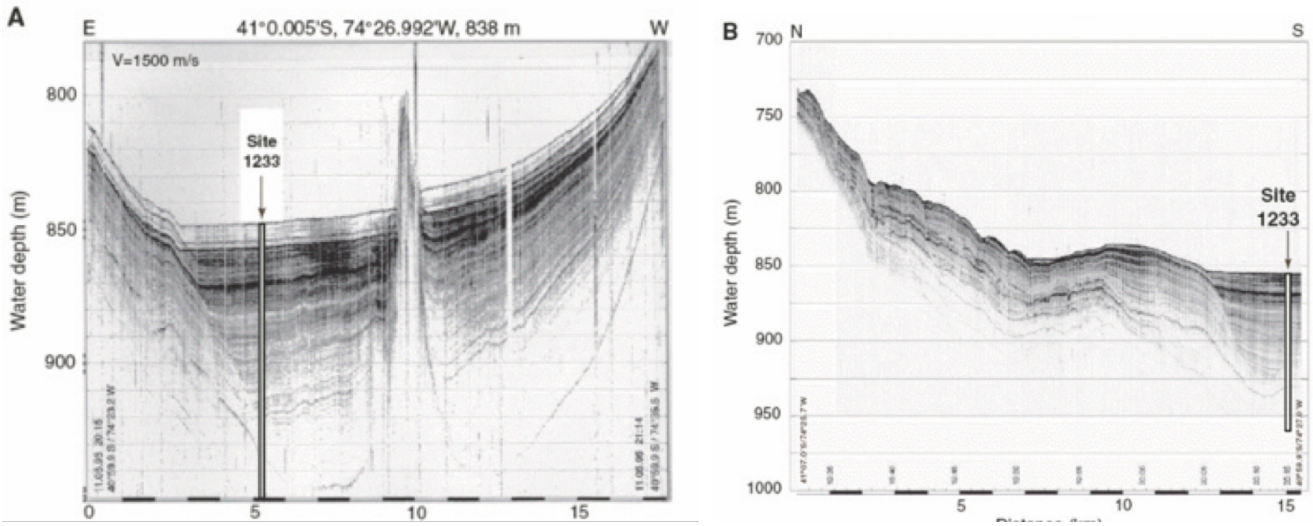

Figure 3.1. The seismic profile of the ODP Site 1233 location, apose to important sedimentological features. A) East-West Profil, the lamination of the sediments are clear from the seismic profil B) North-South Profile. One large turbidite can be seen north of the core site, but the profile also display the undisturbed sediment sequence of Site 1233 (Hebbeln et al., 1995)

.

3.2 Retrieving the core

ODP Site 1233 was drilled using an Advanced Piston Corer (APC). The APC works as follows; a core barrel is placed inside a drill pipe, and when a certain pressure is reached the barrel shoots down into the sediments retrieving, in best case, 9,5 meters of undisturbed sediment (JAMSTEC, 2015)(Figure 3.2). To obtain sufficient quality of the core, five holes were drilled and later spliced together to a 135,65 Meter Composite Depth (MCD). Hole 1233A was terminated after the first core, due lack of mudline. However, Hole 1233B, 1233C, 1233D and 1233E provided a good mudline and were cored to depths of 109.5, 116.3, 112.3 and 101.5 m.b.s.f, respectively. The study material for this thesis is sampled between 34,14 MCD and 66,38 MCD, and it encompass a splice between cores from Hole 1233C and hole 1233D. This means that the best preserved and continuous sections from holes C and D were spliced to enable the best possible recovery of the marine sediments. (Mix et al., 2003). The core splicing and the MCD-scales were enabled through stratigraphic correlation of the whole-cores onboard *RV Joides Resolution* (Figure 3.2) using the Oregon State University (OSU) fast track magnetic susceptibility scanner.

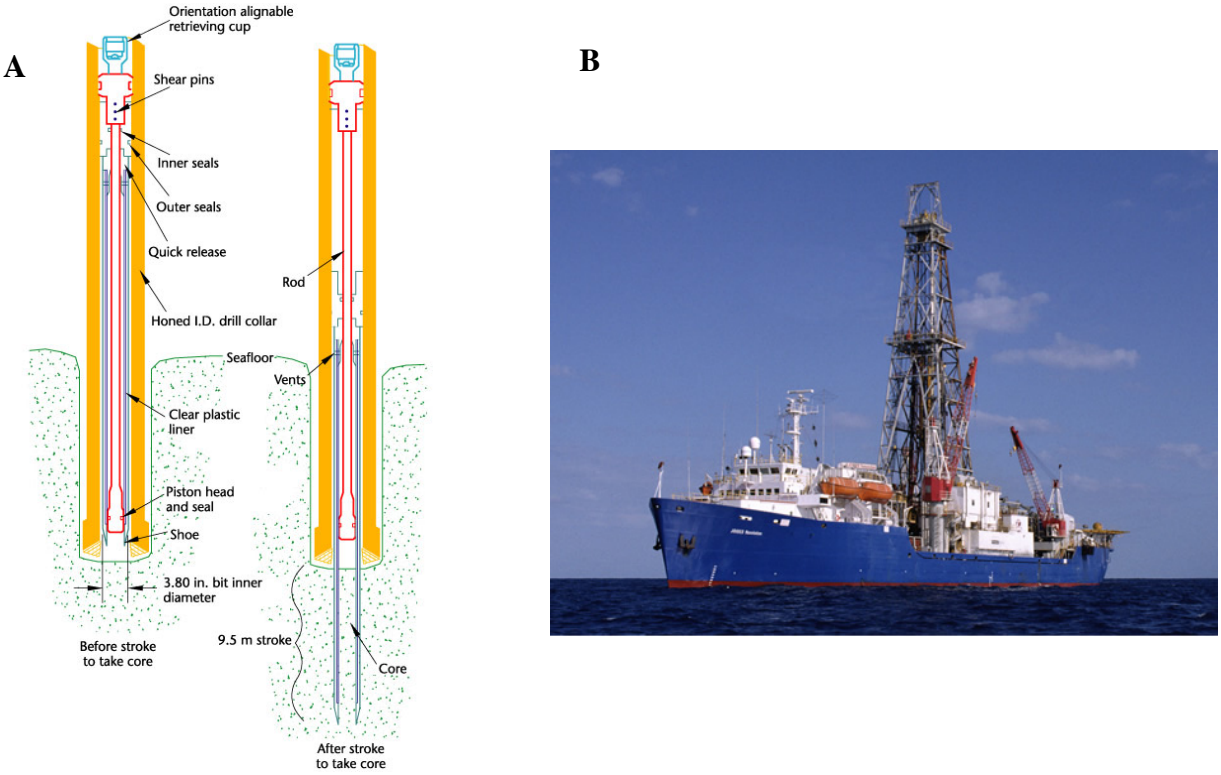

Figure 3.2 The gadgets used when extracting marine cores with Ocean Drilling Program (ODP). A) Illustration of how the Advanced piston core function when the marine sediments are extraxted. From IODP (2019a). B) RV Joides Resolution, the coring platform used for Leg 202. The APC are placed in the drill rig in the middle of the ship IIODP (2019b).

3.3 Lithostratigraphy

Sedimentation rates at ODP Site 1233 are very high. This was established when the 8 m long core GeoB3313-3 were cored in 1995 and suggested a 100cm/kyr sedimentation rate during the Holocene. Areas with high sedimentation rate has previously shown inhabitable for planktic calcareous organisms due to the sediments blocking of sunlight though the water column (Stein, 1990). However, this is not the case at ODP Site 1233, and foraminifera and other biogenic components are present throughout the core. This due to close proximity to upwelling regions driven by westerly winds which brings cold, nutritious water masses to the sea surface (Mix et al., 2003). Thus, terrigenous component, such as clay and silty clay, dominate throughout the core (Figure 3.3). Clay minerals and feldspar are common, with small quantum of quartz. The color of the core is olive-grey to dark olive gray (Shipboard Scientific Party, Leg 202, Chapter 4, 2003).

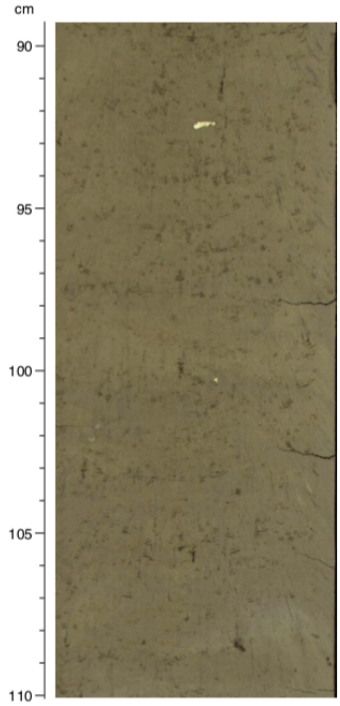

Figure 3.3 Representative core photo of the homogenous high resolution sediments from Site 1233. Shipboard scientific party, Leg 202, Chapter 4, 2003.

4. METHODS

This chapter describes the procedure of foraminiferal and lithic counts. The counts were done by using a Leica microscope at the microscopy lab at Department of Earth science at University of Bergen. Two different species of foraminifera were identified and counted in each sample, in addition to counting the lithic fragments.

4.1 Laboratory work

ODP Site 1233 was sampled at the Bremen Core Repository every 4 cm along the splice. The marine sediment samples were prepared for microscope analyses prior to this study. The interval from 34,14 to 66,38 MCD was wet sieved by H. Kleiven (pers.comm) and by N. Soltvedt (Soltvedt, 2014). The sediment samples were soaked in deionized water, shaken for 12 hours to disperse the clay and silt and later dried at 50ºC. Following this, the samples were wet sieved on 150µm and 63µm sieves, dried and weighed to obtain dry bulk weight per sample and transferred into sample glasses for microscopy analysis.

4.2 Microscopy analyses

A 33 MCD long interval (34,14-66,38 MCD) from ODP Site 1233 were analyzed with a sample spacing of 8 cm, corresponding to a resolution of 36 years (APPENDIX A). In some intervals the sampling interval was increased to every 4 cm, to obtain higher resolution and resolve the proxy signal in even greater detail. A total number of 122 samples were analyzed. Each sample was dry sieved using a 150 µm sieve, and the >150µm fraction was used for the foraminifera assemblage counts (Figure 4.1C). Samples were split when necessary, into smaller batches that contained approximately 300 individual grains (figure 4.1E)(CLIMAP, 1984). Each sample was distributed homogenously on a gridded microscopy tray prior to counting (Figure 4.1).

Figure 4.1 The equipment used to prepare the samples for analyzing in the Leica microscope. A) The microscope used to count a majority of the samples. B) The tray with a prepared sample, ready for analyzing. C) The sieve used to obtain the >150 µm fractions of the foraminifera and IRD. D) The tray used to move a sample from sieve to tray and vice versa and E) The splitter used to divide the samples down to approximately 300 individual specimens.

4.2.1 Planktic foraminiferal counts

The total amount of individual planktic foraminifera in a sample varied from 6 to 690 specimens. Of the 122 samples counted there were 54 samples containing less than 250 individual grains (APPENDIX A). Total planktic foraminifera counted includes two indicator planktic species; *Neogloboquadrina Pachyderma sinistral* (hereafter named *N. Pachyderma*) and *Neogloboquadrina Incompta (*hereafter named *N. Incompta)* and "other planktic

foraminifera" (Figure 4.2). The "other planktic foraminifera" category consists of all planktic species other than the two indicator species used. Exclusively whole, recognizable specimens were counted. The different species are identified using a brush to turn them and move them, moistened with deionized water.

4.2.2 Lithic counts

Lithic fragments (ice-rafted debris (IRD)) were counted from the >150 μm fraction, with a sampling space of 8 cm down core. This was done to estimate calving iceberg discharge from the Patagonian ice sheet. The amount of IRD varied down core from 0 to 50 grains. The lithic grains in this study mainly consist of single quartz grains (Figure 4.2 and 4.7). The relative abundance (%) of the IRD was derived from the total number of foraminifera counted in each sample (total benthic + total planktic + total IRD). The benthic foraminifera were therefore counted as part of a whole faunal assemblage.

4.3 Calculations

The coiling ratio was calculated as the percentage of right (or left) coiling varieties from the total counts of both *N. pachyderma* and *N. incompta* (equation 1). The relative abundance (%) of *N. pachyderma* and *N. incompta* were derived from the total number of planktic foraminifera (equation. 2 and 3). These equations has historically been used to interpret relative temperature change and alteration in the frontal position(Imbrie and Kipp, 1971, CLIMAP, 1984). The relative abundance of IRD is calculated as the percentages of IRD grains relative total from entities (foraminifera) in each sample (eq. 4).

$$\textbf{Coiling ratio } \% = \frac{\mathbf{100 * \textit{N. pachyderma} \text{ counts}}}{\mathbf{\textit{N. incompta} + \textit{N. pachyderma}}} \qquad \textbf{Equation 1}$$

$$\textbf{N. pachyderma } \% = \frac{\mathbf{100 * N. \text{ pachyderma counts}}}{\mathbf{\text{Total Planktic}}} \qquad \textbf{Equation 2}$$

$$\textbf{N. incompta } \% = \frac{\textbf{100} * \textbf{N. incompta counts}}{\textbf{Total planktic}} \qquad \textbf{Equation 3}$$

$$\% \textbf{ IRD} = \frac{\textbf{100} * \textbf{IRD counts}}{\boldsymbol{Total\ benthics + Total\ planktics + Total\ IRD}} \qquad \textbf{Equation 4}$$

4.4 Foraminifera

Foraminifera are calcareous single-celled organisms, that live either in the water column or on the ocean floor, and when they die and sink down their shells contribute to the pelagic ooze of the deep ocean(Kucera, 2007). Foraminifera are the most studied marine microfossils, due to their sensitivity to environmental changes and biostratigraphic significance, which makes them very good proxies for paleo environmental reconstructions and age determination (Hemleben et al., 2012). Foraminifera calcify their shell in equilibrium with the seawater, and the composition of the shells will consequently reflect the physical (temperature and salinity) and chemical (nutrients) characteristics of the both near surface and bottom waters. This allows utilizing foraminifera shells to analyze stable isotopes such as oxygen and carbon. The oxygen isotopes in foraminifera depend mainly on the isotope ratio of the water it is precipitated from and the temperature of calcification. Foraminifera can preserve their original isotope ratio for millions of years, and work on the oxygen isotope ratios of foraminifera was instrumental in the discovery of the orbital theory of the ice ages and continues to be widely used in the study of rapid climate change (Emiliani, 1955, Hays et al., 1976, Zachos et al., 2001, Lisiecki and Raymo, 2005).

4.4.1 Planktic foraminifera

The planktic foraminifera live in the photic zone of the water column. Bradshaw (1959) detected the highest concentration of the planktic foraminifera to be between 6-30 meters depth in the Pacific Ocean. Below 200 meters depth the number of planktic foraminifera declined sharply. Many of the species change their depth habitat through their life cycle, because as they grow their shells, their position in the water column will decline. In the modern ocean,

foraminifera have a latitudinal distribution, with a remarkable similarity in ecology between the corresponding latitude in each hemisphere (Figure 4.3)(Bé and Tolderlund, 1971). The same study reports an increase of <10% during the El Niño in 1997, indicating that an El Niño event only slightly affects the planktic foraminifera assemblage. The highest abundance of planktic foraminifera is found in the subtropical gyres, with *Globigerina bulloides* (hereinafter *G. Bulloides*), *N. Incompta, Globigerina Glutinata and Orbulina Universa* as the most abundant species.

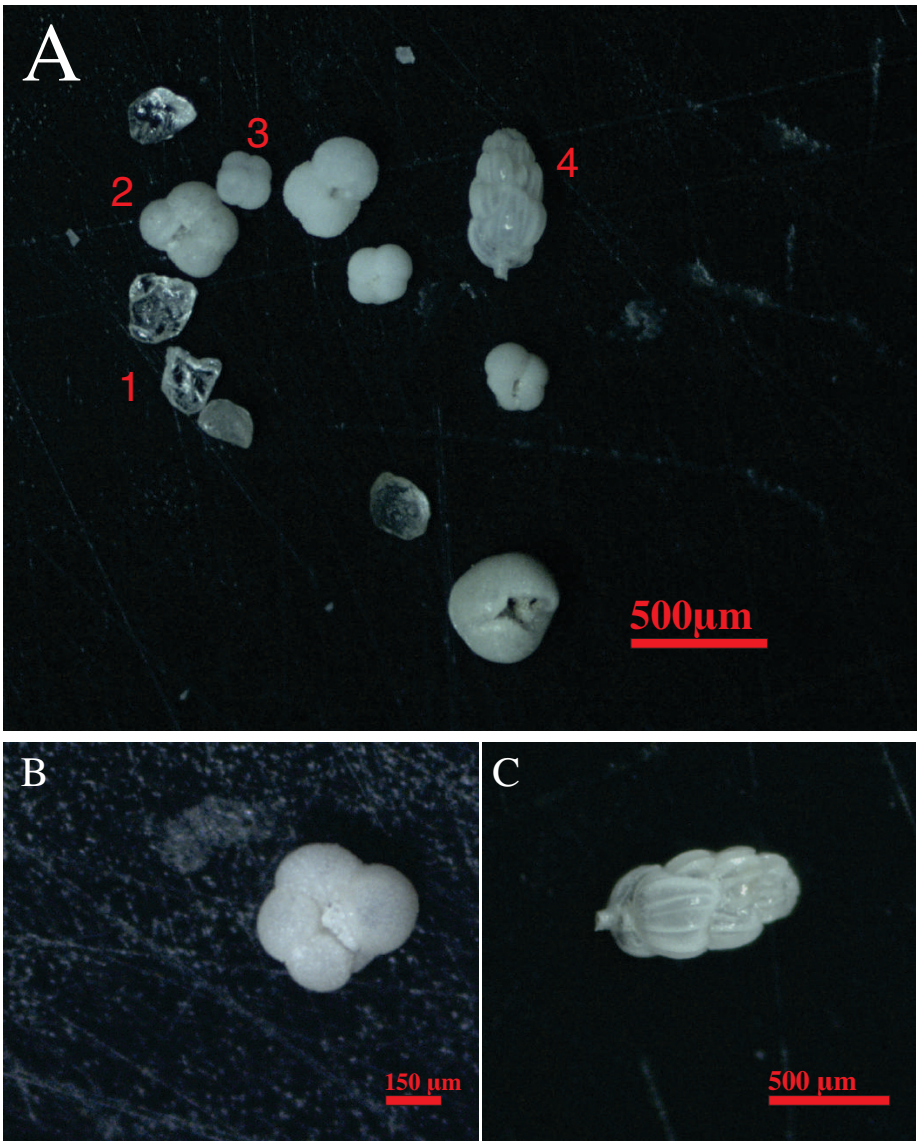

Figure 4.2. Common foraminifera and lithic components of the study interval at Site 1233. Scale are given as a red bar in the right corner. A) Sample selection of the foraminifera and lithics used for calculating the results. IRD (1), N. incompta (2), N. pachyderma (3) and U.peregrina (4). B) Photo close up of a N. pachyderma. C) Photo close up of a Uvigerina peregrina, which was one of the most abundant benthic foraminifera throughout the study interval.

4.4.2 Decisive factors controlling the planktic assemblages

Surface water properties, such as sea surface temperature (SST) in combination with salinity (SSS), is the main decisive factor controlling the planktic foraminifera faunal composition on global scale, while nutrients and light being the dominant factor under the favorable temperature regime on a more local scale (Ortiz et al., 1995, Niebler and Gersonde, 1998, Mohtadi et al., 2005, Morey et al., 2005, Kucera, 2007). Experiments conducted by Bijma et al. (1990) show that planktic foraminifera can live in a variety of different SST zones, but that their optimum range (highest abundance) are narrow (Figure 4.3). The modern distribution of foraminifera in the southern ocean is highly tied to the temperature gradients related to the frontal systems of the ACC (Niebler and Gersonde, 1998). Berger (1969) observed that in warm, nutrient depleted waters, the planktic foraminifera shells were big and rich in phosphate, whereas in cold regions the shells were small and low in phosphate. The species assemblages vary over the seasonal cycle, this is due to movement of oceanic fronts, leading to temperature alterations and changing level of chlorophyll in the mixed layer (Schiebel and Hemleben, 2000, Schiebel et al., 2001). Planktic foraminifera tend to flee the inner continental shelf with high sedimentation flux, that leads to decreasing sunlight penetrating the upper layer of the water column (Bandy and Rodolfo, 1964). However, the foraminifera are abundant and thrive at ODP1233 despite the high sedimentation rate. The explanation lies in the upwelling zone,

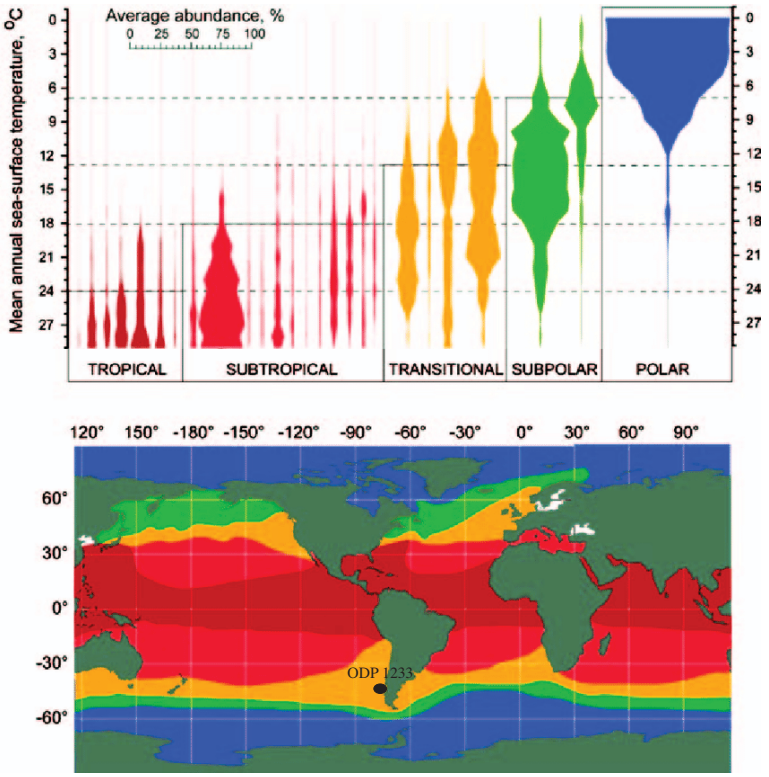

Figure 4.3 – the distribution of the planktic foraminifera of the modern oceans, divided into polar, subpolar, transitional, subtropical and tropic. ODP site 1233 are positioned in the transitional zone. Boundaries after Bé and Tolderlund (1971) and Bé and Hutson (1977). Modified from Kucera (2007).

facilitating a neutrinos water column that feeds a productive ecosystem (Toggweiler et al., 1991, Mix et al., 2003). Note that we do not consider dissolution of the foraminifera to have taken place, with the core site being at 883 m.

4.4.3 *Neogloboquadrina pachyderma*

Near monospecific assemblages from polar regions reflect the dominance of *N. pachyderma* in these regions (Figure 4.3 and 4.4)(Darling et al., 2007). The habitat of *N. pachyderma* is also distributed to subpolar and upwelling sites. This species is most abundant and calcify in the upper 50 to 100 meters (Reynolds and Thunell, 1986, Bauch et al., 1997) The optimum temperature range of *N. pachyderma* are -1 to 9º C (figure 4.5) and they tolerate a salinity range of 32 to 35 psu(Vázquez Riveiros et al., 2016). Carstens et al. (1997) showed that *N. pachyderma* thrive in close proximity to a stable ice front, and that during temperature inversion of the water column the depth habitat of the species drops down to 100 m.b.s.l. However, vertical fluxes from 300 to 50 m.b.s.l is observed during maximum upwelling regions in response to changes in the depth of the thermocline (Ivanova et al., 1999). The morphology of the *N. pachyderma* varies, regarding size, shape and texture (Altuna et al., 2018). The *N.*

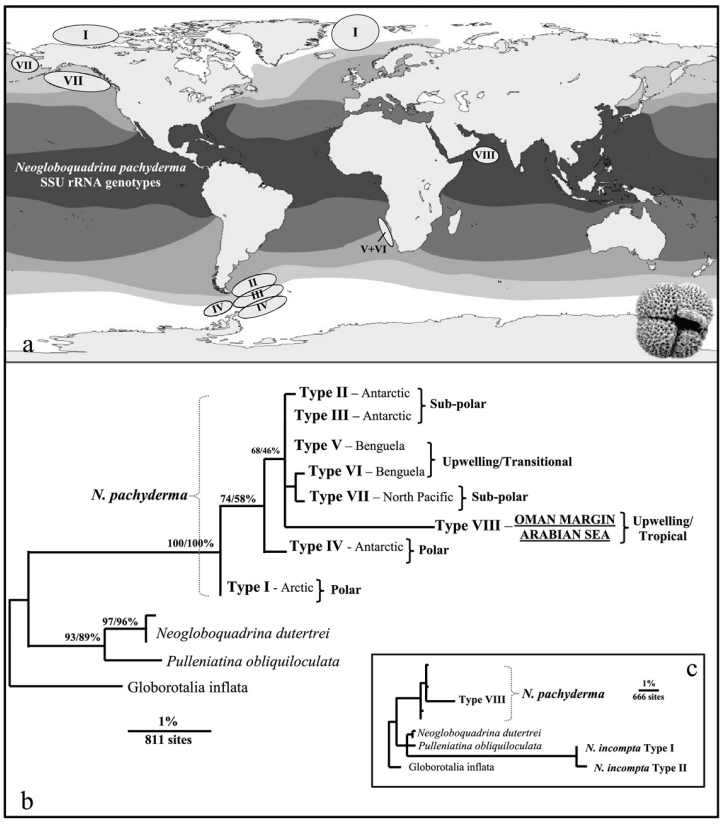

Figure 4.4 displays a genotype map of N. pachyderma. A) illustrate the distribution of the eight genotypes of N. pachyderma that exists in the global surface ocean. Note the high diversity of genotypes (II-VI) in the southern hemisphere. The grey shading shows the five major planktic foraminiferal faunal provinces, as shown in figure 4.3. B) The phylogeny of N. pachyderma. C) The genotype distinction between N. pachyderma and N. incompta. The figure is from Darling et al. (2017).

pachyderma is arranged by four to four and a half round, chambers, where the last chamber might consist of a lip. Darling et al. (2004) recognized four different genotypes inside the sub Antarctic front in the SH, whilst only a single genotype was found in the NH (Figure 4.4). During high latitude glaciations throughout the Pleistocene epoch, the *N. pachyderma* have shown to migrate equatorward in both hemispheres(Hendy and Kennett, 1999).

4.4.4 *Neogloboquadrina incompta*

This species were for a long time regarded as the right coiling morphotype of *N. Pachyderma*, however Darling et al. (2006) found genetic evidence for that it should be considered as a genetically distinct species and should be distinguished from the left-coiling counterpart. Their study documented that the coiling direction is not a signal decided by the environment, but a genetically inherited trait. Moller et al. (2013) report of a linear relationship between shell size and SST in the north Atlantic. In the southern ocean the main habitat of *N. incompta* is between the subpolar front and the subtropical front, with a temperature optimum range from 8-21ºC (Figure 4.5)(Bé and Tolderlund, 1971, Žarić et al., 2005). As Site 1233 lies within the northernmost reach of the Antarctic Circumpolar Current which has a high nutrient/low chlorophyll content (De Baar et al., 1995), *N. incompta* has been observed related to other water

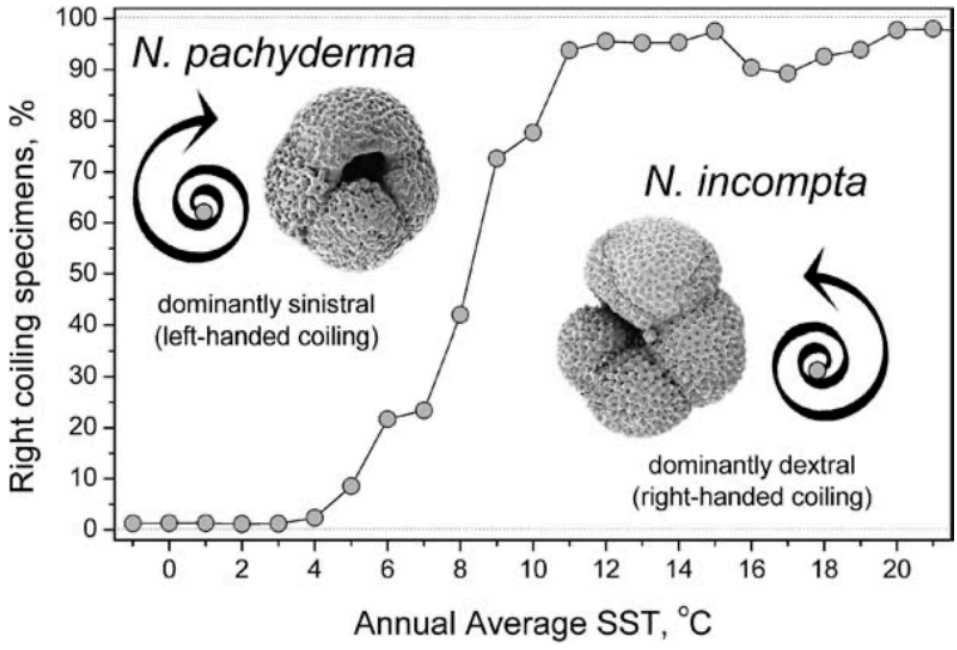

Figure 4.5 The faunal abundance of N. Pacyderma and the N. incompta plotted versus temperature (ºC) range, shown by the black line. Increasing temperatures coincide with increasing abundance of N. incompta (Kucera, 2007).

masses, usually above the pycnocline and waters with a high chlorophyll-a-content (Kuroyanagi and Kawahata, 2004). Marchant et al. (1998) recognizes *N. incompta* as the most abundant planktic foraminifera along the margin of Chile. Its calcification depth is most likely above 50 meters depth, depending on the depth of the pycnocline (Morley et al., 2017), however if the water column is well mixed the habitat could reach down to 100 meter water depth. The distribution of the species on the coastal Chile are tied to the thermal regime and how well wind-mixed the upper water column are (Reynolds and Thunell, 1986, Schiebel et al., 2001, Mohtadi et al., 2005).

4.5 Planktic foraminiferal census counts

One gram of deep-sea sediments will contain thousands of foraminifera, which is larger than 150μm. This enables quantitative analysis of the sediments to determine environmental surroundings (Kucera, 2007). Paleoceanography reconstructions derived from foraminifera faunal assemblage is based on the pioneering work by Schott (1935). He was also one of the first to point out that absence of foraminifera in the sample could be the result of dissolution and not the result of absent planktic foraminifera in the water column. In his studies, as well as mine, it is assumed that the ecological response of a foraminiferal species to chemical and physical parameter of the ocean are the same through time (Imbrie and Kipp, 1971, CLIMAP, 1984)

The census counts-method were tested out by the CLIMAP (Climate Long-age Investigation, Mapping, and Prediction)-project, who needed large amounts of census data, that were statistically reproduceable (CLIMAP, 1976, 1984). The method have later been improved and tested by the MARGO project (Pflaumann et al., 1996, Kucera et al., 2005a, Kucera et al., 2005b), with the goal to provide a tool box of assessing past sea surface properties based on foraminiferal assemblages. The biggest challenge of the quality of the method lies in recognizing the right species, amongst very similar species. Taxonomic accuracy are therefore highly necessary when applying this method(Kucera, 2007).

Relative abundance of *N. pachyderma* and *N. incompta* are used in this thesis to reconstruct movement of the front position, as successfully demonstrated by Mokeddem et al. (2014) and

Barker et al. (2010), amongst other. Because frontal positions are zones with a high gradient in sea surface porperties, movements in the front are altering foraminifera assemblages (Kellogg, 1976, Imbrie et al., 1992). *N.pachyderma* represent polar and subpolar watermasses and are rarely found north of the STF, while *N. Incompta* prefer subpolar to subtropical water masses (Figure 4.3 and 2.8). Increased abundance of *N. pachyderma* and *N. Incompta* will consequently represent a northward and southward frontal displacement, respectively (Imbrie and Kipp, 1971, Kohfeld et al., 1996).

4.6 Lithic counts

The proximity of ODP Site 1233 to the extent of the Patagonian ice sheet during the last glacial cycle suggests that sediments laden ice-bergs calving into the fjords in the Los Logos (Lake district) region could be a dominant factor affecting both the sediment flux and the water mass properties of the site. Andrews (2000) noted that there are three important factors controlling the sediment flux and meltwater discharge derived from icebergs, which are important to keep in mind when interpreting an; 1) how fast do the icebergs track from the fjord outlet and onto the shelf, 2) the route the icebergs take during the transport and, 3) the rate of mechanical destruction and melting en route.

4.6.1 Ice Rafted Detritus deposition ODP Site 1233 from icebergs

Melting icebergs and meltwater discharge from glaciers on land will first and foremost affect the surface water properties, setting the temperature and salinity of the ocean waters. This could alter the habitat and hence the assemblages of the planktic species that live in the upper water column. An iceberg-run off model study from Greenland shows that the melting rate of icebergs is biggest between 20 m.b.s.l and 170 m.b.s.l (Figure 4.6) (Moon et al., 2018). The presence of IRD at ODP Site 1233 suggests that ice berg melting have taken place here as well. Hulton et al. (2002) suggests a main source of regional meltwater pulses coming from the Chilean Lake District (40-44ºS). The limit on survival of icebergs today are occurring at 4ºC in the southern ocean (Hodell et al., 2001). The planktic foraminifera used for this study, as mentioned, calcify their shells during the spring/summer seasons, indicating that the meltwater in the upper 170

meters from icebergs during summer will affect both the foraminiferal assemblage and their isotopic signal.

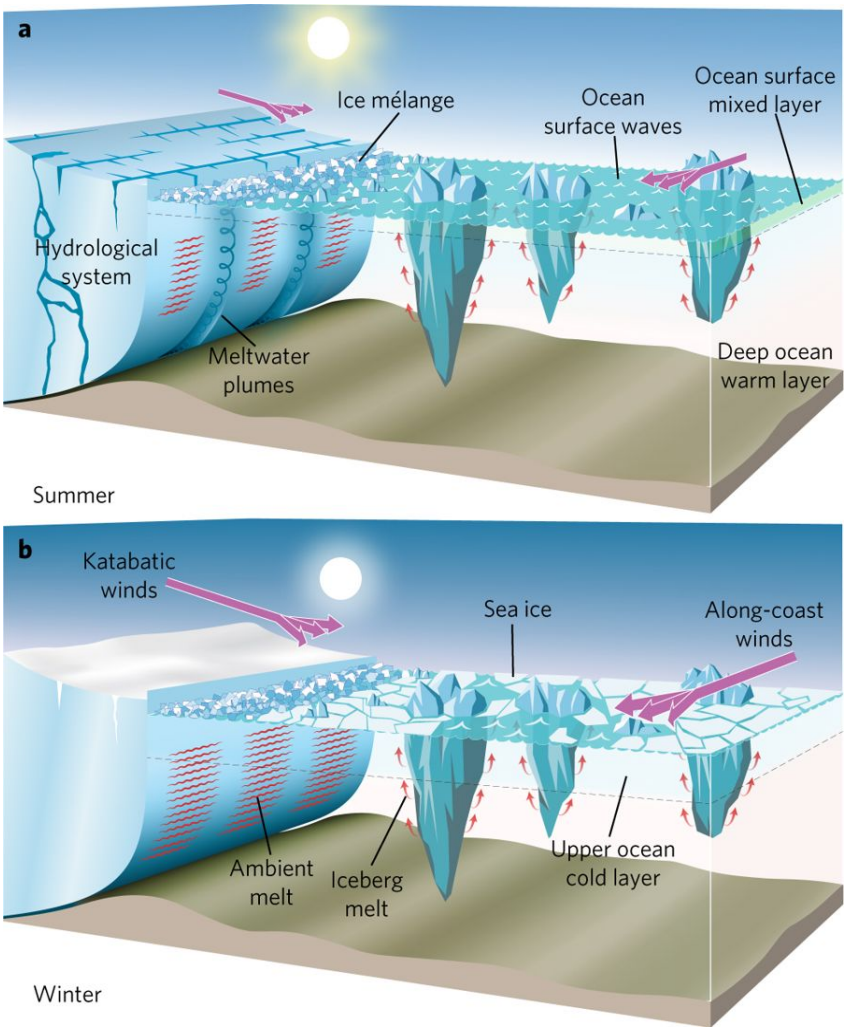

Figure 4.6 Seasonal changes in the hydrological system of a retreating glacier-fjord system. A) During summer, the icebergs break off from the marine terminating shelf. The icebergs melt and meltwater plumes are released from the shelf edge due to positive subsurface temperatures. This will affect the sea surface properties, creating a surface mixed layer. Mechanical erosion from waves ultimately breaks down the icebergs. B) During winter the sea ice increases, while the subsurface temperatures of the ocean are still melting the biggest icebergs. Figure after Moon et al. (2018).

4.6.2 Ice rafted debris

Ice rafted debris (IRD) are mineral grains of >63 μm that has been transported from land to the open sea, either by sea ice or icebergs (Figure 4.7). The prevailing winds and ocean currents are controlling the transport direction of the icebergs, and the sediment settles on the sea floor when the carrying ice melts (Figure 4.8)((Hemming, 2004). Therefore, IRD in marine cores are strong indication of waxing and waning of continental marine termini ice sheets (Baumann et al., 1995). However, there are some implications that should be regarded, when interpreting

IRD records. Andrews (2000) emphasizes that the source rock is important to consider, when choosing a size fraction in a study; because coarse-grained fractions are biased towards rocks with higher density, and subsequently are resistant towards mechanical erosion.

Therefore, knowledge about the adjacent continental bedrock is crucial when analyzing IRD. Further, the concentration of IRD in icebergs are assumed to vary from 0,01-10% and depends on the thermal regime of the glacier. This complicates what the presence of IRD in marine sediments actually mean, and should be taken into account when IRD are used to reconstruct ice sheet variations (Andrews, 2000, Hemming, 2004).

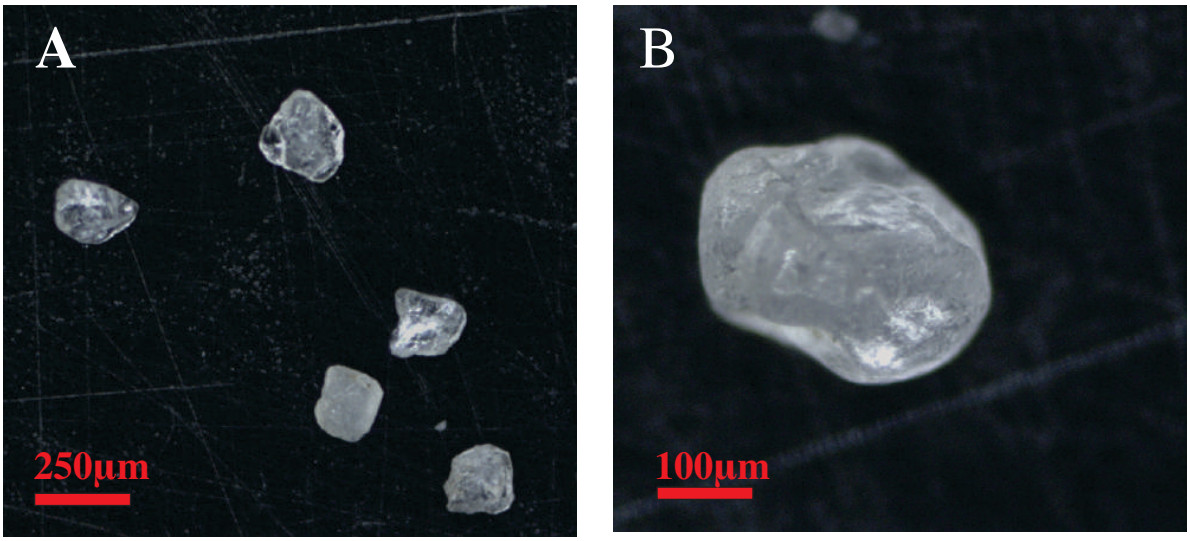

Figure 4.7 IRD from ODP Site 1233. A) . A selection of IRD from the samples. B) IRD with clearly rounded angles.

Earlier studies spanning the Pleistocene in the NH (Ruddiman, 1977, Jansen and Sjøholm, 1991, Bond et al., 1992, Broecker, 1994, Fronval et al., 1995, Kleiven et al., 2002) document that IRD flux is tightly coupled to the waxing and waning of ice sheet on land with the highest flux of IRD occurring at the glacial maxima, the deglacial and Heinrich events. We interpret the IRD record at Site 1233 on the assumption that this is also valid for icebergs in the SH and that maxima and minima in the number of % IRD reflects glacial maxima and minima of the PIS.

A few studies have reconstructed IRD flux in the SH (Kanfoush et al., 2000, Diekmann et al., 2003, Hoem, 2017), but only one is tied to the western marine terminating PIS (Caniupán et al., 2011), which presents an IRD record with a maximum resolution of 230 years spanning MIS 3-2. Hence, the high-resolution IRD record presented in this thesis, with a maximum resolution

of 18 years, is the first of its kind from SE Pacific. The lithic record combined with the high-resolution foraminiferal counts, will further be presented, which can unravel the detailed hydrography and ice sheet variability.

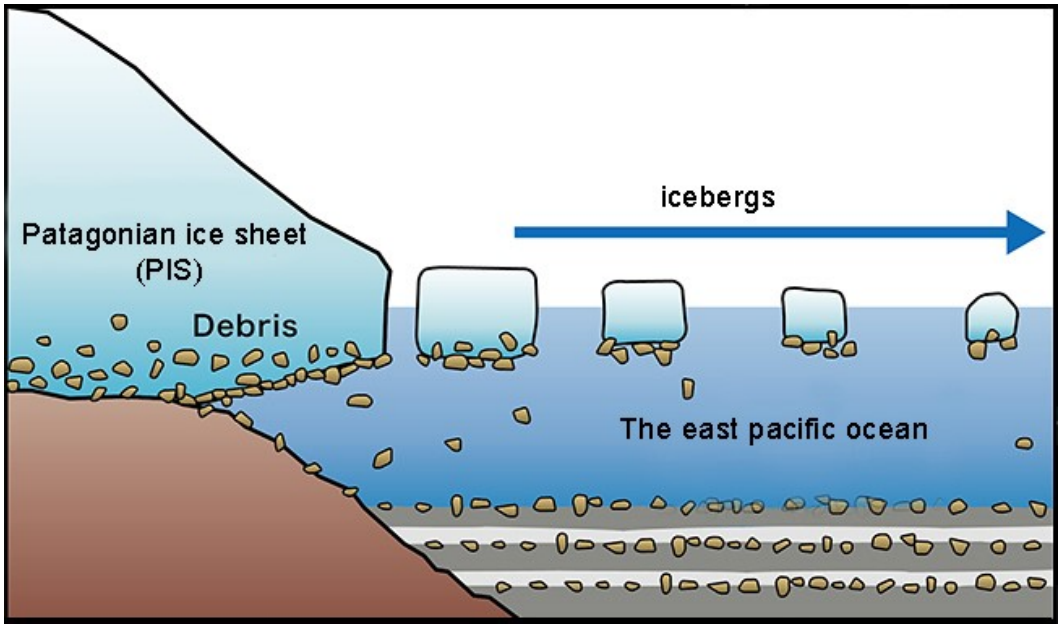

Figure 4.8. The concept of depositing and conservation of ice rafted debris (IRD). Modified from JAMSTEC (2015).

5. CHRONOLOGY

The age model used in this study is constructed by Førde (2008), who established an numeric age model spanning 31 kyr BP to 43 kyr BP (53,11-74,26 MCD) at Site 1233. Førde´s work built on, and suggested improvements on the AMS ^{14}C based age model published by Lamy et al. (2004) and Kaiser et al. (2005). The age model construction was done in two steps: First, by using linear interpolation between nine tie points, assuming constant sedimentation rates (Figure 5.1)(Førde, 2008). Eight of the control points are AMS ^{14}C-dates, while the latter is the Laschamp geomagnetic excursion at 41 kyr BP (Lund et al., 2006). The ^{14}C-dates were calibrated by using calpal 2004 calibration curve. The reservoir effect is assumed to be similar to the global mean, at 400 years, because of a relative distance to upwelling sites, nor close proximity to the southern polar front which can yield higher reservoir ages (Lamy et al., 2004, Lamy et al., 2007). Secondly, fine tuning of the δ^{18}O-signal from ODP1233 to the δ^{18}O from the EPICA DML ice core, thorough visual correlation. This was necessary because of unreliable ^{14} C-dates, with increasing age uncertainty (error bars) beyond 40 kyr BP at Site 1233(Kaiser et al., 2005). Tuning of an age scale is a process where the climate signal in a sediment core (or an ice core, coral, lake core etc.) can be correlated to climate signal in a target core, between two or several fixed ages. (Imbrie et al., 1984).

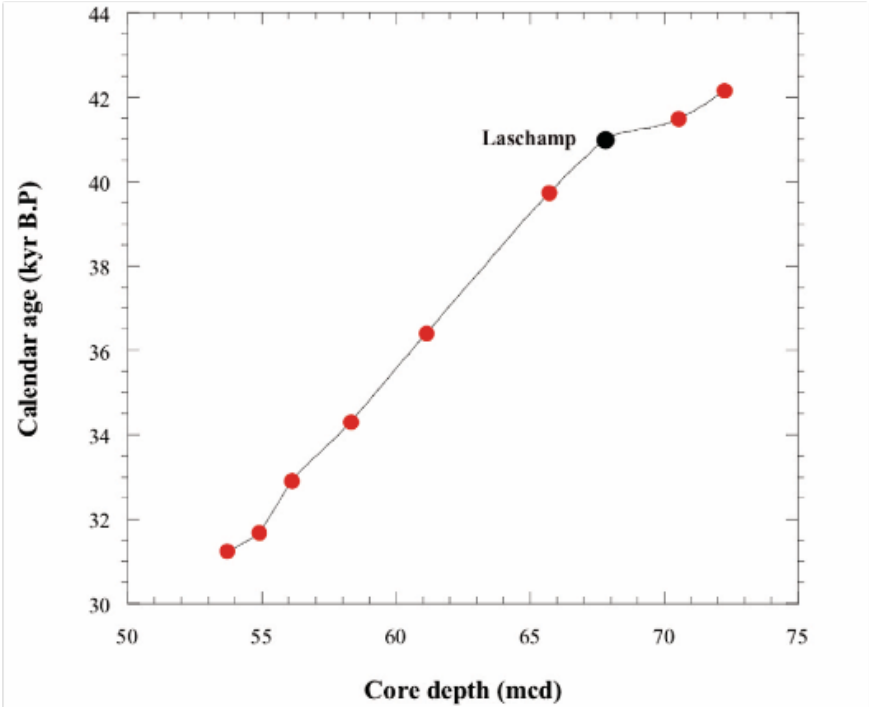

Age (kyr)	Depth (mcd)
31,250	53.700
31,690	54.900
32,910	56.120
34,310	58.310
36,410	61.130
39,740	65.700
41,000	67.800
41,490	70.530
42,170	72.260

Figure 5.1 The control points used by Førde (2008) to construct an age model shown to the right by using linear interpolation, assuming constant sedimentation rate between the control point to the left.

The tuning is based on the assumption that the climate signals from both climate archives occurred synchronized and represent the same age in both records. The EPICA DML Age model is based on annual layer counting of the chemical, dust and conductivity records. These layers are caused by seasonal changes in the source, transport and deposition of aerosols (EPICA community members, 2006). Lamy et al. (2004) established a strong Antarctic timing for the Holocene-Last Glacial Maximum (0-25 kyr BP) records at Site 1233 (Figure 5.2) and we assume that this synchronous behavior of the atmosphere over Antarctica and the ocean-climate proxies at 41ºS continuous through MIS3-4. Between 34 and 40 kyr BP, Førde (2008) detected a lead of 500-800 years between the EDML δ^{18}O-signal, and the ODP site 1233 benthic δ^{18}O-signal. Since the lead is within the AMS ^{14}C age uncertainty of 0,39 - 0,79 kyr (Kaiser et al., 2005), tuning was done, a new age scale was established – exhibiting a clear one-to-one coupling between the major climate events in both records (Figure 5.2).

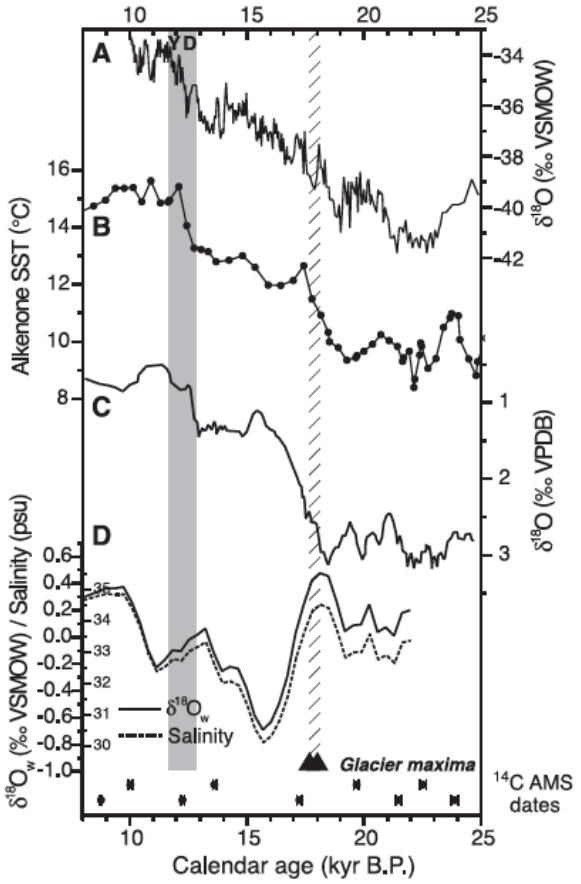

Figure 5.2. The clear one-to-one coupling of ODP Site 1233 and the Byrd ice core of Antarctica during LGM and the deglaciation. The δ^{18}O-signal of Byrd ice core (A) in synchrony with the SST and δ^{18}O of Site1233 (B, C and D), although plotted on different age models. From Lamy et al. (2004).

6. RESULTS

The high-resolution foraminiferal assemblage counts and lithic counts presented in this thesis are performed on the composite sequence of ODP Site 1233 from 57,9 to 66,5 mcd. This interval spans approximately seven millennials during MIS 3, from 34,10 to 40,85 kyr BP (6,75 kyr). The time interval spans over the Antarctic warming interval (A1), which corresponds to the D-O8 event and the subsequent D-O7 event in the NGRIP ice core(Johnsen et al., 2001, EPICA community members, 2006). Detailed lithic and foraminiferal assemblage studies from this region are scarce (i.e. Mohtadi and Hebbeln (2004)), and consequently can this study be regarded as the first high-resolution pilot study documenting changes in MIS 3 SE Pacific hydrography linked with Patagonian Ice Sheet variability. The assemblage data from the planktic species *N. incompta* and *N. pachyderma* together with lithic counts are reported in percentages (%). The high sedimentation rate (220cm/kyr) allows a sampling resolution down to 4 cm (18 years), but the average resolution in this study is 8 cm (36 years). The following chapter describes the data and its character in detail. In the subsequent chapter the most prominent results related to the foraminiferal assemblage work is presented and their potential significance discussed.

6.1 Planktic foraminiferal assemblages

A total of 122 samples were analyzed. Sediment samples of the size fraction >150 μm were split to give approximately 300 planktonic foraminifera for the counts in each sample. The actual number of planktonic foraminifera counted in a sample ranged from 0 to 1101 specimens. The number of total *N. pachyderma* varied from 0 to 301 and *N. incompta* varied from 0 to 213 counts. Of the 122 samples, 50 contained less than 250 planktic foraminifera, requiring that these data points should be treated with more caution (see full overview of counts and calculations in the Appendix). The abundances of the species *N. incompta* and *N. pachyderma* relative to the total planktonic foraminiferal assemblage were calculated. The variability in these two species monitors changes in oceanic water mass properties, related to frontal movements and/or upwelling regions. Other species such as *Globigerina bulloides*, *Globoratalia inflata*, *Globigerinita glutinata*, *Orbulina universa* and *Turborotalita quinquiloba* were also observed, and counted as “other planktics”. The assemblages varied highly from sample to sample.

6.2 *N. pachyderma* Coiling Ratio (%)

6.2.1 Common usage of the *N. pachyderma* Coiling ratio (%)

The coiling ratio is calculated as a percentage of the right (or left) coiling varieties in total (eq.1) and can be used as a sea surface temperature proxy, with increasing (decreasing) *N. pachyderma* coiling ratios representing cooler (warmer) temperature fluctuations.

6.2.1.1 Temperature

N. pachyderma is an excellent recorder of sea surface temperature through geologic time. When the earth experiences periods of lowered temperatures, the oceanic sea surface waters are cooler and the *N. pachyderma* forms its test (shell) with a coiling direction to the left. On the contrary, when the sea surface is warmer the test is formed with a coiling direction towards the right (Kucera, 2007). Consequently, will the coiling ratio fluctuations through time be a result of the changing SST, which creates an environment which is more suitable for either *N. pachyderma* or *N. incompta* in the surface ocean. Decreasing *N. pachyderma* coiling ratio below 50% will thus point to a dominance of *N. incompta* and consequently warmer temperatures of the depth habitat of the species (subsurface). It was for a long time regarded that the right and left coiling shells were morphotypes of the same species. However, DNA analysis reveal that the coiling variety each are their own genetic species. Here we adopted the name *N. incompta* for the right coiling *N. pachyderma* variety as suggested by Darling et al. (2006). The coiling ratio (%) is very suitable as a SST proxy where the planktic foraminifera mainly responds to changes in sea surface temperature (Bauch et al., 2003). However, we know that there are other mechanisms controlling the planktic foraminifera fauna.

6.2.1.2 Upwelling

The *N. pachyderma*, which generally is thought to be a polar species and restricted to temperatures below 8ºC, is found in upwelling regions in west Africa (Volbers et al., 2003), and in the Oman and Somali coast (Ivanova et al., 1999) in SSTs of up to 15ºC. Thus, will *N. pachyderma* act as a proxy for the temporal variability in the amount of upwelling that occurs. Upwelling along the coast of Chile is a result of atmospheric conditions which controls the position and strength of the Southern Westerlies. The wind blows towards the coast and as a result of the Coriolis force the surface water is deflected and replaced by cold, nutrient rich

water. These water masses have proven highly compatible with *N. pachyderma,* however whether it is the cold temperatures or the high nutrient level that controls the species population is not completely established. The study by Giraudeau and Rogers (1994) shows that there are no correlation between *N. incompta* and *N. pachyderma* with respect to nutrients (phytoplankton biomass) and consequently is it likely that the relationship between the two species are controlled by temperature in upwelling regions as well. This study could potentially shed some light on the topic.

6.2.2. *N. pachyderma* coiling ratio record of ODP Site 1233

Figure 6.1 displays the coiling ratio of *N. pachyderma* from ODP Site 1233 plotted versus meter composite depth (mcd). The unsmoothed signal shows a range from 0 to 100% of the left coiling varieties. The record exhibits high variability, which is superimposed on a general trend of 30% to high values of 80-100% takes place over a just a few centimeters of core. Between 64,5 to

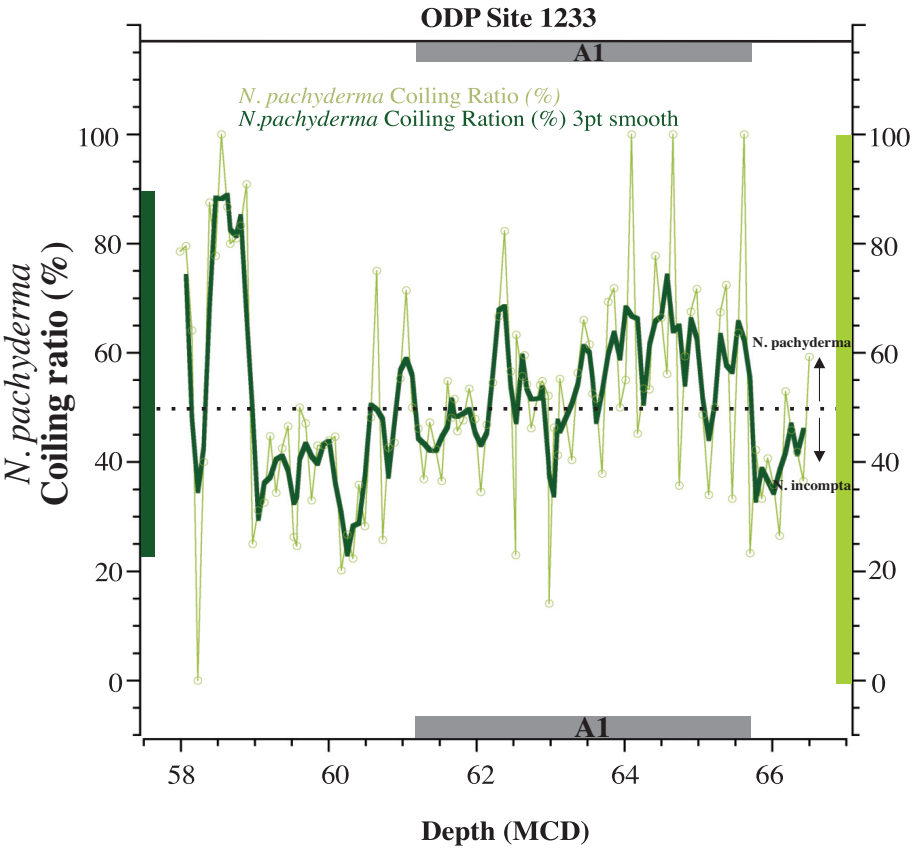

Figure 6.1. The N. pachyderma Coiling Ratio (%) plotted versus depth (mcd). The unsmoothed and smoothed record are shown by light and dark green lines respectively. The range for the records is shown along the y-axes. The Antarctic Warming event (A1) interval is shown as a gray bar on the x-axes. The stippled, horizontal line marks 50%, with the dominance of each species shown by arrows.

65,5 mcd. *N. pachyderma* coiling ratio shows high variability, increasing up to 100% three times during this interval. One of the most prominent fluctuations is observed between 58,98 and 58,52 mcd of the study interval and exhibit a change in the N. pachyderma coiling ratio from 30 to 100%.

The most reliable and robust curves are created when the data are plotted towards depth. It is crucial however, to investigate the variability of the record from a chronological perspective, to make statements about the timing, temporal resolution and to compare the findings to other records and observations, consequently will the following results be plotted towards age and these records are further evaluated and discussed. The age model constructed by Førde (2008), described in the previous chapter, is used for this purpose.

Figure 6.2 exhibit the high temporal variability of the *N. pachyderma* coiling ratio from ODP Site 1233, plotted versus calendar age (kyr BP). The unsmoothed record displays a range from 0 to 100%. The record exhibit four samples consisting of solely *N. pachyderma* repeatedly four times during the record. The smoothed curve shows a range of 65,5%, from a minimum of 23% (35,63 kyr BP) to a maximum of 88,5% (34,61 kyr BP). It is evident from Figure x.2 that two cycles of increasing to decreasing values are superimposed on a gradual ceasing trend, from 100% to 30% (stippled line in figure x.2). The first interval occurs from 39,74 to 37,88 kyr BP and is initiated by a rapid (in ~468 years) 78% increase of coiling ratio. The second interval spans 37,88 kyr BP to 35,60 kyr BP and are initiated by an increase of 62% in ~520 years (from 37,88 to 37,36 kyr BP). The two black arrows in Figure x.2 illustrate these two cycles. These major trends are best observed in the smoothed curve. Subsequently, the most abrupt increase of the record, from 30% (34,38 kyr BP) to 100% (34,57 kyr BP) occurs over a period of ~260 years, before the signal decreases to 0% over a period of 250 years (34,57 to 34,32 kyr BP).Superimposed on these general trends is a high frequency variability, with *N. pachyderma* coiling ratios ranging from 8% to 75,5%. It is evident that the highest variability occurs during the first cycle of A1 (39,77 to 37,88 kyr BP), with multidecadal to centennial oscillations and *N. pachyderma* coiling ratios range from 15 to 78%. Three prominent increases reaching a 100% of *N. pachyderma* coiling ratio occurs over a millennium (39,70 to 38,69 kyr BP). These variations in the faunal abundance are remarkable, because they may indicate large alterations in temperature and/or nutrients over a relatively short duration.

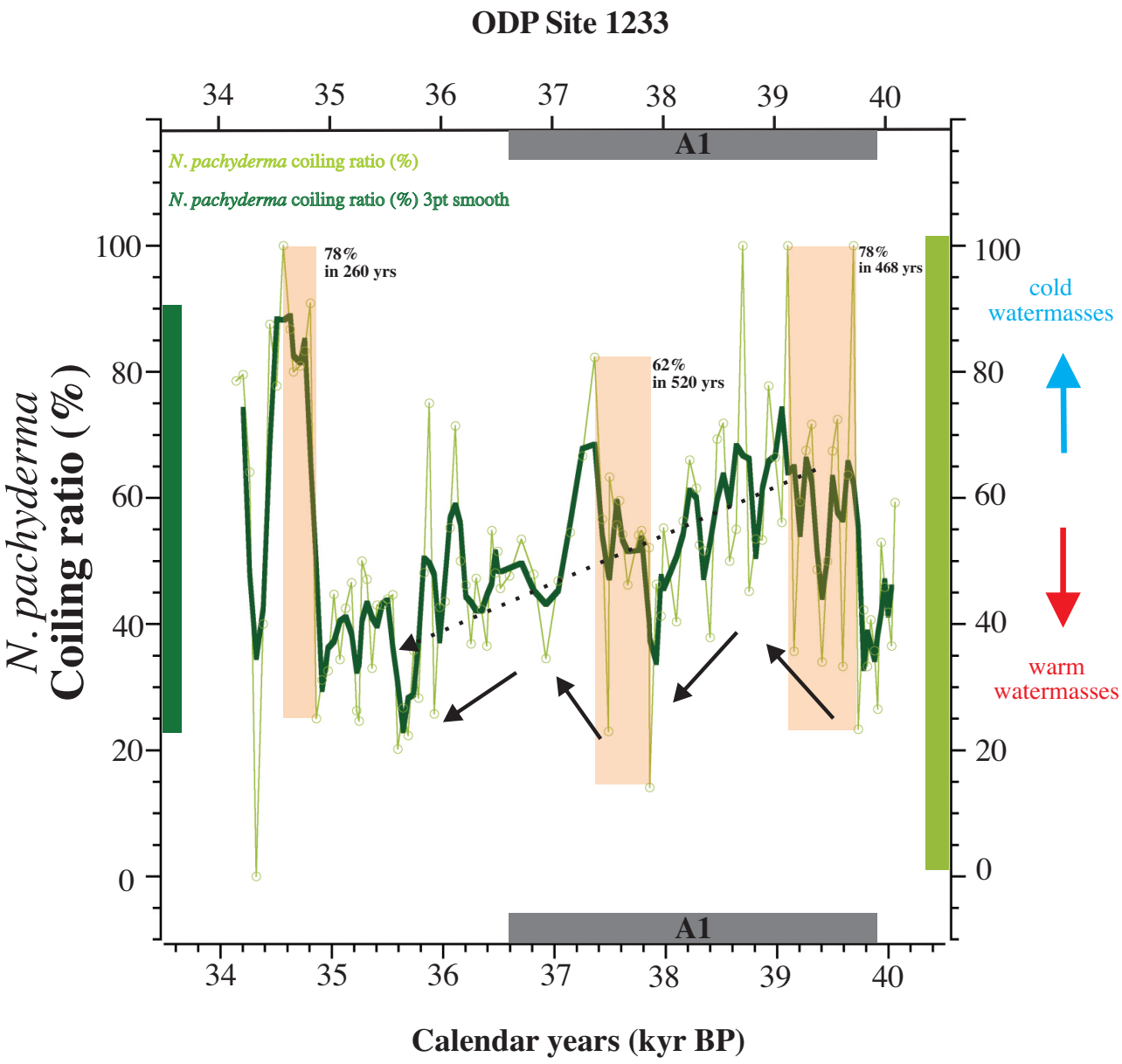

Figure 6.2. N. pachyderma coiling ratio plotted versus age (kyr BP). The non-smoothed and smoothed record is represented by a light green line and dark green line, respectively. The total range for each record is displayed along the y-axes. Orange bars represent the three most rapid increases of the N. pachyderma coiling ratio record. Black arrows illustrate two prominent increase-decrease trends. The stippled line displays the gradual ceasing long-term trend of the study interval. Grey bars along the x-axes show the temporal extent of Antarctic Warming event 1 (A1). Red and blue arrow along the right y-axes display the relative temperature change tied to the variability of the record.

6.3. Relative abundance (%)

The relative abundance (%) of *N. pachyderma* and *N. incompta* are calculated based on the total number of planktic foraminifera (eq. 2 and 3). Variability in the relative abundance is generally tied to alterations in the frontal systems. In this case however, a much more dynamic system must be taken into account when interpreting the signal. The core site is in close proximity to modern day areas of upwelling, which can have migrated during past climate changes, due to a shifting latitudinal location of the Southern Westerlies and its related oceanic fronts.

6.3.1 Relative abundance of *N. pachyderma* at ODP Site 1233

Figure 6.3 illustrates the relative abundance of *N. pachyderma*, plotted versus age (kyr BP). The unsmoothed *N. pachyderma* record displays a high frequency, with a total range of 0 (34,14 kyr BP) to 68% (39,08 kyr BP). The smoothed, more subdued signal exhibits a total range of 38% (from 4% at 34,44 kyr BP to 42% at 37,50 kyr BP). The record illustrates high variability, with centennial to multidecadal fluctuations with amplitudes of 5 to 25%. The smoothed and unsmoothed record of figure x.3 clearly illustrate that superimposed on the frequency signal is a rapid increasing and gradual decreasing trend, as inferred with black arrows.

The orange bars illustrate the two most prominent oscillations of the record, which both occur during the A1 interval, these peaks illustrate the maximum value of *N. pachyderma%* that occurs at 39,09 kyr BP, after an abrupt increase of 63% which takes place over approximately 500 years. This increase represents the largest peak of the record. The second peak has an abrupt step-wise increase starting at 37,85 kyr BP and peaks at 37,49 kyr BP followed by an immediate decrease. The overall increase in *N. pachyderma%* is 50% over 360 years. These prominent peaks infer a complete change of the near surface water properties. The interval in-between the peaks, exhibit several rapid, low range oscillations with amplitudes of 20%, 10% and is superimposed on a high-frequent oscillation with amplitudes of 5 to 20%.

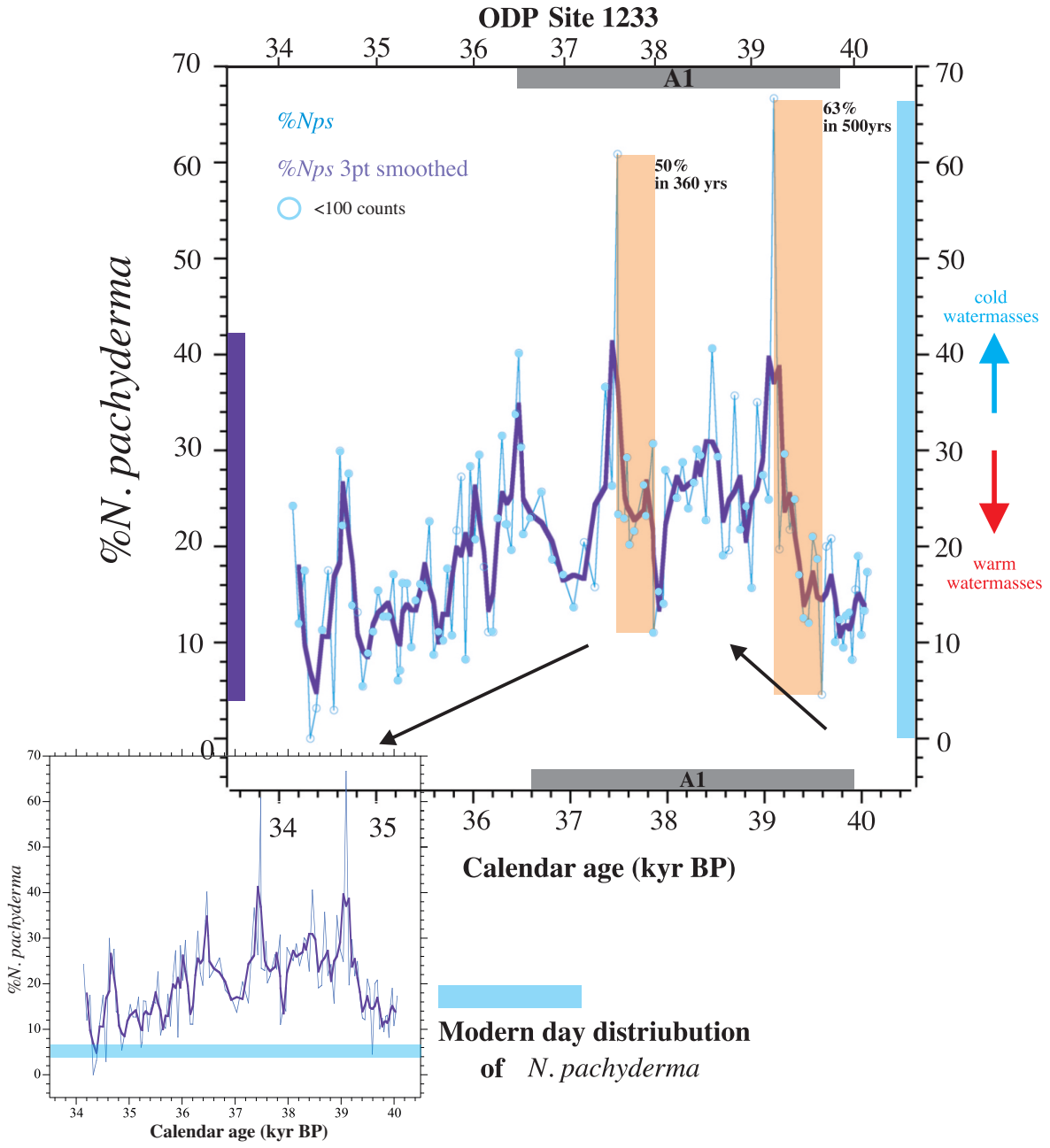

Figure 6.3 shows the relative abundance (%) of N. pachyderma plotted versus age (kyr BP). Smoothed and un-smoothed record are shown by dark and light blue lines, respectively. The total range for each record is displayed along the y-axes. The gray bar along the x-axis display the temporal extent of Antarctic warming event 1 (A1). The orange bars represent abrupt, high amplitude increases in the species abundance. It is important to mark that both of these increases occur within the A1. Black arrows indicate the general increasing-decreasing long-term trend. Red and blue arrows along the right y-axes indicates relative temperature change. Open blue circles mark samples consisting of <100 total number of planktic foraminifera. Inset in the lower left corner illustrates the modern-day relative abundance of N. pachyderma with a blue horizontal line. The modern day relative abundance close to ODP Site 1233 is 6,8%, derived from core top RR9702A-24MC-1 (41,297° S 74,320° W).

It should be noted that the two most prominent peaks (at 39,08 and 37,49 kyr BP) of the unsmoothed record are samples containing less than 100 total number of planktic foraminifera, creating a signal which is less statistically robust. These peaks should consequently be interpreted more carefully.

The 3-pt smoothed record of *N. pachyderma,* emphasizes the evident increase-decrease trend, however what stands out from the smoothed record are four peaks occurring on centennial timescales over five millennia (Figure 6.4). The four peaks are prominent features of the general trend and occur with the approximately same duration. The peaks occur at 39,08 kyr BP, 37,49 kyr BP, 36,46 kyr BP and 34,62 kyr BP, separated by 1600 year, 800 years and 1800 years, respectively.

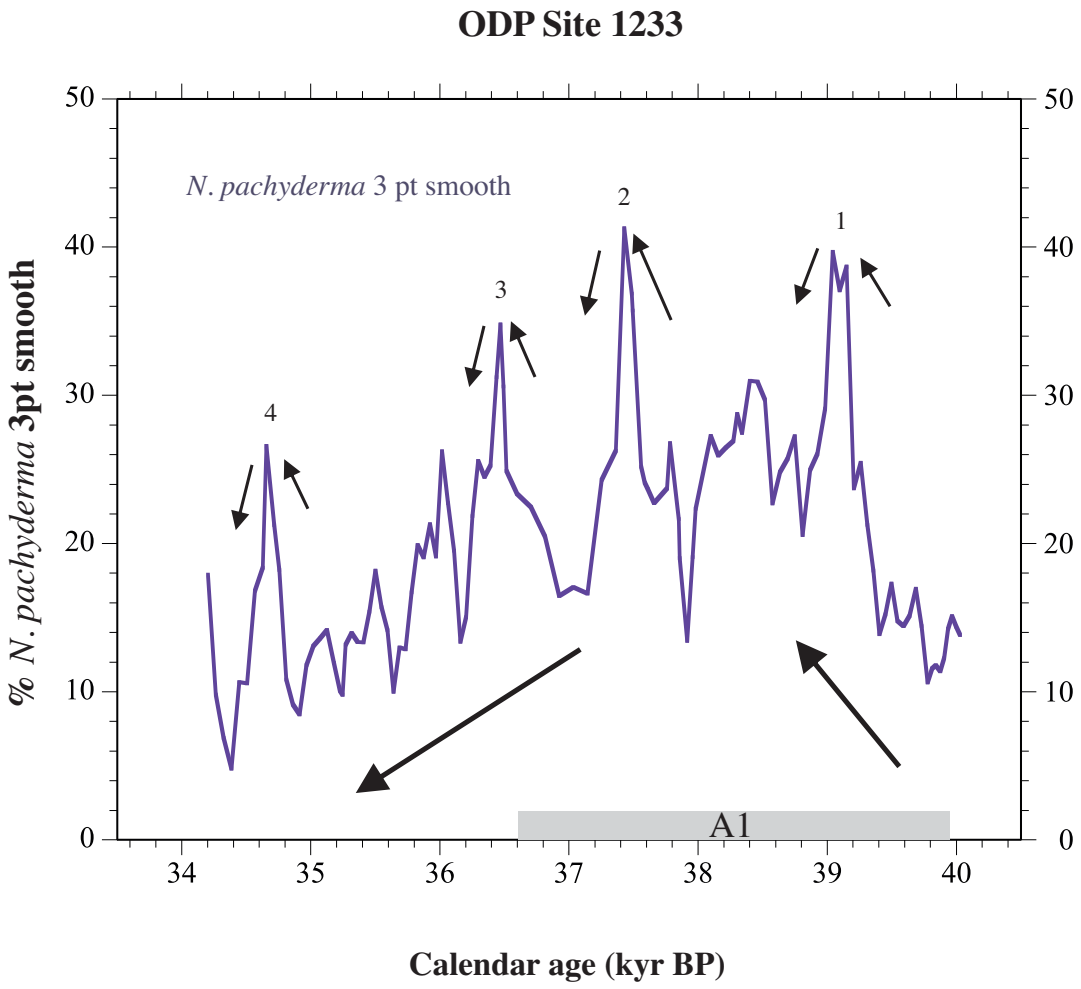

Figure 6.4 The 3-pt smoothed record of %N. pachyderma plotted versus age (kyr BP) to better illustrate the general trends of the record. Four prominent peaks that are superimposed on the long-term increase-decrease trend are highlighted with arrows and numbers in this plot.

6.3.2 Relative abundance (%) of *N. incompta* at ODP Site 1233

Figure 6.5 displays the relative abundance of *N. incompta* plotted versus age (kyr BP). The unsmoothed signal exhibits a range of 43% (36,47 kyr BP), while the 3pt smoothed record display a total range of 35% (36,47 kyr BP). The record is characterized by an overall high variability, but with varying frequency.

It is evident from the figure 6.5 that the relative abundance of *N. incompta* exhibits millennial and centennial scale oscillations throughout the study interval. The smoothed and unsmoothed records clearly exhibit the same pattern. 13 distinct peaks in *N. incompta %* is evident between 40 and 35 kyr BP. The most rapid oscillations of the record are highlighted by blue bars in Figure 6.5. The *N. incompta %* increases with 36% from 38,68 to 38,40 kyr BP and 35% later in the study interval from 37,27 to 36,47 kyr BP.

From 40.08 to 37.40 kyr BP a high-frequency signal dominates, with clear multidecadal oscillations of 20-30%. The signal is superimposed on a rapid increasing, gradual decreasing trend, with a maximum range of 36%. Between the multidecadal frequency there is a low amplitude variance with a range to 10-15%. A variability of over >30% over 36 years occurs three times in the study interval (38,68-38,40 kyr BP, 37,27-36,47 kyr BP, and 35,97-36,12 kyr BP). Which is remarkable because this suggests rapidly varying physical (temperature and salinity) and chemical (nutrients) properties at the core site.

The highest *N. incompta %* abundance occurs at 36,47 kyr BP and it is worth noting that this closely falls in line with the end of the A1 interval (36,6 kyr BP). From 37.40 to 35,55 kyr BP several oscillations on centennial timescale are observed, with varying amplitude, ranging from 8 to 35%. The youngest part of the record is characterized by a two-step 35% decrease in abundance, occurring over a few decades, with a decadal frequency and low amplitude (2-8%) sequence in each step. This is a rapid and prominent change, which could indicate shifts in atmosphere and ocean dynamics at the core site.

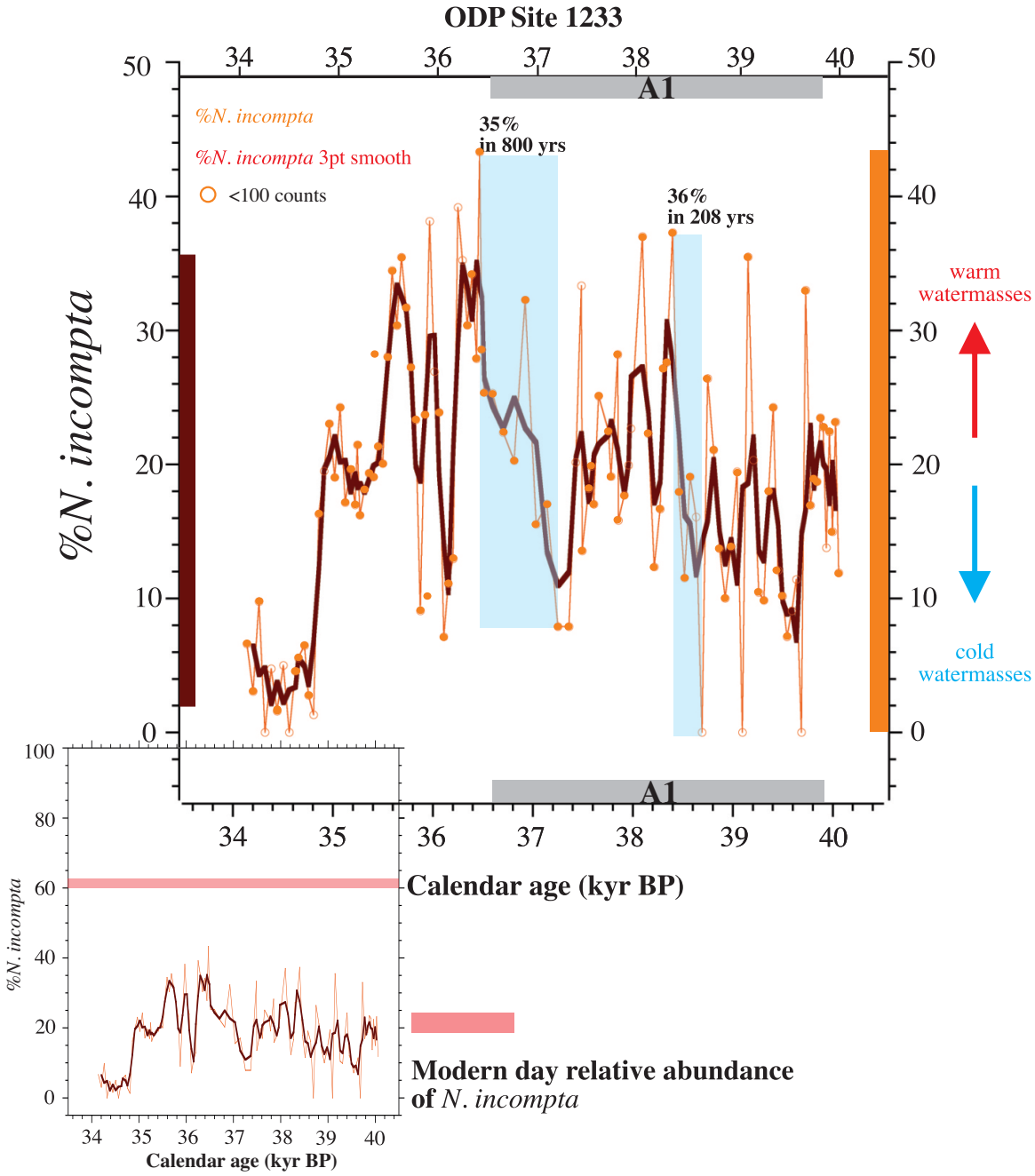

Figure 6.5 shows the relative abundance (%) of N. incompta plotted versus age (kyr BP). Smoothed and un-smoothed record is shown by red and orange line, respectively. The total range of each record are given along the y-axes. The blue bars represent intervals where the variability is high. Relative temperature is illustrated with the red and blue arrow along the outside of the right y-axis. The Antarctic Warm Event 1 (A1) is shown by dark grey bar along the x-axes. The samples containing <100 planktic foraminifera in total are marked with open orange circles. Inset in the lower left corner illustrates the modern-day relative abundance of N. incompta with a red horizontal line. The value of 62% is derived from Core top RR9702A-24MC-1 (41,297° S 74,320° W) close to ODP Site 1233.

6.4 Lithic counts (%)

The lithic counts from ODP site 1233 monitors variability of the North Western edge of the Patagonian ice sheet, possibly from icebergs calving from the marine drainage route through Golfo de Ancud (figure 2.6). However, icebergs drifting from further along the coast could also be contemplated as a source since the marine terminating margin of the PIS reach as far south as 56ºS (Glasser et al., 2008).

Figure 6.6 displays the abundance of lithic grains in percentages and plotted versus age (kyr BP). The individual IRD grains varied from 0 to 50 in the studied samples. The calculated relative abundance of the IRD exhibit a range of 25%, with 24% being the largest range occurring from one sample to another. The most prominent feature of the lithic curve is the abrupt increases of IRD between 37,50 to 37,25 kyr BP and between 36,14 to 35,67 kyr BP, marking four episodes of massive iceberg discharge. These peaks in %IRD is superimposed on a less prominent, yet consistent, IRD content between 2 to 5% from 39 to 34 kyr BP. The duration of the individual peaks in the interval vary from 36 to 108 years, indicating repeated rapid calving events. Between 40 and 39 kyr BP the IRD-signal exhibit no variability. The dynamic and nature of the IRD-signal is complex and will be discussed in a regional climate context in the subsequent chapter.

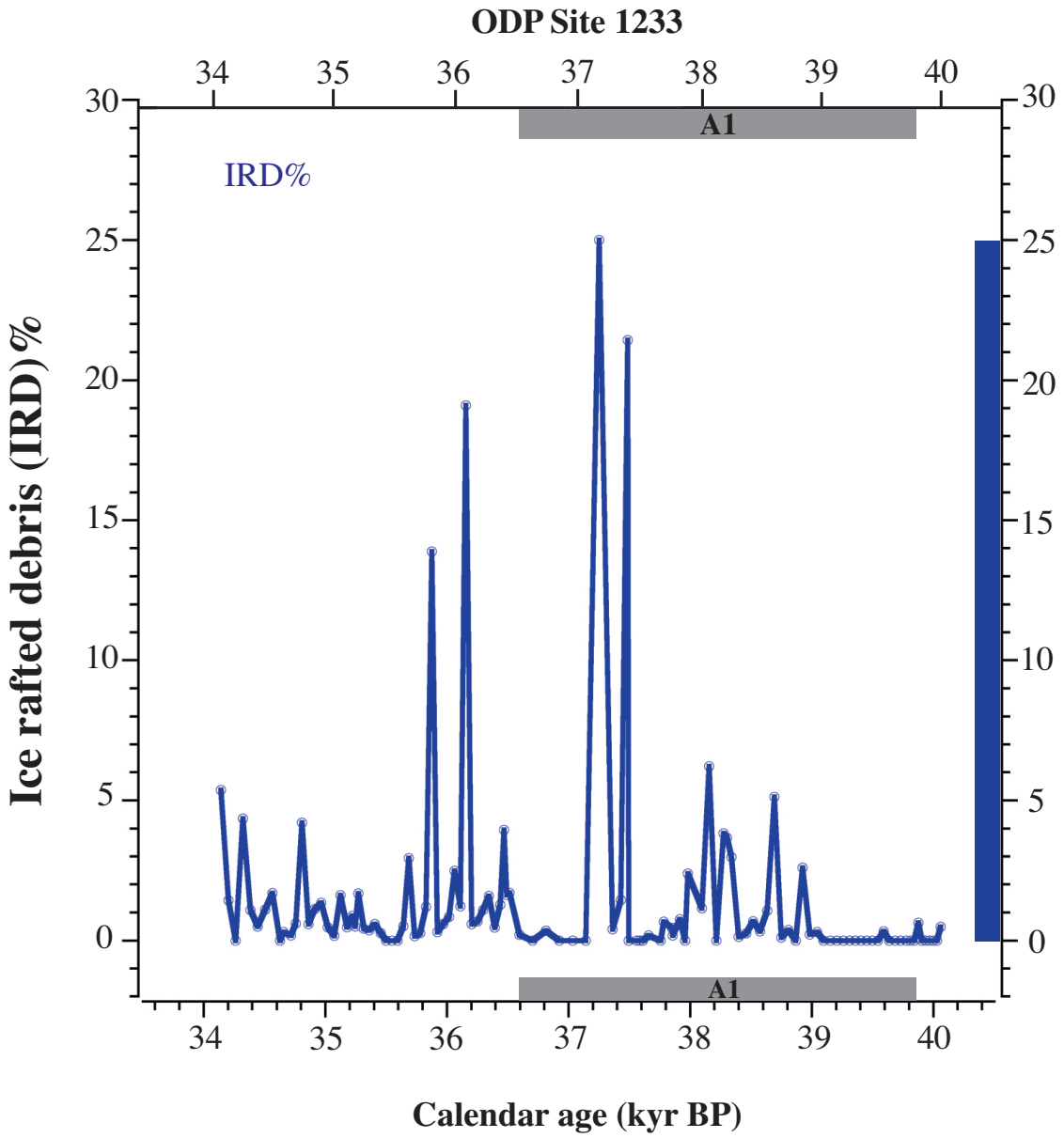

Figure 6.6 Ice rafted debris (IRD) plotted versus age (kyr BP). The blue line represents the IRD record from the northernmost margin of the marine terminating Patagonian ice sheet. The range is shown along the right y-axis. The temporal extent of the Antarctic Warming event (A1) is shown by horizontal gray bar, along the x-axes.

6.5 Combined planktic foraminiferal counts spanning A1

Figure 6.7 show the variability of the planktic foraminiferal assemblages counts spanning the study interval. The figure illustrates that the highest frequencies occur during A1. At 39,08 kyr BP both the coiling ratio and the relative abundance of *N. pachyderma* show high values, coinciding with a *N. incompta* value reaching 0% in the same time span. The *N. pachyderma* % and *N. pachyderma* coiling ratio display highest abundance during A1, however the relative abundance of *N. incompta* does not follow the same trend, exhibiting its highest abundance 153 years after the termination of A1 (36,47 kyr BP).

The curve of the relative abundance of *N. incompta* and *N. pachyderma* are both characterized by a strong decrease at 37,25, before a rapid increase at 36,46 kyr BP. This indicates the dominance of other species in the 800 years interval. The coiling ratio show a drop from 80 to 34%, illustrating a shifting dominance from *N. pachyderma* to *N. incompta* in the same time interval, potentially reflecting changes in the surface water properties. This shift in the coiling ratio coincides with the changing variability of *N. incompta,* from centennial in the older part of the record (40,1-37,2 kyr BP) to millennial in the younger parts (37,2-34,1 kyr BP).

It should be noted that the highest total number of both *N. pachyderma* and *N.incompta* occur at 36,46 kyr BP. At this time the planktic assemblages consists of 82% *N. pachyderma* and *N. incompta (*combined*),* indicating small amounts of other species. The planktic species records of *N. incompta %*, *N. pachyderma %* and *N. pachyderma* coiling ratio deviate most from each other in types of trending and peaks towards the end of the study interval.

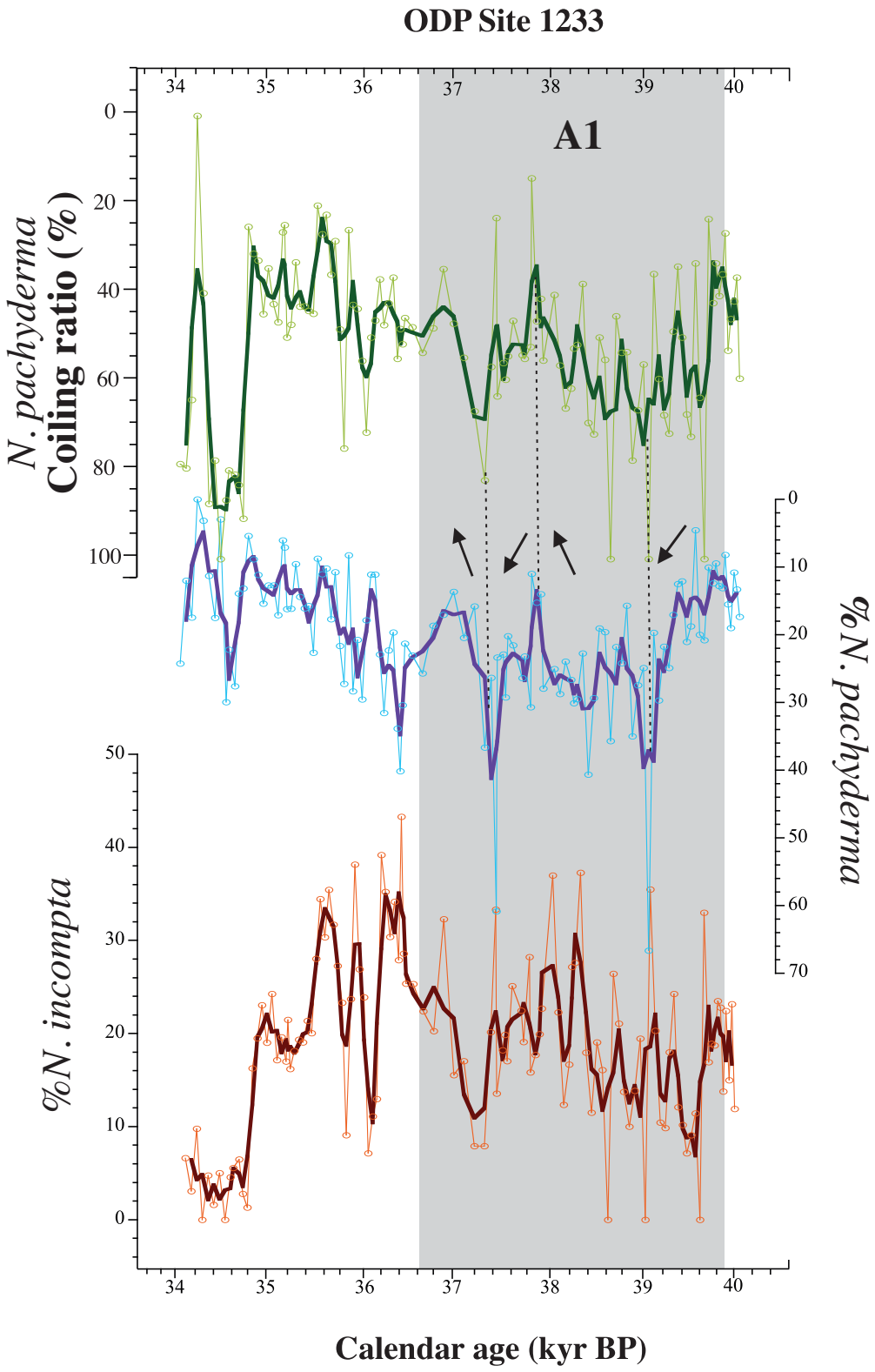

Figure 6.7 The stacked planktic foraminiferal assemblages of ODP Site 1233 plotted versus age (kyr BP). The records of N. pachyderma coiling ratio, N. pachyderma% and N. incompta% and are shown by green, blue and red lines, respectively. Coiling ratio is inverted to better illustrate warming (increasing) and cooling (decreasing). The gray bar illustrates the duration of Antarctic warming event (A1). The arrows and stippled lines indicate rapid fluctuations in both the relative abundance of N. pachyderma and N. pachyderma coiling ratio.

6.6 Combined planktic and lithic counts spanning A1

In figure 6.8 the relative abundance of *N. pachyderma* and *N. incompta,* the *N. pachyderma* coiling ratio and the %IRD are plotted versus age. The first IRD peak coincides with a peak in *N. pachyderma* and an abrupt decrease in the *N. incompta,* and a coiling ratio signal pointing towards a dominance of *N. pachyderma*. The second, high peak of IRD coincides with both a small peak in *N. pachyderma* and the highest value of the *N. incompta* % record.

In summary there is evidence for an overall increase-decrease trend in the cold-water species *N. pacyderma*, with maximum abundance during A1. The warm species *N. incompta* exhibit two general cycles of increase-decrease trends, with the maximum abundance occurring at the peak of the second cycle. The IRD-record display a general low-amplitude trend, with two prominent peaks occurring towards the end and straight after A1, indicating rapid calving events from the North-Western PIS. These records demonstrate large variation in the hydrographic state of the sub surface water mass over centennial timescales.

The foraminifera abundance and IRD records presented here have the potential to give insight into the oceanic and atmospheric setting of ODP Site 1233. To further contextualize the origin and scale of these paleo-hydrographic changes, these records will be compared to oxygen isotope records, Alkenone derived SSTs and XRF-data. The subsequent chapter contains a full discussion of the significance of the newly derived foraminifera assemblages and IRD counts.

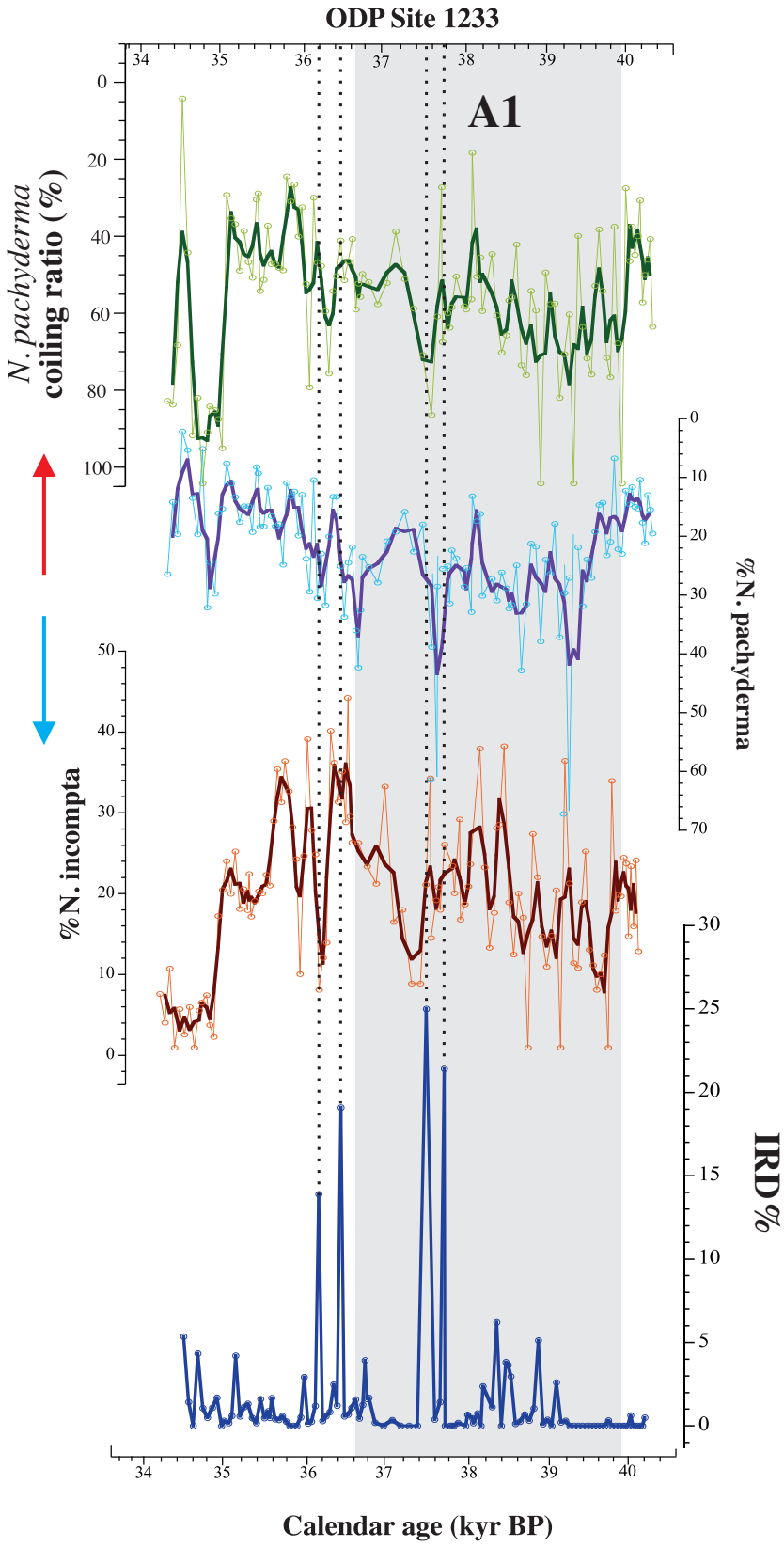

Figure 6.8 shows all the proxy records derived in this study plotted versus age (kyr BP);The relative abundance of N. pachyderma and N. incompta, together with the N. pachyderma coiling ratio and relative abundance of IRD at ODP1233. Note the inverted axis on N. pachyderma coiling ratio and %N. pachyderma. Red and blue arrows along the y-axes indicates increasing (decreasing) N. pachyderma coiling ratios representing cooler (warmer) temperatures. This is also indicated by red and blue arrows along the left y-axis. The grey bar illustrates the temporal extent of Antarctic Warm event (A1). Stippled lines follow the IRD peaks.

7. DISCUSSION

This multiproxy pilot study, producing the first IRD counts and foraminiferal assemblage's data from ODP Site 1233, offers an excellent opportunity of viewing both the atmospheric and the oceanic forcing and their connection at the study site Antarctic warming event 1 (A1). Interpretation of the results presented in chapter 6, reveals that upwelling cells along the coast shifted southward during A1 and influenced the foraminiferal assemblage composition at ODP Site 1233. This shift is tied to latitudinal migration of the SWW-belt, which is dynamically tied to the STF and the ITCZ. This frontal shift would also influence the Patagonian Ice Sheet. Our new IRD counts, unraveling the dynamics of the Northwestern PIS, will also be discussed through comparing with other marine and land-based studies reconstructing the variability of the PIS.

In the following subchapters, the variations in the relative abundance of *N. incompta* and *N. pachyderma* will be discussed in comparison to modern day assemblages at the study site, along with other marine and land-based records spanning the study interval. Conclusively the results will be reviewed in context of regional records in the SH and assessed in relation to the bipolar seesaw and the atmospheric teleconnection.

7.1 Paleoproductivity along the Chilean coast

The planktic foraminiferal assemblages along the coast of the Chilean margin, including at the study site, are affected by several factors stimulating and controlling the primary productivity, which is controlled by the unique terrestrial, atmospheric and oceanic setting (Marchant et al., 1998, Hebbeln et al., 2000). The eastward flowing ACC impinges the South American continents and brings macro-nutrients to the site. The heavy run-off from the continent supplies the ocean with iron and meltwater, facilitating a productive and relatively fresh surface ocean along the southern margin. The upwelling, which takes place north of the study site today, brings nutrients and cold water to the surface. However, the major controlling factors on the foraminiferal faunal assemblages are temperature, nutrients and salinity (Mohtadi et al., 2005, Morey et al., 2005). Through this knowledge, along with the depth habitat and water mass preferences of the different foraminiferal species, our newly derived records can be used to

interpret water mass variability tied to the study site. However, the *N. pachyderma* abundance should be interpreted cautiously as the species have shown to be able to adjust to a variety of salinities and to tolerate a large range of temperatures by migrating down in the water column (Wu and Hillaire-Marcel, 1994, Darling et al., 2017).

When interpreting the past changes in foraminiferal assemblages as frontal movements, several assumptions are involved. Firstly, we assume that the foraminiferal behavior towards changes in water mass properties has stayed constant through time. Evidence from the cryptic genetic traits of planktonic foraminifera species such as *N. pachyderma* (Darling et al., 2004) and variation in the foraminiferal ecological preference (Schmidt et al., 2003) indicate that modern foraminiferal assemblages are well suited for reconstructing past environments spanning at least the last glacial cycle. Secondly, it is still debated how wind translates into ocean circulation changes and further altering the biological productivity (Watson and Naveira Garabato, 2006). This implies that the interpretations of frontal movements in the subsequent discussion are based on general assumptions. Thirdly, our interpretations of frontal movements are derived from a single core. Although, the study site is located along the fringes of the subtropical front, which is an ideal place for monitoring frontal movements, the inferred temperature shifts are only tied to relative movements causing changes in the ocean-atmosphere dynamics, which alters the properties of the surface ocean on short time scales. To get an even better constrain on the subtropical front, a transect of cores in a N-S direction should be investigated (Kucera et al., 2005b, Kohfeld et al., 2013)

7.2 Comparison to modern faunal assemblages in the SE Pacific Ocean

To get a better scope on the faunal assemblages records we will start with a comparison to the modern-day assemblages, derived from core top samples in close proximity to ODP Site 1233. Note that with a full assemblage count, a transfer function could be applied to derive SST. In this study, only *N. pachyderma* and *N. incompta* were identified and counted limiting these possibilities, although SST through *N. pachyderma* counts is achievable, it is not derived in this study.

7.2.1 *Neogloboquadrina incompta*

The modern day Peru-Chile current holds a temperature and climatic setting which favors the dominance of *N. incompta* (Marchant et al., 1998). *N. incompta* thrives along coastal Chile due to warmer temperatures, with spring-summer seasonal SST of 14-16ºC, which corresponds to the optimum temperature range of *N. incompta* (Kucera, 2007) (4.5 in methods).

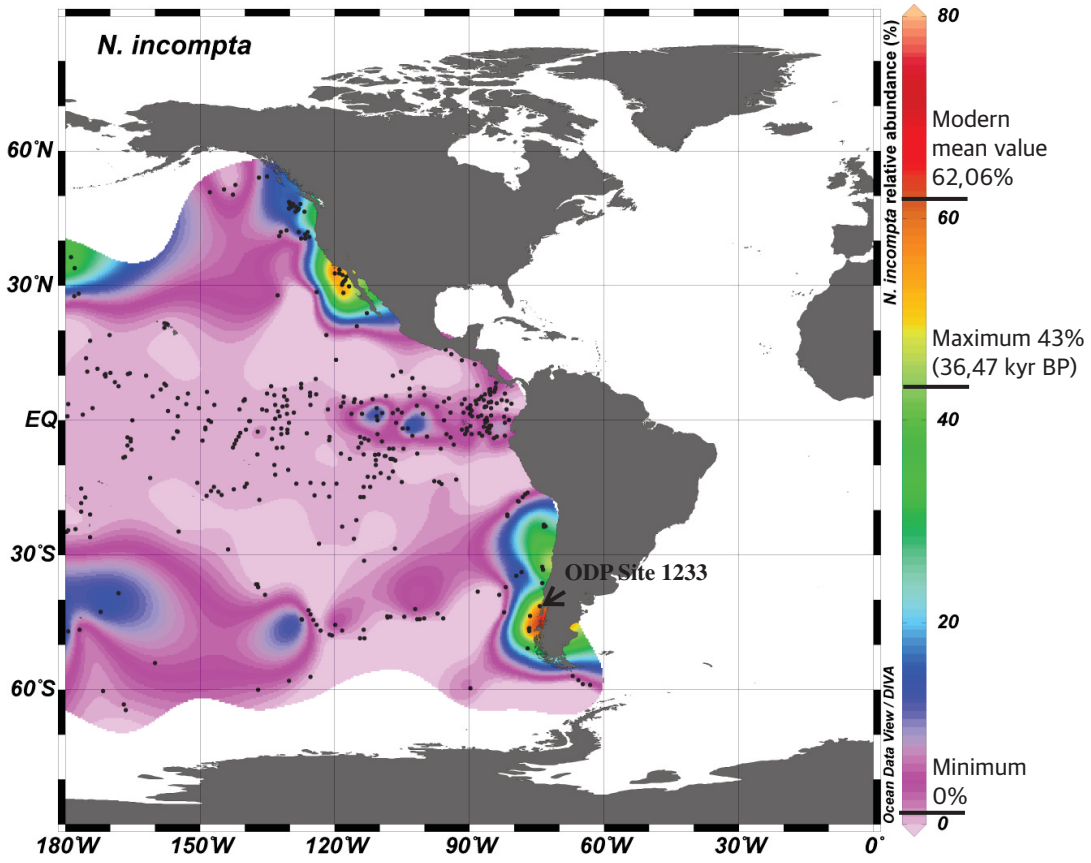

Figure 7.1 Distribution of N. incompta in the East Pacific retrieved from the MARGO project modern planktonic foraminifera-database for the Pacific Ocean (Kucera et al., 2005a) and plotted using Ocean Data View (version 4.6.2 2011). The scale on the right side indicates % abundance, with red being the highest and pink the lowest abundance. Location of ODP Site 1233 is marked with an arrow. The maximum and minimum abundance of ODP Site 1233 and modern-day relative abundance are marked on the scale. Notice that the modern-day highest abundance is located in close proximity to ODP Site 1233.

However, the most decisive factor controlling the abundance today is the high amount of land derived nutrients, which is controlled by the high precipitation rate of the region facilitating high fluvial discharge to the coast (Mohtadi et al., 2005). This is also evident from figure 7.1, which illustrates a decreasing amount of *N. incompta* offshore. A core-top (core RR9702A-

24MC-1 at 41,297º S 74,320º W) located near the location of ODP Site 1233 shows a relative *N. incompta* abundance of 62%, which is among the highest abundances along the coastal Chile (Marchant et al., 2004) (Figure 7.1). A similar abundance is confirmed by Mohtadi et al. (2005) who found a *N. incompta* abundance of 64,2% in a core-top sample slightly further north-east (41,12º S 74,25ºW) of ODP Site 1233. The *N. incompta* % record of ODP Site 1233, spanning 40-34 kyr BP, produced in this study show a substantial colder setting, compared to the modern-day conditions (Figure 7.3). The lower percentages of *N. incompta* abundance clearly demonstrate a general influence of water-masses containing different physical and/or chemical properties dominating the core site during the study interval when compared to modern day conditions. This means a less suitable environment for *N. incompta*. The abundance over A1 varies from 0 to 43% and the large variability within the record shows the sensitivity of *N. incompta* to a rapid shifting climate and hence, water mass properties. This demonstrates the importance of studying the climate variability in this region.

7.2.2 *Neogloboquadrina pachyderma*

The modern-day relative abundance of *N. pachyderma* increases north of 39ºS, due to increased upwelling (Mohtadi et al., 2005). Although the SSTs increase northwards along the coast, *N. pachyderma* thrives due to upwelled cold nutrient rich waters from the deep, which stimulates primary productivity. In the South Pacific the *N. pachyderma* abundance is strongly associated with the temperature change that are within the frontal system of the ACC (figure 7.2 and figure 2.8). The relative abundance of *N. pachyderma* near the location of ODP Site 1233 (Core RR9702A-24MC-1 at 41,297º S 74,320º W) is 6,8%. This is due to an annual mean summer SST of up to 16ºC, which is higher than the optimum temperature range for *N. pachyderma (*figure 4.5*)*. The ODP Site 1233 *N. pachyderma* record exhibit a maximum relative abundance of 68% (figure 4.5). This, if interpreted as temperature, would suggest a dramatic cooling at the study site, compared to today. Similar relative abundances of *N. pachyderma* are today found associated with the sub Antarctic front, around 55ºS, where the optimum temperature range (-1 to 9ºC) for *N.pachyderma* is obtained (Kucera, 2007).

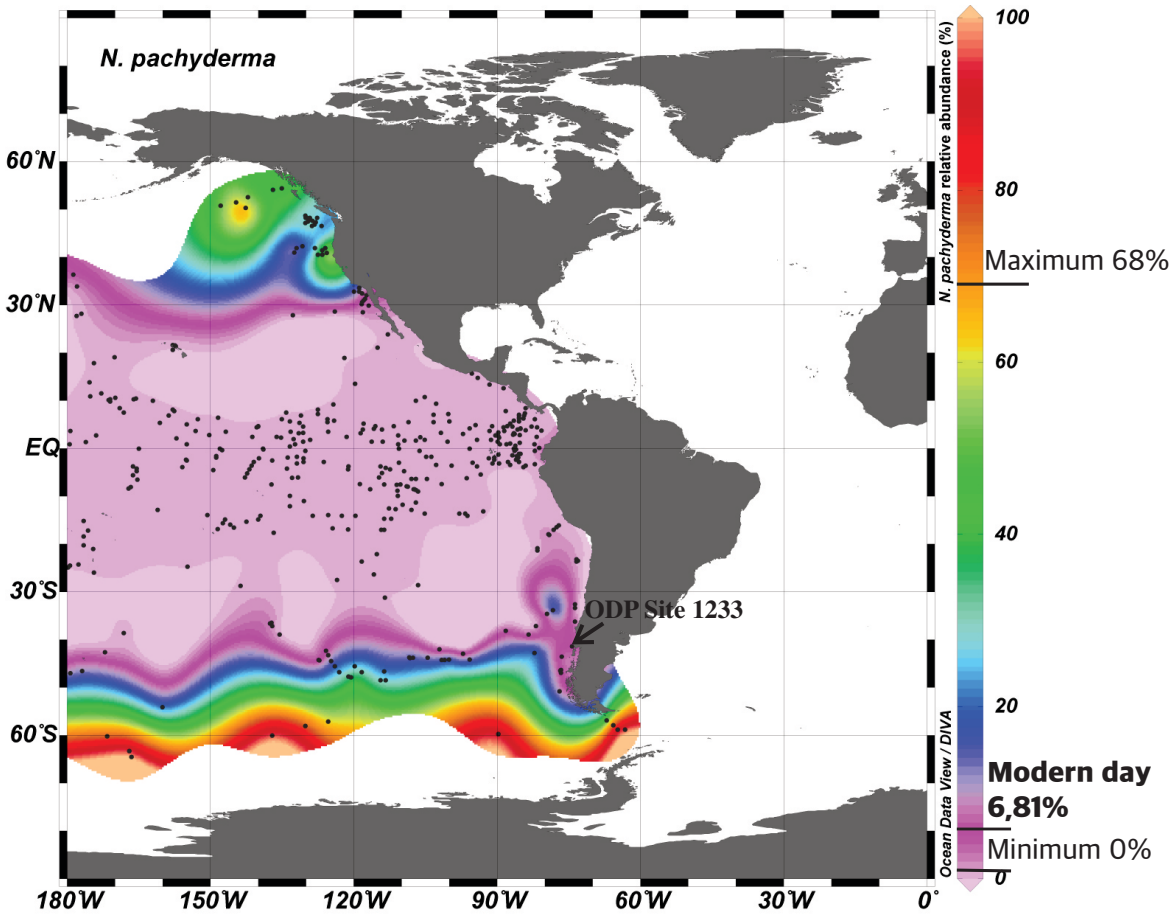

Figure 7.2 Distribution of N. pachyderma% in the East Pacific retrieved from the MARGO project modern planktonic foraminifera-database for the Pacific Ocean (Kucera et al., 2005a) and plotted using Ocean Data View (version 4.6.2 2011). Location of ODP Site 1233 is marked with an arrow. Notice the scale to the right, where red indicate high and pink indicate low abundance of N. pachyderma. The maximum and minimum abundance of ODP Site 1233 and modern-day relative abundance are marked on the scale.

7.3 Cooling of the Peru-Chile Current

What could cause the general cooling observed in both the *N. pachyderma* % and *N. incompta* % records? Especially the *N. pachyderma* % increase indicates strong cooling in the region, but also the decrease in the *N. incompta* % indicates cooling to below their optimum temperature range of 8ºC. Since the most dominant water mass along the coast of Chile are the PCC, cooling in this water mass could alter the faunal assemblages. The overall general cooling of the PCC during the last glacial cycle is associated with an enhanced formation rate of the AAIW, which is initiated by equatorward frontal shifts (Liu et al., 2002, Muratli et al., 2010, Bostock et al.,

2013), together with cooling through upwelling along coastal Chile. The current is further cooled by chilled continental air masses, along with katabatic winds from the Patagonian ice sheet. This strong eastern boundary current is contributing to cool the tropics, together with the upwelled intermediate water masses, through the oceanic tunnel (Mix et al., 1999, Sarmiento et al., 2004, Liu and Alexander, 2007). Mix et al. (1999) investigated the foraminiferal assemblages along the PCC current and reconstructed temperatures using transfer functions. They found a 5-6ºC drop in SST, along with a deviation in the assemblages tied to low salinity layers during LGM. Soltvedt (2014) reports of a covariation in the foraminifera derived $\delta^{18}O$-signal at both intermediate and near surface depths, suggesting a rapid transmission of properties through the water column at Site 1233. This indicates that temperature, driving the variation in the planktic foraminiferal assemblage, is controlled by changes at higher latitudes.

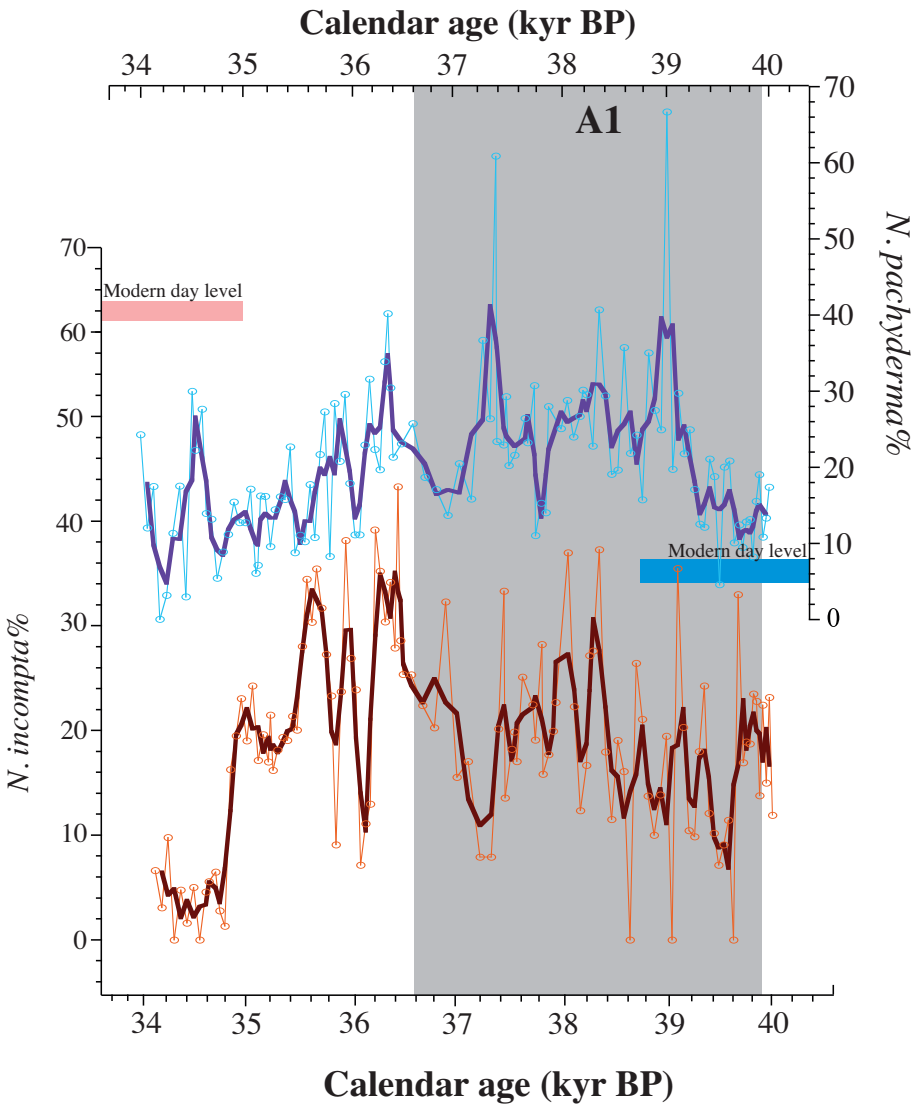

Figure 7.3 show the record of N. Pachyderma % and N. incompta %, plotted versus age (kyr BP). Blue and pink vertical bar represents the modern-day level for N. pachyderma % and N. incompta %, respectively. Grey shading represents the Antarctic warm interval (A1).

However, the trend observed in the planktic assemblages is suggesting something else than just «glacial temperature change» (i.e. Milankovitch forcing) as a driver for the signals. The main dynamic process that changes the sub surface temperature at ODP Site 1233 is related to shifts in the subtropical front, which varies in sync with the cooling and warming of Antarctica (Lamy et al., 2004). The frontal system of the ACC has a strong temperature gradient, creating large changes in the water mass properties at the site, and hence the foraminiferal assemblages, due to minor frontal movements (Locarnini et al., 2013). Towards the peak of A1 (39,9 to 36,6 kyr BP) the subtropical front gradually migrated poleward, facilitating a warming in the surface water masses, as seen in the *N. incompta* $\delta^{18}O$ signal (figure 7.3). This warming is accompanied in our records by an increase in the *N. incompta* % and *N. pachyderma* % towards the peak of A1 (Figure 7.3).

Superimposed on the general trend in the foraminifer assemblages is a high centennial scale variability, which suggests another mechanism altering the environment for *N. incompta* and *N. pachyderma* and possibly their depth habitat. In figure 7.4, the Alkenone derived SST reconstructions are plotted versus the *N. pachyderma* % and the *N.incompta* $\delta^{18}O$ signal. From 37 to 40 kyr BP, the Alkenones and foraminifera assemblages exhibit similar variability, but at 36 kyr BP, the Alkenones peak at temperatures of 12ºC, which are close to the optimum temperature range for *N. pachyderma*. Yet, the N. *pachyderma* % abundance does not increase, but instead exhibit high variability superimposed on a trend towards lower %. This points to something other than temperature, which appears near optimal, as a mechanism or driver influencing the abundance of *N. pachyderma*. We interpret this to be; either caused by increased upwelling as or meltwater discharge from the marine terminating Patagonian ice sheet. These interpretations will be discussed in the following subchapters. Note that the following subchapter contains comparisons to the high-resolution *N. incompta* $\delta^{18}O$ signal produced by Soltvedt (2014), which interpreted the oxygen isotope variability as mainly temperature driven. We support this hypothesis when interpreting the faunal assemblages with relation to the $\delta^{18}O$ signal but will also elaborate on possible other changes that our data can indicate.

7.4 *N. pachyderma* % as an upwelling indicator

Because indirect proxies, such as those based on foraminifera, by definition do not provide exact information about past environmental conditions the following section contains interpretations which will be based on multiple and partially independent lines of information such as isotope data, alkenones, glacier responses, and inferences of how foraminifera would react to these variables based on modern day evidence.

The polar species *N. pachyderma* generally inhabits cold, nutritious water, and constitutes the mono assemblage at high latitudes both in the NH and SH. However, the presence of *N. pachyderma* in a faunal assemblages is also used as an upwelling indicator along the coast of Chile (Mohtadi and Hebbeln, 2004, Mohtadi et al., 2005) in both present day, and during glacial periods. Consequently, the dominance of *N. pachyderma* would point toward either upwelling or polar conditions at the study site. One way to differentiate between these two mechanisms for increasing *N. pachyderma* % at Site 1233 is with independent lines of evidence for either polar or subpolar (upwelling conditions) temperatures. The highest relative abundance occurs during A1, despite that the Alkenone derived SST increases rapidly over the same time interval and exceed the temperature levels optimal for *N. pachyderma* (-1 to 9ºC) (Figure 7.4). This suggests local water mass conditions that are more consistent with general warmth but seasonally upwelling and production of *N. pachyderma,* even though the mean or peak temperatures at the core site might be sub optimal. It should also be noted that other upwelling indicators such as *T. quinqueloba* and *G. bulloides* were also present in many samples throughout the study interval.

Consequently, despite the high Alkenone SSTs, the high % of *N. pachyderma* and the proximity of Site 1233 to the modern major upwelling regions (figure 2.11), could explain that the variability of the signal can be caused by various amount of upwelling drawing cool, nutrient rich water towards the surface This suggest that the relative abundance of *N. pachyderma* at Site 1233 is not controlled only by (peak seasonal) temperature, but mostly by the accessibility of nutrients. For the 40-34 kyr BP time period, the source water for the upwelled water was probably the poleward flowing, nutrient rich Gunther undercurrent, as upwelled water usually originates from 200-300 meters water depth (Neshyba, 1979). Detailed oxygen isotope analyses

and trace metal measurement based on *N. pachyderma* shells could be applied to further evaluate this theory because each ocean current has their specific source region and consequently their unique physical and chemical properties.

That the opposing signals of both warming in the subsurface from the *N.incompta* $\delta^{18}O$ and an increase of the relative abundance *of N. pachyderma* are inherent in one core site, points to a possible differentiation in the depth habitat for *N. incompta* and *N. pachyderma*. Several studies

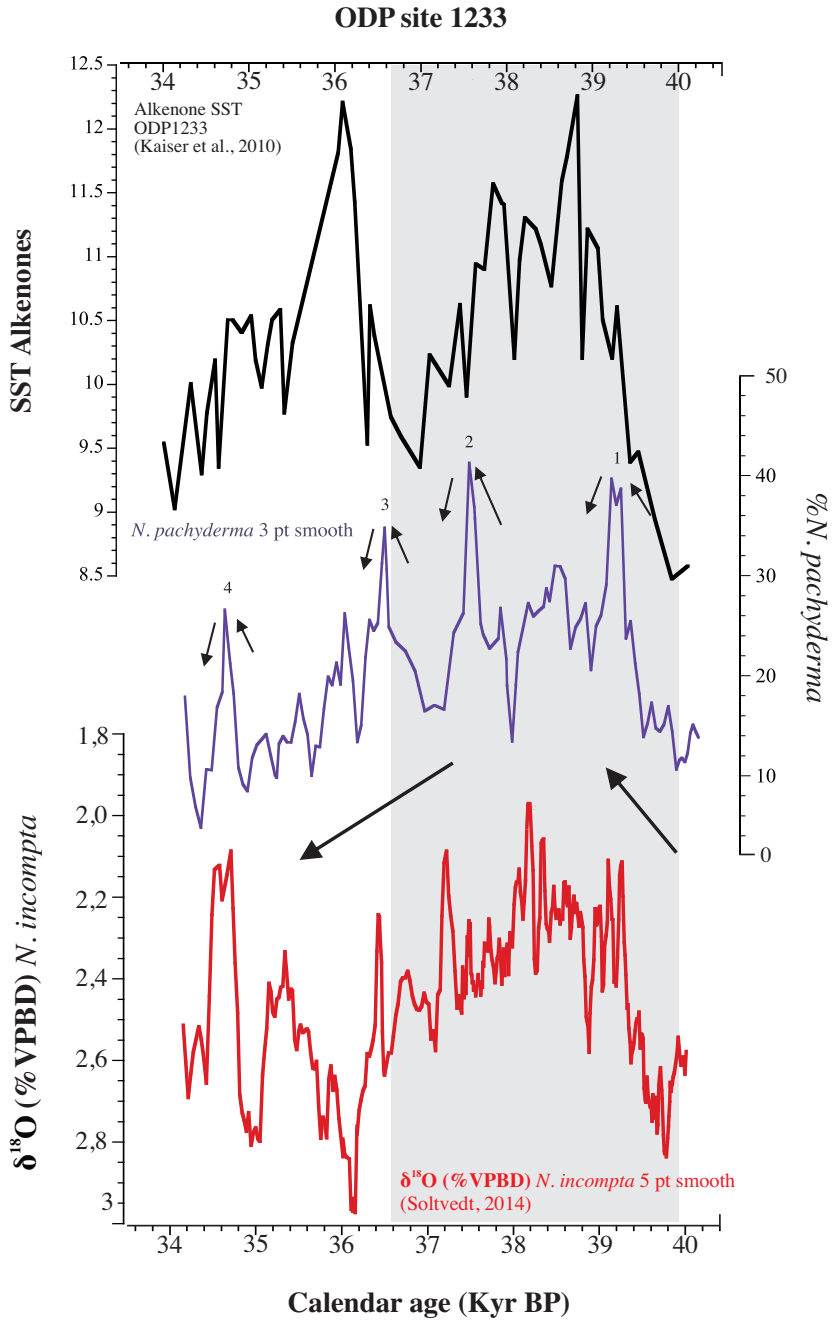

Figure 7.4 Oxygen isotopes from Soltvedt (2014) compared to relative abundance of N. pachyderma (%) and alkenone derived SST (°C) data from Kaiser and Lamy (2010). Note that the axis on the N. pachyderma and Incompta $\delta^{18}O$ are reversed to mirror relative temperature alterations. Shading represents the temporal marks the A1.

have shown that *N. incompta* inhabit the upper parts of the water column, above the pycnocline, while *N. pachyderma,* especially in upwelling zones, dwells deeper(Darling et al., 2017). Upwelling creates a more uniform water column that will enable the *N. pachyderma* to inhabit deeper parts of the water column (Ortiz et al., 1995, Ivanova et al., 1999), facilitating a clear distinction between the environments affecting these two species. However, upwelling usually leads to a (seasonally) well-mixed upper water column, and consequently the *N. incompta* signal could also be affected by the upwelling if it calcified its test during the upwelling season. Mohtadi et al. (2005) reports that nutrients are the most important variable when it comes to foraminiferal assemblages along the coast of Chile. This was probably also the major variable during 40-34 kyr BP, as inferred from the *N. pachyderma* abundance at ODP Site 1233 – explaining the high abundance and variability of the polar species within a warm period (A1).

The modern-day core of the SWW impinges the South American continent between 38-42ºS. The northward deflected coastal wind creates Ekman pumping in the region and consequently water is drawn up towards the surface. With a more poleward located SWW core, the coastal wind would originate further south on the continent and facilitate upwelling further south along the coast (figure 7.5). However, these evidences point towards an even further poleward displaced SWW as compared to today, (a warm interglacial), and thus adds new insight to the variability of the SWW during interstadials. Our data support a more southward located SWW during peak A1, which is observed in multiple recent studies and supports the bipolar seesawhypothesis involving both the atmosphere and ocean changes (Markle et al., 2017, Buizert et al., 2018)

Episodic upwelling driven increases in *N. pachyderma* are observed in other Southern Hemisphere upwelling/margin locations during the last glaciation. Along the Benguela boundary current in West Africa, similar relative abundances, trends and variability of *N. pachyderma* is observed during late MIS 3 and interpreted as increased upwelling (Little et al., 1997a). This study is conducted at lower resolution sites than Site 1233, but exhibit similar trends: The planktic foraminiferal assemblages from core along the continental slope of Namibia (19-23ºS) show peaks of up to 70% *N. pachyderma* during intervals of maximum upwelling. The upwelling variability in this region is ultimately tied to variations in the Angola-Benguela front and the trade winds. The link between increased upwelling and increased *N.*

pachyderma spans two glacial cycles, and is thus a robust feature in a boundary current associated with shifting winds (Little et al., 1997a, Little et al., 1997b, Volbers et al., 2003). Since these two EBC settings; along the west coast of Namibia and Chile are fairly similar, this supports our theory that the *% N. pachyderma* increase, observed over A1 at Site 1233 is caused by upwelling.

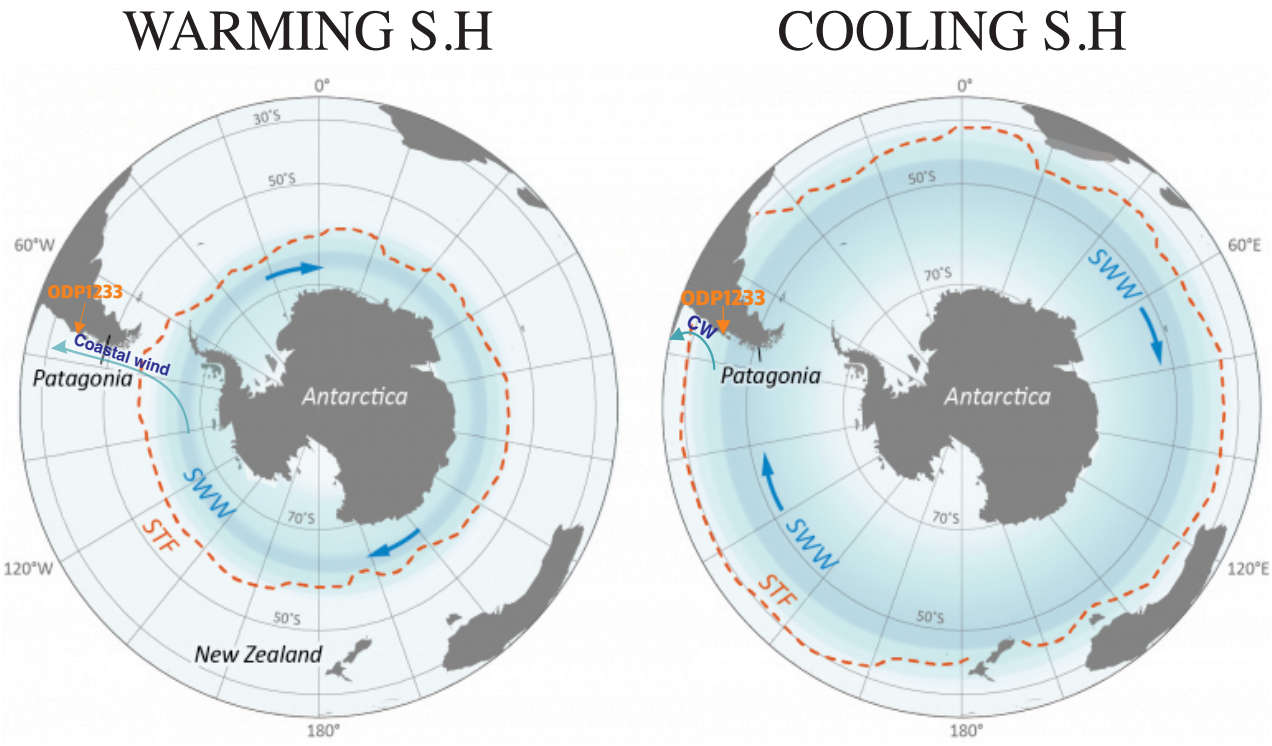

Figure 7.5 display the S.H with its landmasses and subtropical front (STF) from 30ºS and southwards. Contraction of the Subtropical front and the SWW belt, creates warming in the extra tropics. More tropical water can influence the region. In addition, the SWW will carry less precipitation to Patagonia, reducing the ice sheets. In a warming SH the coastal wind (CW) will be initiated further south on the continent and facilitate increased upwelling further south along the coast. Cooling of the SH leads to expansion of the STF and the SWW, which facilitates a more polar signal to the core site. SWW impinges the south American continent and increased precipitation will lead to expanded ice sheet. Modified after Bendle (2018).

Previous studies based on ODP Site 1233 material assumed that upwelling never reached the core site but were positioned further north. Consequently, the reservoir age has been attributed to the global mean of 400 yrs. The results from this study could therefore potentially have some implications for the corrected ^{14}C-dates used as a basis for the age model. However, since the *N. incompta* δ^{18}O signal at Site 1233 has a near one-to-one coupling with the Site 1233 AAIW δ^{18}O signal and the EDML record from Antarctica, there is no evidence that the upwelled water

from 200-300 meters depth was particularly "old" perhaps indicating it originated from a shallow/intermediate source.

7.5 Unravelling the *N. incompta* % variability

Based on both the oxygen isotope signal and the relative assemblage of *N. incompta*, both of which indicate a general warmth (generally low isotope values and high to increasing *N. incompta* %) during A1, it is reasonable to assume that the relative abundance of *N. incompta* is also highly affected by temperature change due to frontal movements. However, there is strong high frequency variability during A1 in both proxy sequences, but most strongly evident in the *N. incompta* % record. This centennial variability could have originated from a number of sources, which until now have never been assessed.

The most likely cause for the observed high frequency, centennial scale variability in both *N. incompta* $\delta^{18}O$ and *N. incompta* % is alternating freshwater discharge from the PIS into the Southeast Pacific. Massive melting of the PIS might have occurred over A1 due to rapid warming, as observed during the deglacial (Kaiser et al., 2007). As *N. incompta* is a species, which does not thrive in water masses with low salinities, the low abundances of *N. incompta* could be interpreted as increased meltwater discharge. Increased meltwater from the PIS would also carry large amounts of sediments into the fjord and coastal regions, thus there is also a possibility that the upper water column occasionally became uninhabitable for *N. incompta* because of high sediment flux creating too high density of particles in the water column for the foraminifera to survive (Kucera, 2007). On the other hand, increased nutrient levels from upwelling and sustainable temperatures (>8ºC) could create a nourishing water column for *N. incompta* despite the meltwater discharge. Hence, the high frequency variability could be a response to alternating temperatures and nutrient supply. The highest abundance of *N. incompta* occurs right after the A1 interval (36,47 kyr BP). This could be a response to decreased meltwater discharge, and possibly better living conditions for the species, facilitated by higher nutrients, despite the lower temperatures (figure 7.6).

G. bulloides dwells shallow in the water column and are consequently a good recorder of changes in meltwater supply at ODP Site 1233. Euler (2010) disentangled the temperature and salinity-change by using Mg/Ca on the $\delta^{18}O$-signal from *G. bulloides* over A2. Her results showed that ~50% of the $\delta^{18}O$-signal came from temperature change, while the rest came from changes in decreased salinity most likely from meltwater discharge. The same distinction has not been done with the signal from *G. bulloides* (4 cm sampling) derived by Førde (2008) over A1, however clues can be found when compared to the relative abundance of the unsmoothed record of *N. incompta (*figure 7.6). The two records hold similar variability during A1 (figure 7.6.), and consequently are a combination of temperature and freshwater supply a plausible explanation for the large amplitudes displayed in the *N. incompta* record.

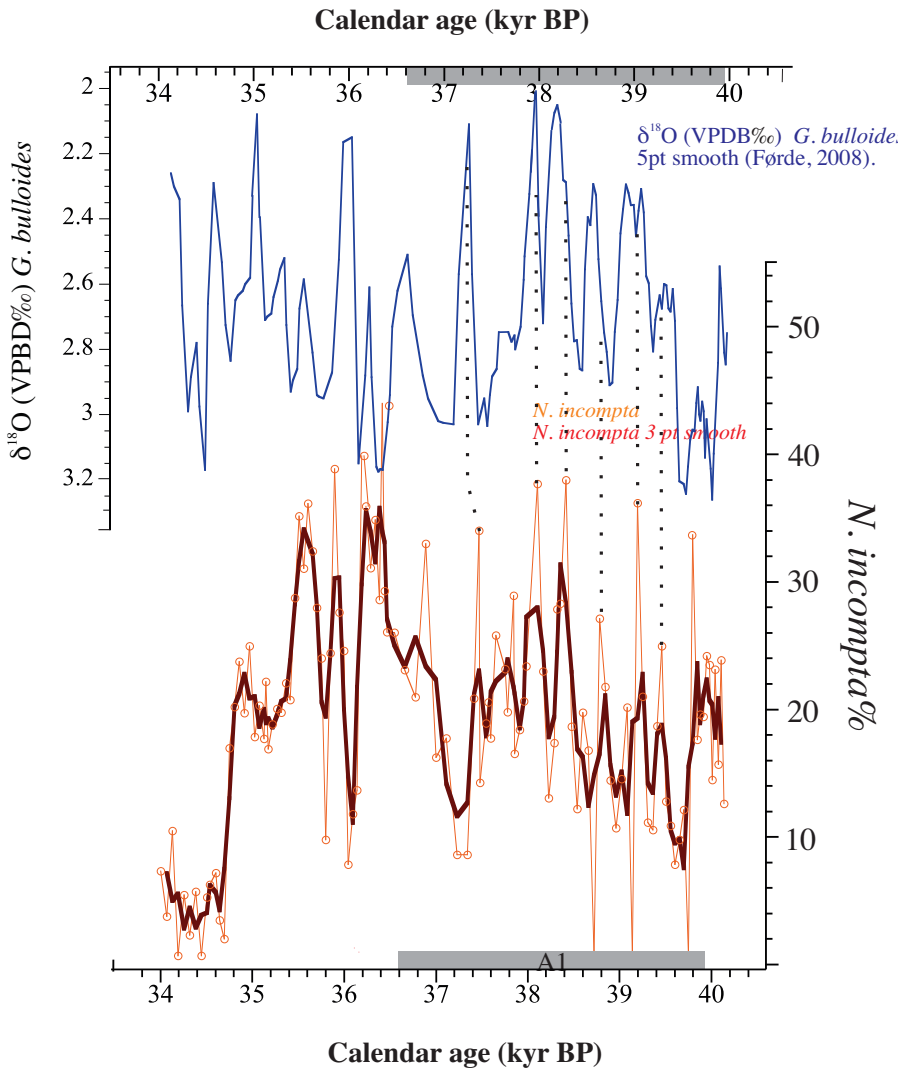

Figure 7.6 show G. Bulloides $\delta^{18}O$ (Førde, 2008) and N. incompta% for ODP Site 1233, plotted versus age (kyr BP). Stippled line indicates possible correlating variability. Grey bar along the x-axes displays the temporal extent of Antarctic Warming event (A1).

However, it is also important to note that in modern day upwelling regions the abundance of *N.incompta* are scarce, indicating that *N. incompta* diverge away from intense upwelling (Darling et al., 2017). From 39,70 to 38,68 kyr BP *N. incompta* % reaches 0 three times. In summary, this points towards either upwelling or meltwater being the dominant factor limiting the abundance of *N. incompta*. Further faunal assemblages' studies depicting changes at multiple water depths and latitudes along the Chilean coast are needed to evaluate the possibilities of either meltwater or upwelling as the dominant cause limiting the *N. incompta* %.

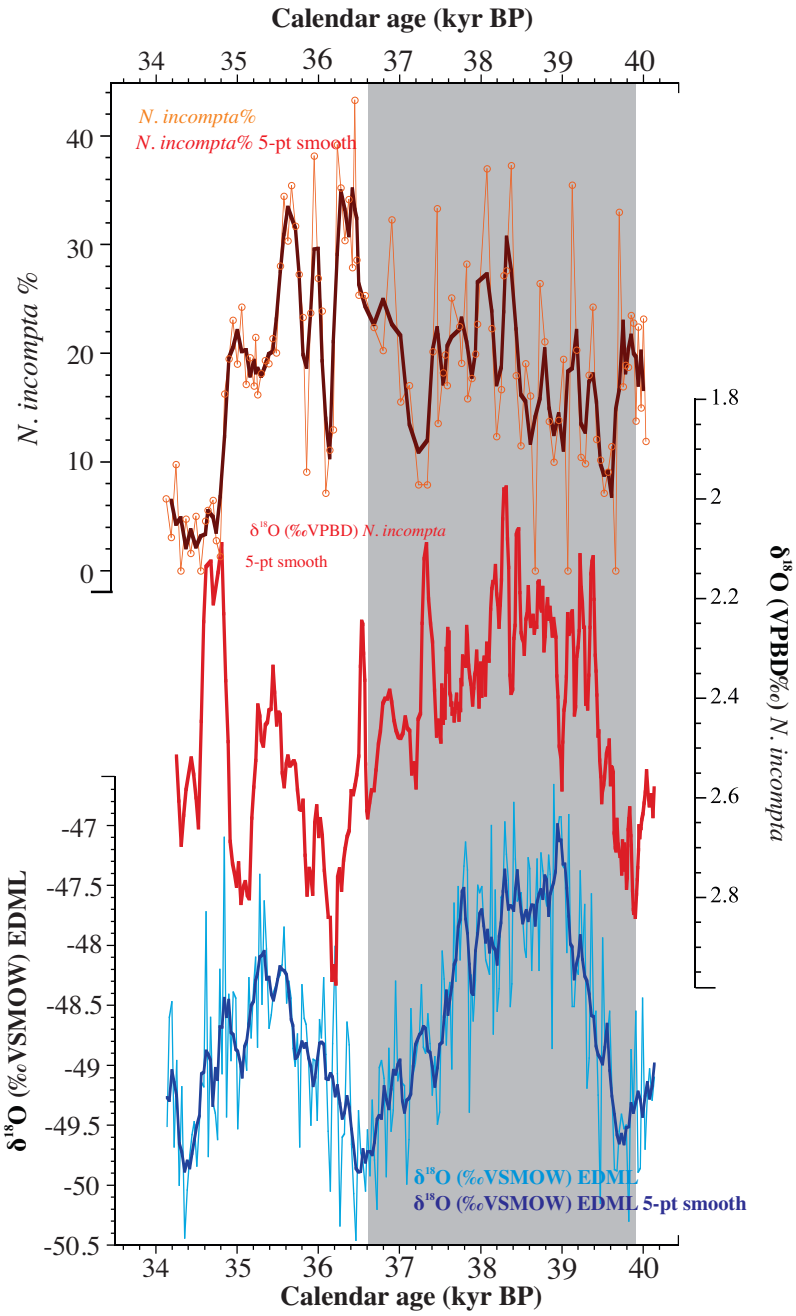

Figure 7.7 shows the stacked record of $\delta^{18}O$ from the EDML ice core (EPICA community members, 2006), N. incompta $\delta^{18}O$ (Soltvedt, 2014) and N. incompta% (this study) of ODP Site 1233, plotted versus age (kyr BP). The Antarctic warm event (A1) is marked

7.6 Species preferences in depth habitat

The sudden changes in relative abundance of *N. incompta* and N. *pachyderma* document that fast extratropical dynamics varied during a warm interval spanning the last glacial cycle. As one of the main indicators of species variability is temperature, we interpret the combined records of increased *N. pachyderma* % and *N. incompta* % relative to the modern assemblage at the site to indicate generally colder conditions during the glaciation. But there are some differences to take note of; during A1, when the relative abundance of *N. incompta* exhibit high variability, the abundance of *N. pachyderma* peak repeatedly but does not exhibit the same high amplitudes as *N. incompta* (figure 7.3). This indicates either a different response to the same environmental change, or separate depth habitats, which ultimately make the species, record different habitat environments. As there are several indices suggesting that the two species inhabit different depths in the water column, we provide a short review of the possible depth habitats of the two species, in response to the environmental forcing's at the study site.

In general, *N. incompta* have been observed to inhabit shallower depths compared to *N. pachyderma* (Simstich et al., 2003). Several studies demonstrate that *N. pachyderma* can dwell down to 500 m.b.s.l in upwelling regimes, (Ivanova et al., 1999, Darling et al., 2017, Greco et al., 2019). However, it is not clear if *N. pachyderma* migrate down to these depths due to higher food availability or if this is the preferred depth habitat through their whole life cycle. In comparison, *N. incompta* prefer a shallower depth habitat to obtain the preferred temperature range of >8ºC. Another observation is that, *N. pachyderma* migrate deeper in the water column as a response to the increasing temperatures, to obtain temperatures closer to its optimum range (Wu and Hillaire-Marcel, 1994). However, *N. pachyderma* has also been observed to tolerate a large range of SSTs and salinities, as long as nutrients are accessible, which would make them more tolerable to changes in frontal movements and meltwater discharge. *N. incompta* favors nutrient rich waters as well, but has a narrower temperature and salinity range, when compared to *N. pachyderma* (Ortiz et al., 1995).

7.7 Observed covariance of *N. pachyerma* and *N. incompta* and its possible causes

For a millennium, from 37.49 to 36.45 kyr BP, both the *Neogloboquadrina* counterparts decrease and increase simultaneously (figure 7.8). These simultaneous shifts could be interpreted as a well-mixed water column, where nutrients reach both of the depth habitats, or that *N. pachyderma* migrate to shallower depths.

The joint decrease from 37,5 to 37,1 kyr BP coincides with one of the most prominent peaks in the $\delta^{18}O$ *N. incompta* record (figure 7.8). The low *N. incompta* $\delta^{18}O$ values could be a result of meltwater with low $\delta^{18}O$ values originating from the waning ice sheet, as a last response to the warming during A1. This could explain the less favorable conditions for the two species. However, the peak in *N. incompta* $\delta^{18}O$ could also be explained by a rapid southward migrating STF, introducing warmer waters to the study site. A southward migrating front would initiate increased upwelling and introduce more nutrients to the site and sustain increased abundance of the two species. Hence, a frontal location change might not best explain the combined decrease of the relative abundance of *N. incompta* and *N. pachyderma*. An alternative explanation, building on the frontal shift hypothesis, is that other upwelling indicator species such as *T. quinqueloba* or *G. bulloides*, had favorable habitat and thus dominated the assemblage during this time. Indeed, during this time interval we observe an increase in the «other planktic» foraminifera abundance *(*figure 7.9*)*, which could point to increased production of *T. quinqueloba* and *G. bulloides*; perhaps indicating that despite upwelling overall conditions were too warm for either of the (sub)polar *pachyderma* species and favored other species during this interval.

The following concurrent increase of *N. pachyderma* % and *N. incompta* % from 37.10 to 36.45 kyr BP (figure 7.8) at the very end of A1, coincides with higher *N. incompta* $\delta^{18}O$ values, interpreted as colder temperatures by Soltvedt (2014), which, if derived from equatorward frontal movements, would cause the core of the SWW more proximal to ODP Site 1233 and hence reflect less upwelling and consequently less nutrients to the study site. However, colder temperatures could also reflect a more uniform upper water column, where the fresh water from melting of the PIS are less prominent, creating an environment in the surface water where *N.*

incompta thrives. *N. incompta* also show the highest abundance for the whole study interval at the peak of this % increase.

Also, a more equatorward displaced frontal system, would pull the nutrient-rich ACC northwards, and possibly facilitate the observed abundance of *N. pachyderma*. The study by Mohtadi and Hebbeln (2004) from the same region, points to the ACC as the most important factor controlling the supply of phosphate and nitrate to the coast of Chile, and consequently

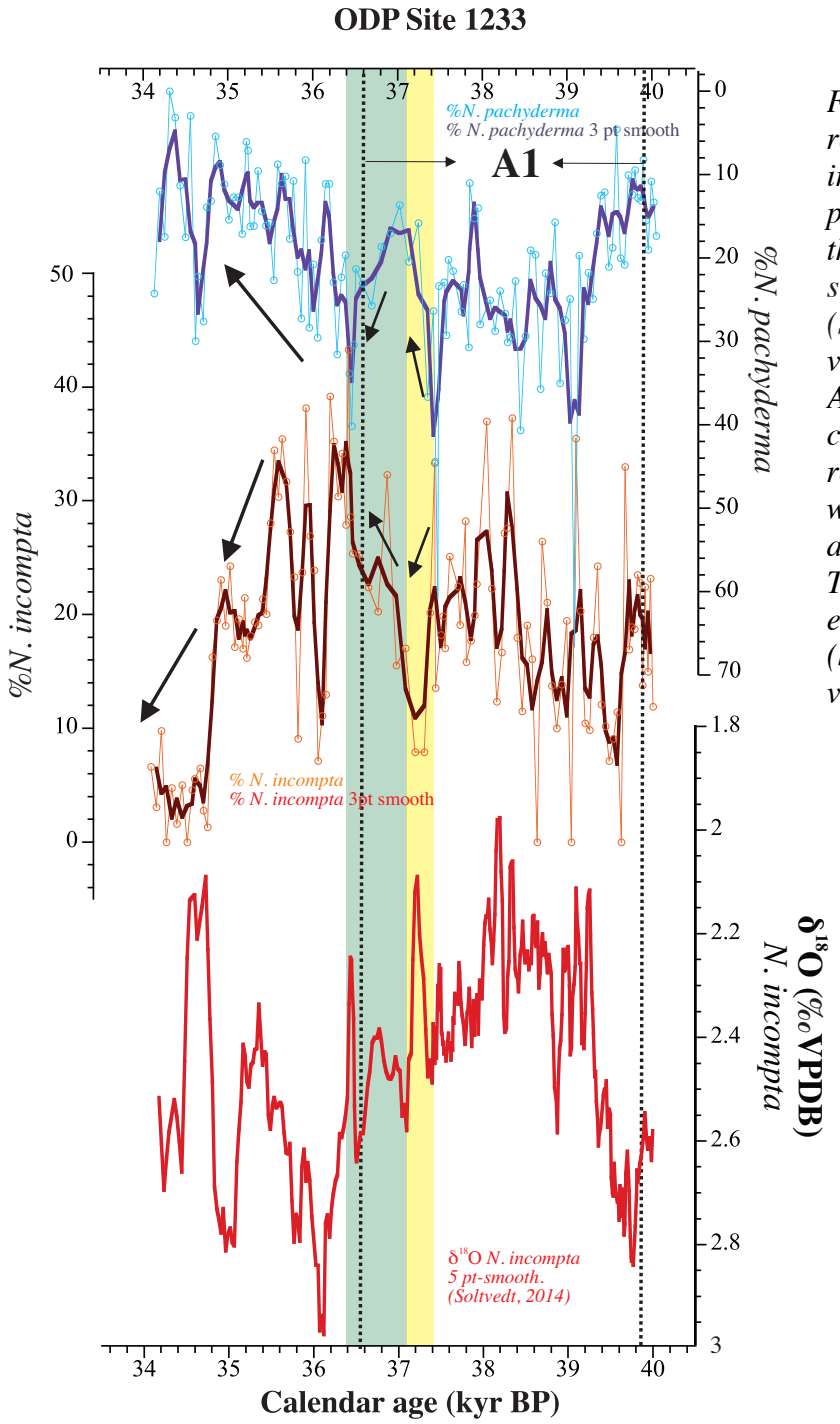

Figure 7.8 show the relative abundance of N. incompta and N. pachyderma, along with the $\delta^{18}O$ 5-pt smooth signal of N. incompta (Soltvedt, 2014) plotted versus age (kyr BP). Arrows indicate coeval changes between the relative abundance, along with yellow (decrease) and green (increase) bar. The Antarctic warming event (A1) is denoted (between the dashed vertical lines).

stimulating the primary production. However, our results show that this is not a dominating control factor, since the *N. pachyderma* % increase is synchronized with the *N. incompta* $\delta^{18}O$.

7.8 The combined record vs «other planktics»

The «other planktic» record constitutes both subpolar and subtropical planktic foraminifera and are generally interpreted as species which prefer in general warmer temperatures than *N. incompta* and *N. pachyderma*.

The «other planktic» % record is characterized with a plateau of low amounts during A1, however the variability is high. The decrease in «other planktic» % towards the low at 36.20 kyr BP (figure 7.9) represent the time interval were other sub-polar and transitional species are least present at the core site and coincides with the highest *N. incompta* $\delta^{18}O$ values, possibly reflecting a decrease in meltwater as indicated by a peak in *N. incompta* % over the same time span. A similar stepwise decrease in «other planktic» % occurs toward the peak of A1, possibly resulting from an increase in *N. pachyderma* %, due to increased upwelling.

After 36.20 kyr BP, as indicated by the «other planktic» % record, where the dominance of subpolar to subtropical species increases towards 34.24 kyr BP, both *N. pachyderma* and *N. incompta* abundance decrease gradually and at 34.24 kyr BP they are almost completely absent at ODP Site 1233. An adverse influence of colder waters, through an equatorward displaced STF that drive the upwelling regions further north, could explain the gradual decrease of *N. pachyderma%*. However, the decrease in *N. incompta* % is more difficult to explain. As «other planktics» are characterized as mostly subtropical species, this increase towards 34 kyr BP does not coincide with temperature to gradually decrease, as a result of the northward shifted STF and facilitate the recorded PIS advance at 34 kyr BP (Caniupán et al., 2011, García et al., 2018). To further utilize the information contained in the "other planktic" record, a full identification and counts of the foraminiferal assemblages is required. Given that these species represent a significant fraction of the total assemblage (often 60% or greater) they likely hold crucial information useful to further unravel the dynamics and water mass characteristics in the region.

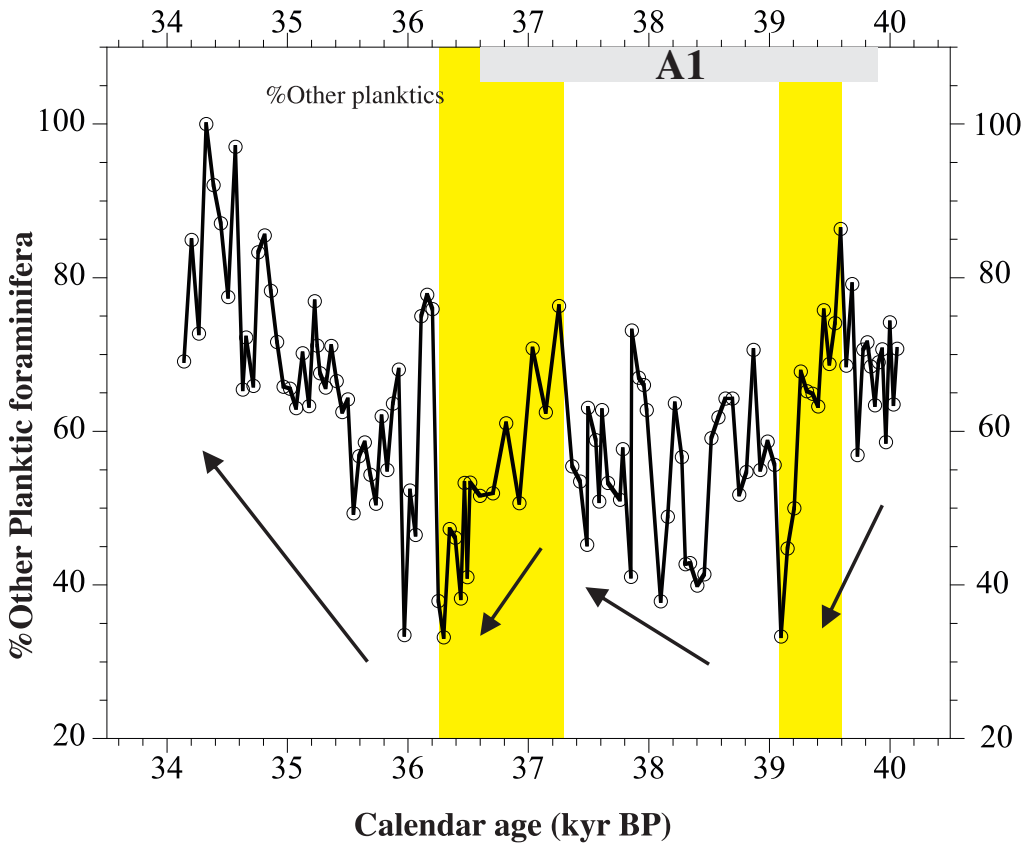

Figure 7.9 shows the relative abundance (%) of other planktic foraminifera through the study interval. The maximum abundance of other planktic foraminifera occurs at 34.30 kyr BP where all of the planktic foraminifera were characterized as "other". Other planktic foraminifera % includes all foraminifers, excluding N. pachyderma and N. incompta, and therefore reflects the abundance of subpolar to subtropical species (i.e., "warmer" species). These species were counted as "others", but not identified.

Both today and during glacial periods, the productivity along the southern coast of Chile has been attributed to large volumes of run-off entering the ocean through fluvial discharge, from precipitation in the iron-rich Andean mountains (Carr and Kearns, 2003, Dezileau et al., 2004, Mohtadi and Hebbeln, 2004). However, the XRF Fe-record from Lamy et al. (2004) and the foraminiferal assemblage records exhibit no clear covariance and exclude Fe (as a micronutrient) as the most important factor controlling the faunal assemblages.

In this study we suggest that the main factors controlling *N. incompta* and *N. pachyderma* assemblages are temperature, salinity, and nutrients, respectively. The coiling ratio, which has been used successfully in other studies to infer relative temperature change in the North Atlantic

(Bauch et al., 2003), assuming that both of the *Neogloboquadrina* react to temperature, clearly cannot be used in the same way here given that large deviations in this ratio occur during both warm and cold intervals of A1 (based on Alkenones and $\delta^{18}O$). The coiling ratio have never before been properly tested as a temperature proxy in the SE Pacific and this study can conclude that the hydrography and competing influences such as seasonal upwelling is too complex/dynamic for the coiling ratio to exhibit a simple temperature dependent signal. Conversely however, this means that changes in coiling ratio may provide additional insights into these other (extra-temperature) influences.

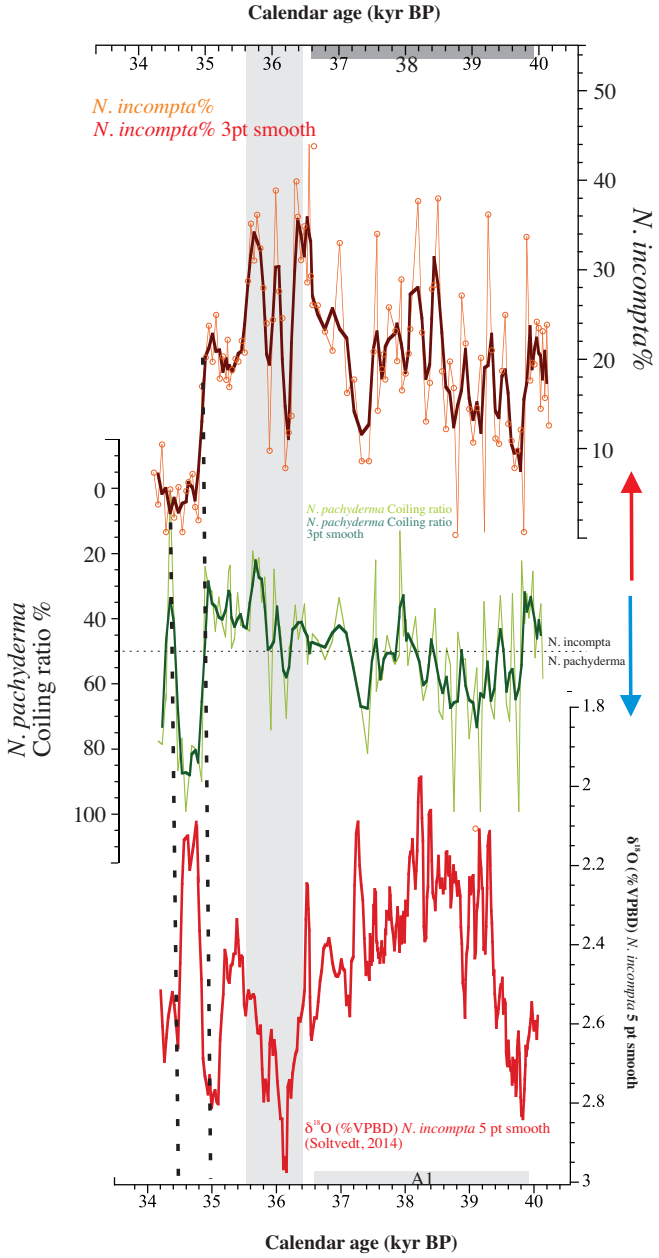

Figure 7.10. The relative abundance of N. incompta and N. pachyderma coiling ratio plotted versus the 5pt smoothed N. incompta $\delta^{18}O$ signal (Soltvedt, 2014)From bottom: The coiling ratio are plotted reversed, to infer relative temperature change (arrows indicate relative warming in all the three records). A stippled line indicates 50%, to infer N. pachyderma vs. N. incompta dominated signals. The highest values for N. incompta%, coincides with the heaviest values of the $\delta^{18}O$-signal of N. incompta, inferred with a gray bar. Vertical stippled lines indicate large shifts in all of the three records, most conspicuous between the coiling ratio and the $\delta^{18}O$-signal of N. incompta. G. bulloides are plotted on a reversed axis.

7.9 The Patagonian Ice Sheet variability

The new foraminiferal assemblage records from ODP Site 1233 suggests two main shifts in frontal location during the study interval. First at the onset of A1, where the STF were shifted southwards, and secondly a northward shift following A1, as a result of gradual cooling towards LGM. These frontal movements would affect the NPIS in two ways; firstly, though changes in the SST, which a marine terminating ice sheet is very sensitive to, and secondly through a shift of the precipitation center, tied to the SWW which fluctuates in sync with the STF. A southward migrated STF would introduce a drier, warmer climate to northern Patagonia, which would lead to an ice sheet retreat. Simultaneously, a southward shifted precipitation center would favor a SPIS advance. The maximum extent of the NPIS and SPIS are separated by up to 30 kyr, which underscores the ice sheets sensitivity towards changes in latitudinal changing fronts (Darvill et al., 2015b, Moreno et al., 2015, García et al., 2018).

Under a warming climate, as inferred from increased relative abundance of *N. incompta* and decreased *N. incompta* $\delta^{18}O$ (figure 7.6), the peaks of IRD at the core site are interpreted as a calving response to the 4ºC warming observed from the Alkenones that occurred during the first 1600 years spanning A1 (Kaiser and Lamy, 2010, Soltvedt, 2014). The ice sheet would consequently retreat through both meltwater plumes and massive calving events, as observed in the modern day Greenland (Thomas et al., 2000, Moon et al., 2018). Further, the calved icebergs would, steered by the prevailing wind and the PCC, drift towards our study site, 38 km off the coastline. There is a possibility that the icebergs were not advected towards the study site, due to a prevailing onshore SWW. However, a direct onshore wind direction is highly unlikely, as our foraminiferal assemblages record points towards upwelling in the same time span, which requires at least some component of northward blowing winds and thus offshore Ekman transport and advection.

Ruddiman (1977) stated that lithic grains of >150 μm definitely are transported by icebergs. The possibility that the lithic grains are being transported by sea ice or icebergs coming from the Antarctica peninsula are unlikely, given the mean annual SST is varying from 12 to 8.5ºC in the study interval (Kaiser and Lamy, 2010) (Figure 7.11).

Lamy et al. (2004) and Kaiser et al. (2007) suggested that the XRF Fe counts per second (cps) records the terrestrial bulk input from the NW-Patagonian ice sheet. A close synchronization with temperature indicates that the ice sheet is highly sensitive towards SST changes. Although an offset between Fe and SST is found during the last 70 kyr, where the offset increases towards

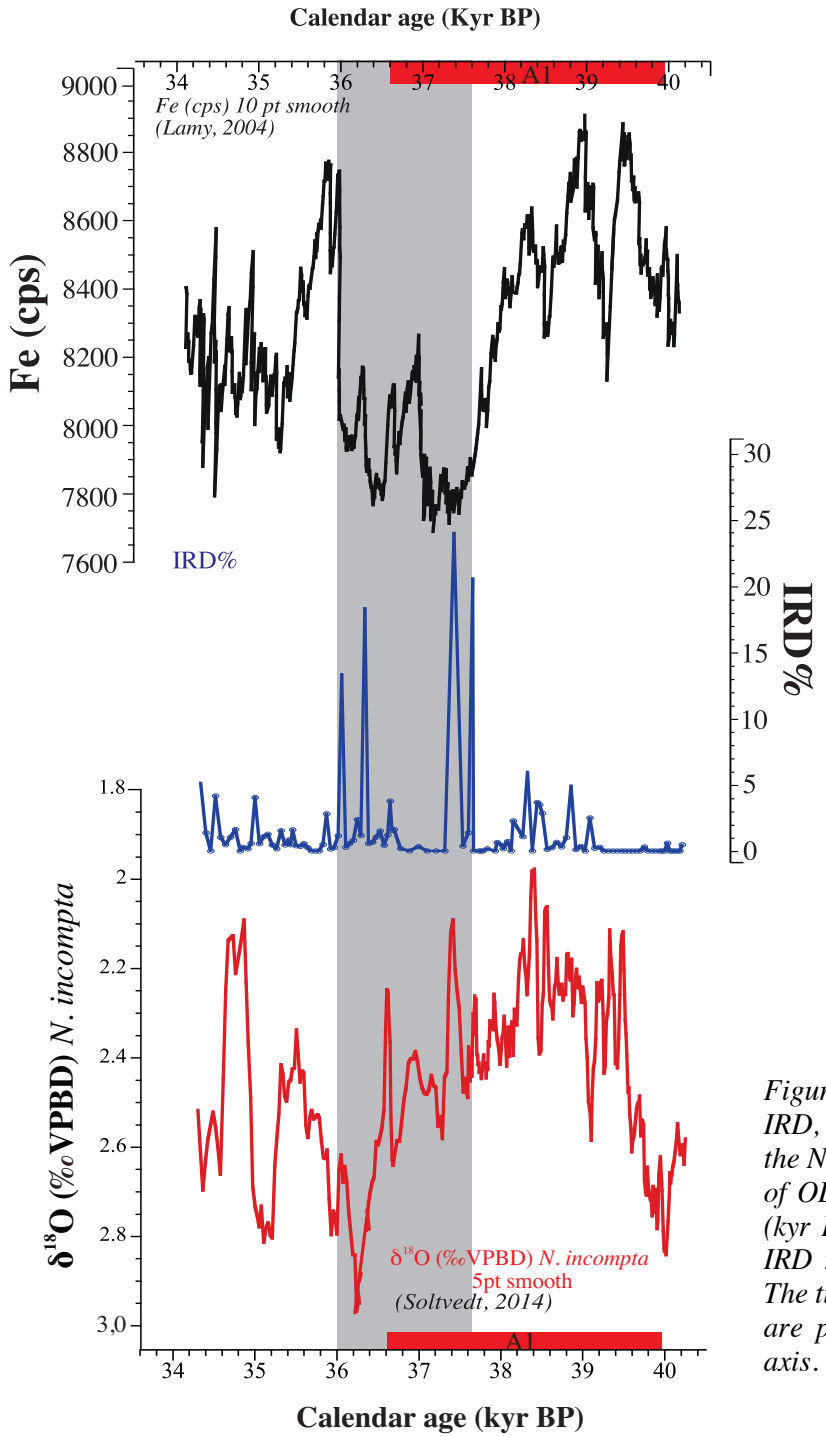

Figure 7.11 The stacked record of IRD, iron (Fe) cps (Lamy, 2004) and the N. incompta $\delta^{18}O$ (Soltvedt, 2014) of ODP site 1233 plotted versus age (kyr BP). The two main peaks of the IRD record are shown by gray bar. The time period of the warm-event A1 are plotted as red bar along the x-axis.

LGM, indicating that an extensive ice sheet responds slower to temperature change. An ice sheet (Fe) lag of 500-600 years compared to temperature is found in the study interval (Soltvedt, 2014), indicating that there is something else than SST controlling the ice sheet dynamics or that Fe is a complex/imperfect proxy for ice sheet dynamics. Is there a possibility that the IRD can give additional insights to the processes and timing of PIS dynamics?

The timing of the IRD-peaks at ODP Site 1233 are rather ambiguous compared the Fe-content. The largest IRD peaks generally coincide with low or declining Fe-content during the waning stages of A1 and the following cold period (figure 7.11). Thus paradoxically, peak IRD does not coincide with the high Fe input interval during early and peak A1 when the NPIS is thought to be declining. Multiple factors could explain the differences between these two ice sensitive proxies. Fe is sensitive to total weathered input by precipitation and integrated ice delivery and cannot differentiate between a fast streaming ice sheet and a decaying ice sheet. IRD on the other hand only monitors iceberg melt at the core site and is subject to the potential influences of varying proximity to iceberg sources (marine calving glaciers), iceberg survival and routing.

The first IRD peak occurs 800 years after the temperature maxima of A1 (based on *N. incompta* $\delta^{18}O$ from Soltvedt (2014)). This lag could either point to a strong atmospheric control of the ice sheet, where the SWW brings more moisture to the ice sheet, keeping the ice margin stable and in balance, delaying the collapse/rapid retreat of the ice sheet. However, our own records suggest greater upwelling (*N. pachyderma* peaks) during A1 suggesting the main belt of precipitation was shifted further south at this time. Thus, the most plausible explanation for the lack of IRD peaks during high Fe input during peak warmth of A1 could be that the ocean temperatures influence iceberg survival and transport of IRD to the study site. During peak A1 temperatures were likely too high in the subsurface ocean for many icebergs to survive and reach the core site; except for the two intervals of IRD-peaks when the icebergs survived due to lower sea surface temperatures. In addition, the NPIS may have retreated from the coast during peak A1, reducing the amount of proximal marine calving of icebergs. Thus, IRD at the core site is strongly sensitive to NPIS extent (proximal calving) consistent with that it was reduced in extent during peak warmth of A1 (Lamy et al., 2004, Kaiser et al., 2007)

Declining amounts of Fe at ODP Site 1233 during a glacial period has previously been attributed to wetter conditions, creating a dilution of the total Fe-signal, tied to more erosion and consequently fluvial discharge from the Fe-poor Coastal Range (Kaiser et al., 2007). This could ultimately indicate that the precipitation belt at the core of the SWW was positioned more proximal to ODP Site 1233, creating wetter conditions and possibly support the hypothesis from Kaiser et al. (2007). As a consequence, wetter conditions would increase the precipitation over the NPIS, make more snow to fall in the abrasion area, possibly keeping the marine terminating ice sheet margin to calve, due to a large ice sheet. However, this hypothesis match rather poorly with the faunal assemblages at the time, which indicate that SWW and associated precipitation must have been located poleward of even their modern position during much of A1 to explain the southward shifted upwelling zone—arguing strongly against such an explanation.

7.9.1 IRD versus terrestrial and marine records

There are two well-constrained glacier advances dated within the study interval, from both the terrestrial and the marine domains, at 34 and 39 kyr BP. The advances are well documented, both in the north, central and south terrestrial Patagonia (Andersen et al., 1999, Sagredo et al., 2011, Moreno et al., 2015, Smedley et al., 2016, García et al., 2018). Only one former PIS reconstruction with IRD have been conducted, and this findings will be discussed further (Caniupán et al., 2011) (figure 7.12). These two main advances, along with the general climatic setting tied to the A1 warming, underscores that the IRD signal derived from this study is not a result of the same advances recorded in the terrestrial domain. However, it is important to note that terrestrial dating methods, like exposure and luminescence, has a higher uncertainty, hence making the correlation with our IRD peaks less precise.

The comparison between the ODP Site 1233 (41ºS) and MD07-3128 (53ºS) is an unique opportunity to assess the variability of the northern and southern PIS, as a response to both atmospheric and oceanic changes, which is observed to be highly coupled (Lamy et al., 2010).

Caniupán et al. (2011) investigated the marine perspective of the southern Patagonian ice sheet at 53ºS. They interpret increases of IRD to represent advances of the marine terminating SPIS. As the majority of the IRD-peaks from this record correlate well with terrestrial records on the eastern side of the ice divide, the peaks are interpreted as general expansions of the SPIS. Figure 7.12 demonstrates that from a marine perspective the IRD content in the south, differ a lot from

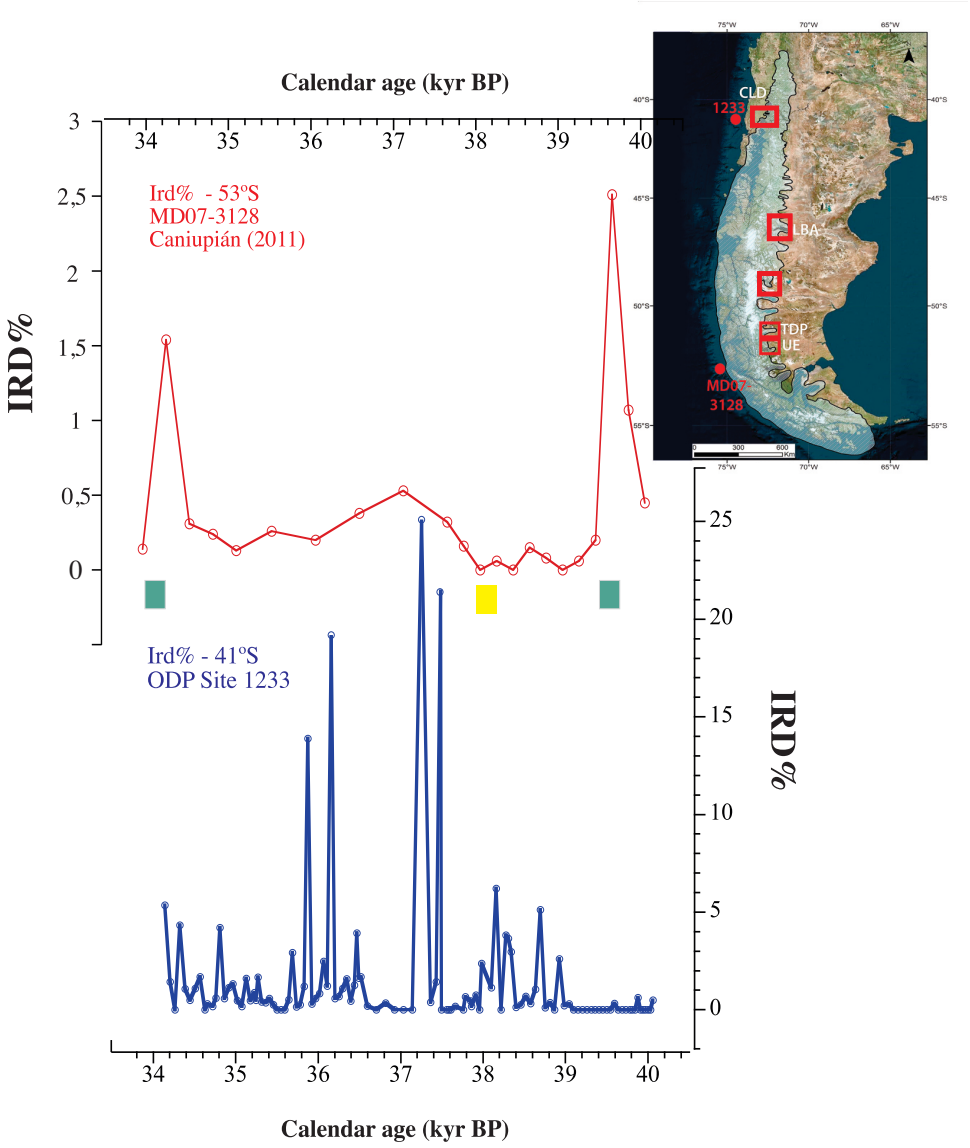

Figure 7.12 % IRD at ODP Site 1233 at 41ºS compared to the low resolution IRD-study by Caniupán et al. (2011) at 53ºS. Note that the two records are plotted on independent time scales. The green squares represent two well-dated terrestrial advances, whereas the yellow bar represents a poorly dated terrestrial advance. The red squares on the map in the right upper corner, represents the areas where the terrestrial records are derived from. The red dots show the position of the marine records. Samples with few grains of IRD at ODP Site 1233 are marked with closed blue circles. Overview map modified after García et al. (2018).

the signal in the north, at ODP Site 1233. In the south the highest peaks occur around 39.5 kyr BP, and at ODP site 1233 the peaks occur around 37.5 kyr BP. However, it should be noted that a gradual IRD increase (at 53ºS) between 38.2 to 36.0 kyr BP coincide with the two main IRD peaks at ODP Site 1233. The most plausible explained is tied to a latitudinal migration of the SWW-belt and its precipitation core, during the study interval, but no clear pattern is observed.

However, the low resolution of the southern record makes it difficult to do a complete assessment between the two records. It is important to note that the relative abundance of IRD (%) is much higher at ODP 1233, reaching 25%, than at MD07-21, where the maximum is 2.51%. The relative abundance of IRD is controlled by the total number of grains (the number of foraminifera and lithic grains). Some of the IRD peaks during the study interval from ODP Site 1233 are from samples that have too few total numbers of grains (<10) and are therefore statistically less robust and should be interpreted with caution. Overall, the IRD data do not indicate coherent behavior between the northern and southern PIS over A1. However, these differences need validation prior to further detailed interpretation as the southern record has very low IRD % , low resolution and not so well dated. Thus, new high resolution IRD-studies are required, both during the full MIS 3 at Site 1233 and also from sites preferentially further south of ODP Site 1233, as well as a paleo-salinity reconstruction at the core site to more directly monitor meltwater influences.

7.10 The SWW and interhemispheric influences

Lamy et al. (2010) attributed the changes in the core strength of the SWW impinging the Chilean coast during the Holocene to SST. The observed pattern of strong and poleward contracted SWW during the early Holocene covary with the strongly increased SST, the opposite occurred during the late Holocene as the SST cooled and the SWW shifted northwards and weakened (Figure 7.13). They suggest that similar mechanism is important during glacial times as well. Our data supports this, as the *N. pachyderma* (upwelling indicator) increased during periods of warmer SST, implying a southward shifted, and possibly also intensified core, of the SWW. This would also support the idea of meltwater plumes from the NW-PIS, as a response to both SST increases and southward displaced precipitation core of the SWW. Plausibly this could also help explain offsets in the timing of the northern and southern limbs of the PIS IRD records, as the influence of the SWW (and accumulation) would be felt oppositely at these two locations.

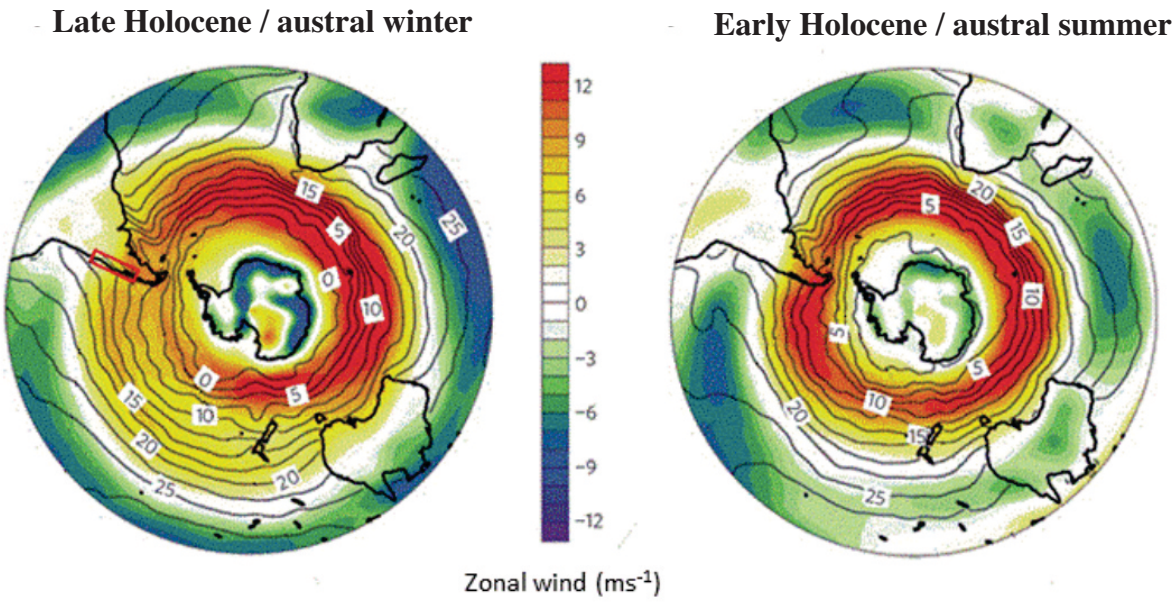

Figure 7.13 The zonal SWW of the SH. Late Holocene with decreased wind zonality over Patagonia, correlating with low SST. Early Holocene increased zonality over Patagonia, as a result of increased SST. Figure from Soltvedt (2014) modified after Lamy et al. (2010)

When comparing our *N. pachyderma %* to the same proxy from core TNO57-21 at 41ºS in the Atlantic Ocean cape basin, a similar pattern is observed (Figure 7.8). The *N. pachyderma%* record from TNO57-21 is interpreted as a result of an equatorward shifted STF is response to D-O8, and consequently contradicting our theory of a southward shifted front on an Antarctic timing. However, the records do show a great deal of similarity, and could hold some information about the interhemispheric coupling. Note that the records are plotted on different age scales (ODP 1233 tuned to the new EDML time scale, TN057-21 on the GICC05 timescale) and thus, impossible to fully compare.

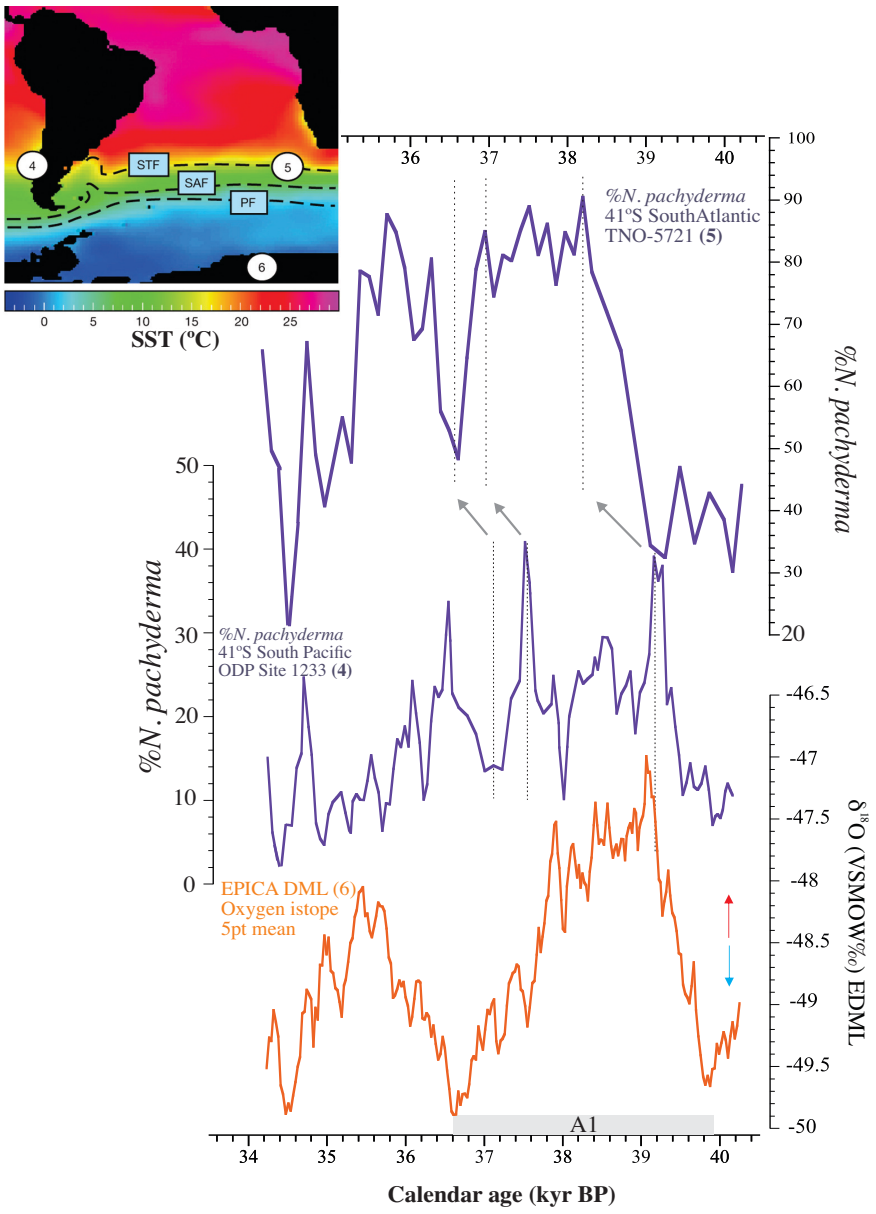

Figure 7.14 Overview map demonstrates the location of the core sites ODP Site 1233(4), TNO57-21(5) and EDML(6), with the temperature gradient of the Southern Ocean, which is strongly related to the frontal system of the ACC; the subtropical front (STF), the sub Antarctic front (SAF) and the polar front (PF).The 3-pt smoothed N. pachyderma% record from ODP Site 1233 (4) in the South Pacific and TNO57-21 (5) from the south Atlantic at 41ºS, where the major increases and decreases are obvious in both records, despite the two cores being in different ocean basins. The data from Barker et al. (2010), closely mirrors warming over Greenland related to D-O 8. ODP Site 1233 and EDML are plotted on the same age scale (EPICA community members, 2006) Map overview modified after Barker et al. (2009)

Our data provide new insights into the absolute position of the SWW during millennial scale changes in climate (A1). The upwelling inferred from the increased *N. pachyderma* record of ODP Site 1233 illustrates that the northern margin of the SWW were located even further south during A1 than it is at present; this poleward wind shifts apparently occurred despite the cooler conditions (relative to today). Thus, the magnitude of the southward shift during A1 is greater than that expected from the general relationship (warm = poleward SWW) outlined by Lamy et al., 2010 as it exceeds the poleward position achieved even during the warm Holocene. Why would the SWW be located even more south during the millennial scale warming of A1 than today when the climate was not as warm? Cooling and expanded ice sheets over the NH tends to drive the ITCZ and SWW southwards (Cheng et al., 2016), through an atmospheric teleconnection. At present the ice sheets in the NH are substantially smaller and thus, the ITCZ and SWW are positioned further north. Extensive NH glaciation during A1 however would have cooled the NH, driving the ITCZ and SWW south during the A1 warming and resulted in upwelling shifting at least as far south as ODP Site 1233. This is the atmospheric component of the ocean-atmosphere bipolar seesaw, which links climate of the two hemispheres during rapid climate change (Markle et al., 2017, Buizert et al., 2018). The new faunal records presented here strongly support a shift by the atmosphere during the millennial scale warming of A1 as the only way to increase upwelling at the site in conjunction with the ocean driven warming related to reduced North Atlantic overturning circulation. Thus, the faunal counts provide new insights into the (atmospheric) dynamics of millennial scale climate events that cannot be derived or inferred from ocean temperature changes alone and seem to confirm that Northern Hemisphere cryosphere changes play a role in driving the ITCZ and SWW further south than they would be in their absence (i.e. currently). Interestingly, the high frequency variability in our records may indicate that the position of the SWW also varied on century timescales and revealing a more variable atmospheric and oceanic circulation pattern than has been previously identified during these millennial scale events.

8. CONCLUSION

The derived foraminiferal assemblages from ODP Site 1233 spanning A1 demonstrates the crucial coupling between the interhemispheric oceanic and atmospheric teleconnections to alter the hydrography of the coastal Chile, tied to the latitudinal position of SWW. We observe a potential centennial variability in this connection, which previously never have been attributed to MIS 3. However, we must also take into account that local factors like melt water from the PIS could alter the hydrography of the core site, and hence the foraminiferal assemblages.

- Foraminiferal assemblages and IRD counts have been conducted on multi-decadal timescales to assess the productivity and water mass properties of the surface ocean, along with variability of the PIS, as a response to frontal migration, at ODP Site 1233 during A1.

- The foraminiferal assemblage's reconstruction points to centennial variability during A1 and a general colder climatic setting throughout the whole study interval compared to the modern faunal assemblages at Site 1233, tied to colder temperatures in the Peru-Chile current.

- A large-scale poleward displaced SWW during A1 facilitated a southward migration of the upwelling cells, reflected by increased *N. pachyderma* at Site 1233.

- The combined *N. incompta%* and *N. pachyderma%* record indicate a separate depth habitat for the two species during A1, sustained by the well-mixed upper water column during upwelling, which facilitates the migration of *N. pachyderma* deeper in the water column.

- The four peaks of IRD at the end of, and after the warming event A1, reflects calving from the northernmost part of the marine terminating Patagonian ice sheet, tied to a more proximal position of the ice sheet, or colder SSTs facilitating iceberg survival and migration towards the study site.

- The marine record of northern and the southern limb of the Patagonian ice sheet show no clear synchronicity, which demonstrates the importance of the latitudinal migration of the SWW to alter the western ice sheet extents.

- From 36,2 kyr BP the foraminiferal assemblages record of ODP Site 1233 displays a decreasing abundance of both *N. pachyderma* and *N. incompta*, possibly reflecting a reorganization and cooling of the climate system related to the Patagonian ice sheet advance at 34 kyr BP and possibly the onset of the LGM.

9. REFERENCES

Aguirre, C., et al. (2018) Insight into anthropogenic forcing on coastal upwelling off south-central Chile. *Elementa: Science of the Anthropocene,* 6 (1)**,** p. 59.

Allen, J. R., et al. (1999) Rapid environmental changes in southern Europe during the last glacial period. *Nature,* 400 (6746)**,** p. 740-743.

Altuna, N. E. B., et al. (2018) The morphotypes of Neogloboquadrina pachyderma: Isotopic signature and distribution patterns in the Canadian Arctic Archipelago and adjacent regions. *Marine Micropaleontology,* 142**,** p. 13-24.

Andersen, B., et al. (1999) Glacial geomorphologic maps of Llanquihue drift in the area of the southern Lake District, Chile. *Geografiska Annaler: Series A, Physical Geography,* 81 (2)**,** p. 155-166.

Anderson, J. (1999) *Antarctic marine geology,* New York, Cambrdige University Press.

Anderson, R., et al. (2009) Wind-driven upwelling in the Southern Ocean and the deglacial rise in atmospheric CO2. *Science,* 323 (5920)**,** p. 1443-1448.

Andrews, J. T. (2000) Icebergs and iceberg rafted detritus (IRD) in the North Atlantic: facts and assumptions. *Oceangraphy,* 13 (3)**,** p. 100-108.

Asmerom, Y., et al. (2010) Variable winter moisture in the southwestern United States linked to rapid glacial climate shifts. *Nature Geoscience,* 3 (2)**,** p. 114-117.

Bandy, O. L. & Rodolfo, K. S. Year. Distribution of foraminifera and sediments, Peru-Chile Trench area. *In:* Deep Sea Research and Oceanographic Abstracts, 1964. Elsevier, 817-837.

Bard, E. & Rickaby, R. E. (2009) Migration of the subtropical front as a modulator of glacial climate. *Nature,* 460 (7253)**,** p. 380-383.

Barker, S., et al. (2009) Interhemispheric Atlantic seesaw response during the last deglaciation. *Nature,* 457 (7233)**,** p. 1097-1102.

Barker, S., et al. (2010) Extreme deepening of the Atlantic overturning circulation during deglaciation. *Nature Geoscience,* 3 (8)**,** p. 567-571.

Basak, C., et al. (2018) Breakup of last glacial deep stratification in the South Pacific. *Science,* 359 (6378)**,** p. 900-904.

Bauch, D., et al. (1997) Oxygen isotope composition of living Neogloboquadrina pachyderma (sin.) in the Arctic Ocean. *Earth and Planetary Science Letters,* 146 (1-2)**,** p. 47-58.

Bauch, D., et al. (2003) Palaeoceanographic implications of genetic variation in living North Atlantic Neogloboquadrina pachyderma. *Nature,* 424 (6946)**,** p. 299-301.

Baumann, K.-H., et al. (1995) Reflection of Scandinavian ice sheet fluctuations in Norwegian Sea sediments during the past 150,000 years. *Quaternary Research,* 43 (2)**,** p. 185-197.

Bé & Tolderlund (1971) Distribution and ecology of living planktonic foraminifera in surface waters of the Atlantic and Indian Oceans. *Micropaleontology of Oceans: Cambridge University Press, New York***,** p. 105-149.

Bé, A. W. & Hutson, W. H. (1977) Ecology of planktonic foraminifera and biogeographic patterns of life and fossil assemblages in the Indian Ocean. *Micropaleontology***,** p. 369-414.

Beers, J. M. & Jayasundara, N. (2015) Antarctic notothenioid fish: what are the future consequences of 'losses' and 'gains' acquired during long-term evolution at cold and stable temperatures? *Journal of Experimental Biology,* 218 (12)**,** p. 1834-1845.

Bendle, J. 2018. *The westerly winds and the Patagonian Ice Sheet* [Online]. Antarctic glaciers Available: http://www.antarcticglaciers.org/glacial-geology/patagonian-ice-sheet/westerly-winds-patagonian-ice-sheet/ [Accessed 28.4 2019].

Berg, A., et al. (2016) Land–atmosphere feedbacks amplify aridity increase over land under global warming. *Nature Climate Change,* 6 (9)**,** p. 869-874.

Berger, W. H. (1969) Ecologic patterns of living planktonic foraminifera. *Deep Sea Research and Oceanographic Abstracts,* 16 (1)**,** p. 1-24.

Bijma, J., et al. (1990) Temperature and salinity limits for growth and survival of some planktonic foraminifers in laboratory cultures. *Journal of Foraminiferal Research,* 20 (2)**,** p. 95-116.

Boex, J., et al. (2013) Rapid thinning of the late Pleistocene Patagonian Ice Sheet followed migration of the Southern Westerlies. *Scientific reports,* 3 (1)**,** p. 2118.

Bond, G., et al. (1992) Evidence for massive discharges of icebergs into the North Atlantic ocean during the last glacial period. *Nature,* 360 (6401)**,** p. 245-249.

Borsdorf, A. & Stadel, C. (2015) *The Andes - a geographical portrait,* Berlin, Springer.

Bostock, H. C., et al. (2013) Reviewing the circulation and mixing of Antarctic Intermediate Water in the South Pacific using evidence from geochemical tracers and Argo float trajectories. *Deep Sea Research Part I: Oceanographic Research Papers,* 73**,** p. 84-98.

Bradshaw, J. S. (1959) Ecology of living planktonic foraminifera of the North and equatorial pacific Ocean *Cushman Found. Foram. Res,. Contr.,* , 10 (2)**,** p. 37-45.

Broecker, W. S. (1982) Ocean chemistry during glacial time. *Geochimica et Cosmochimica Acta,* 46 (10)**,** p. 1689-1705.

Broecker, W. S. (1994) Massive iceberg discharges as triggers for global climate change. *Nature,* 372 (6505)**,** p. 421-424.

Broecker, W. S. (1998) Paleocean circulation during the last deglaciation: a bipolar seesaw? *Paleoceanography,* 13 (2)**,** p. 119-121.

Brook, E. J., et al. (2005) Timing of millennial-scale climate change at Siple Dome, West Antarctica, during the last glacial period. *Quaternary Science Reviews,* 24 (12-13)**,** p. 1333-1343.

Buiron, D., et al. (2012) Regional imprints of millennial variability during the MIS 3 period around Antarctica. *Quaternary Science Reviews,* 48**,** p. 99-112.

Buizert, C., et al. (2015) Precise interpolar phasing of abrupt climate change during the last ice age. *Nature,* 520 (7549)**,** p. 661-665.

Buizert, C., et al. (2018) Abrupt ice-age shifts in southern westerly winds and Antarctic climate forced from the north. *Nature,* 563 (7733)**,** p. 681-685.

Caniupán, M., et al. (2011) Millennial-scale sea surface temperature and Patagonian Ice Sheet changes off southernmost Chile (53 S) over the past~ 60 kyr. *Paleoceanography* 26 (3).

Carr, M.-E. & Kearns, E. J. (2003) Production regimes in four Eastern Boundary Current systems. *Deep Sea Research Part II: Topical Studies in Oceanography,* 50 (22-26)**,** p. 3199-3221.

Carstens, J., et al. (1997) Distribution of planktic foraminifera at the ice margin in the Arctic (Fram Strait). *Marine Micropaleontology,* 29 (3-4)**,** p. 257-269.

Cheng, H., et al. (2016) The Asian monsoon over the past 640,000 years and ice age terminations. *nature,* 534 (7609)**,** p. 640-646.

CLIMAP, P. M. (1976) The surface of the ice-age Earth. *Science,* 191**,** p. 1131-1137.

CLIMAP, P. M. (1984) The last interglacial ocean. *Quaternary Research,* 21**,** p. 123-224.

Conkright, M. E., et al. (1994) *World Ocean Atlas. Volume 1: Nutrients,* Washington DC, NOAA.

Dansgaard, W., et al. (1993) Evidence for general instability of past climate from a 250-kyr ice-core record. *Nature,* 364 (6434)**,** p. 218-220.

Darling, K. F., et al. (2006) A resolution for the coiling direction paradox in Neogloboquadrina pachyderma. *Paleoceanography and Paleoclimatology,* 21 (2).

Darling, K. F., et al. (2004) Molecular evidence links cryptic diversification in polar planktonic protists to Quaternary climate dynamics. *Proceedings of the National Academy of Sciences,* 101 (20)**,** p. 7657-7662.

Darling, K. F., et al. (2007) Global molecular phylogeography reveals persistent Arctic circumpolar isolation in a marine planktonic protist. *Proceedings of the National Academy of Sciences,* 104 (12)**,** p. 5002-5007.

Darling, K. F., et al. (2017) Genetic diversity and ecology of the planktonic foraminifers Globigerina bulloides, Turborotalita quinqueloba and Neogloboquadrina pachyderma off the Oman margin during the late SW Monsoon. *Marine Micropaleontology,* 137**,** p. 64-77.

Darvill, C. M., et al. (2015a) Geomorphology and weathering characteristics of erratic boulder trains on Tierra del Fuego, southernmost South America: Implications for dating of glacial deposits. *Geomorphology,* 228**,** p. 382-397.

Darvill, C. M., et al. (2015b) Extensive MIS 3 glaciation in southernmost Patagonia revealed by cosmogenic nuclide dating of outwash sediments. *Earth and Planetary Science Letters,* 429**,** p. 157-169.

DaSilva, J. L., et al. (1997) Seismic facies changes along a nearly continuous 24 latitudinal transect: the fjords of Chile and the northern Antarctic Peninsula. *Marine Geology,* 143 (1-4)**,** p. 103-123.

De Baar, H. J., et al. (1995) Importance of iron for plankton blooms and carbon dioxide drawdown in the Southern Ocean. *Nature,* 373 (6513)**,** p. 412-415.

Denton, G. H., et al. (1999a) Interhemispheric linkage of paleoclimate during the last glaciation. *Geografiska Annaler: Series A, Physical Geography,* 81 (2)**,** p. 107-153.

Denton, G. H., et al. (1999b) Geomorphology, stratigraphy, and radiocarbon chronology of LlanquihueDrift in the area of the Southern Lake District, Seno Reloncaví, and Isla Grande de Chiloé, Chile. *Geografiska Annaler: Series A, Physical Geography,* 81 (2)**,** p. 167-229.

Deplazes, G., et al. (2013) Links between tropical rainfall and North Atlantic climate during the last glacial period. *Nature Geoscience,* 6 (3)**,** p. 213-217.

Dezileau, L., et al. (2004) Iron control of past productivity in the coastal upwelling system off the Atacama Desert, Chile. *Paleoceanography,* 19 (3).

Diekmann, B., et al. (2003) Terrigenous sediment supply in the polar to temperate South Atlantic: Land-ocean links of environmental changes during the late Quaternary. *The South Atlantic in the Late Quaternary*. Springer, p. 375-399.

Djurfeldt, L. (1989) Circulation and mixing in a coastal upwelling embayment; Gulf of Arauco, Chile. *Continental Shelf Research,* 9 (11)**,** p. 1003-1016.

Emiliani, C. (1955) Pleistocene temperatures. *The Journal of Geology,* 63 (6)**,** p. 538-578.

EPICA community members (2006) One-to-one coupling of glacial climate variability in Greenland and Antarctica. *Nature,* 444 (7116)**,** p. 195.

Euler, C. & Ninnemann, U. S. (2010) Climate and Antarctic Intermediate Water coupling during the late Holocene. *Geology,* 38 (7)**,** p. 647-650.

Fasullo, J., et al. (2018) ENSO's changing influence on temperature, precipitation, and wildfire in a warming climate. *Geophysical Research Letters,* 45 (17)**,** p. 9216-9225.

Fedorov, K. N. (1986) *The physical nature and structure of oceanic fronts*, Springer-Verlag.

Feldberg, M. J. & Mix, A. C. (2003) Planktonic foraminifera, sea surface temperatures, and mechanisms of oceanic change in the Peru and south equatorial currents, 0–150 ka BP. *Paleoceanography,* 18 (1).

Ferrari, R., et al. (2014) Antarctic sea ice control on ocean circulation in present and glacial climates. *Proceedings of the National Academy of Sciences,* 111 (24)**,** p. 8753-8758.

Figueroa, D. & Moffat, C. (2000) On the influence of topography in the induction of coastal upwelling along the Chilean coast. *Geophysical Research Letters,* 27 (23)**,** p. 3905-3908.

Førde, A.-E. 2008. *Millennial to sub-millennial scale variability in sub Antarctic near surface and intermediate water properties across the Antarctic warming event 1 and the Laschamp geomagnetic excursion at ODP Site 1233*. Master, Department of Earth Sciences University of Bergen

Fronval, T., et al. (1995) Oceanic evidence for coherent fluctuations in Fennoscandian and Laurentide ice sheets on millennium timescales. *Nature,* 374 (6521)**,** p. 443-446.

García, J.-L., et al. (2018) The MIS 3 maximum of the Torres del Paine and Última Esperanza ice lobes in Patagonia and the pacing of southern mountain glaciation. *Quaternary Science Reviews,* 185**,** p. 9-26.

Garreaud, R. (2007) Precipitation and circulation covariability in the extratropics. *Journal of Climate,* 20 (18)**,** p. 4789-4797.

Garreaud, R., et al. (2013) Large-scale control on the Patagonian climate. *Journal of Climate,* 26 (1)**,** p. 215-230.

Garreaud, R. D., et al. (2009) Present-day south american climate. *Palaeogeography, Palaeoclimatology, Palaeoecology,* 281 (3-4)**,** p. 180-195.

Gersonde, R. & Zielinski, U. (2000) The reconstruction of late Quaternary Antarctic sea-ice distribution—the use of diatoms as a proxy for sea-ice. *Palaeogeography, Palaeoclimatology, Palaeoecology,* 162 (3-4)**,** p. 263-286.

Giraudeau, J. & Rogers, J. (1994) Phytoplankton biomass and sea-surface temperature estimates from sea-bed distribution of nannofossils and planktonic foraminifera in the Benguela upwelling system. *Micropaleontology***,** p. 275-285.

Glasser, N. F. & Ghiglione, M. C. (2009) Structural, tectonic and glaciological controls on the evolution of fjord landscapes. *Geomorphology,* 105 (3-4)**,** p. 291-302.

Glasser, N. F. & Jansson, K. N. (2005) Fast-flowing outlet glaciers of the last glacial maximum Patagonian Icefield. *Quaternary Research,* 63 (2)**,** p. 206-211.

Glasser, N. F., et al. (2011) Cosmogenic nuclide exposure ages for moraines in the Lago San Martin Valley, Argentina. *Quaternary Research,* 75 (3)**,** p. 636-646.

Glasser, N. F., et al. (2008) The glacial geomorphology and Pleistocene history of South America between 38 S and 56 S. *Quaternary Science Reviews,* 27 (3-4)**,** p. 365-390.

González, H., et al. (2013) Land–ocean gradient in haline stratification and its effects on plankton dynamics and trophic carbon fluxes in Chilean Patagonian fjords (47–50 S). *Progress in Oceanography,* 119**,** p. 32-47.

Greco, M., et al. (2019) Depth habitat of the planktonic foraminifera Neogloboquadrina pachyderma in the northern high latitudes explained by sea-ice and chlorophyll concentrations. *Biogeosciences,* 16 (17)**,** p. 3425-3437.

Grootes, P. M., et al. (1993) Comparison of oxygen isotope records from the GISP2 and GRIP Greenland ice cores. *Nature,* 366 (6455)**,** p. 552-554.

Hanawa, K. & Talley, L. D. (2001) Mode waters. *International Geophysics,* 77**,** p. 373-386.

Hays, J., et al. (1976) 1976: Variations in the earth's orbit: pacemaker of the ice ages. Science 194, 1121-1132.

Hebbeln, D., et al. (2000) Surface sediment distribution along the Chilean continental slope related to upwelling and productivity. *Marine Geology,* 164 (3-4)**,** p. 119-137.

Hebbeln, D., et al. (1995) Cruise Report of R/V SONNE Cruise 102, Valparaíso–Valparaíso, 9.5.–28.6. 95. *Berichte, Fachbereich Geowissenschaften, Universität Bremen,* 68**,** p. 126.

Hemleben, C., et al. (2012) *Modern planktonic foraminifera,* New York, Springer-Verlag.

Hemming, S. R. (2004) Heinrich events: Massive late Pleistocene detritus layers of the North Atlantic and their global climate imprint. *Reviews of Geophysics,* 42 (1).

Hendy, I. L. & Kennett, J. P. (1999) Latest Quaternary North Pacific surface-water responses imply atmosphere-driven climate instability. *Geology,* 27 (4)**,** p. 291-294.

Heusser, C. J. (2003) *Ice age southern Andes: a chronicle of palaeoecological events,* Elsevier, Tuxedo, US.

Heusser, L., et al. (2006) Vegetation and climate dynamics of southern Chile during the past 50,000 years: results of ODP Site 1233 pollen analysis. *Quaternary Science Reviews,* 25 (5-6)**,** p. 474-485.

Hodell, D. A., et al. (2001) Abrupt cooling of Antarctic surface waters and sea ice expansion in the South Atlantic sector of the Southern Ocean at 5000 cal yr BP. *Quaternary Research,* 56 (2)**,** p. 191-198.

Hodell, D. A., et al. (2003) Pleistocene vertical carbon isotope and carbonate gradients in the South Atlantic sector of the Southern Ocean. *Geochemistry, Geophysics, Geosystems,* 4 (1)**,** p. 1-19.

Hoem, F. S. 2017. *Centennial-millennial scale variations in West Antarctic Ice Sheet discharge and their relationship to climate and ocean changes during the late Holocene*. Master, Department of Earth Science University of Bergen.

Hulton, N. R., et al. (2002) The last glacial maximum and deglaciation in southern South America. *Quaternary Science Reviews,* 21 (1-3)**,** p. 233-241.

Huybers, P. & Denton, G. (2008) Antarctic temperature at orbital timescales controlled by local summer duration. *Nature Geoscience,* 1 (11)**,** p. 787-792.

Imbrie, J., et al. (1992) On the structure and origin of major glaciation cycles 1. Linear responses to Milankovitch forcing. *Paleoceanography,* 7 (6)**,** p. 701-738.

Imbrie, J., et al. (1984) The orbital theory of Pleistocene climate: support from a revised chronology of the marine δ18O record. *Milankovitch and Climate,* 3**,** p. 269-305.

Imbrie, J., et al. (1971) The late Cenozoic glacial ages. *Yale University Press, New Haven, Conn***,** p. 71-182.

Imbrie, J. T., KK, & Kipp, N. (1971) A new micropaleontological method for quantitative paleoclimatology: application to a late Pleistocene Caribbean core. *The late Cenozoic glacial ages* Yale University Press, New Haven**,** p. 71-91.

Ingle Jr, J. C., et al. (1980) Benthic foraminiferal biofacies, sediments and water masses of the southern Peru-Chile Trench area, southeastern Pacific Ocean. *Micropaleontology,* 26 (2)**,** p. 113-150.

IODP. 2019a. *Coring tools and technology* [Online]. Available: http://www-odp.tamu.edu/publications/tnotes/tn31/apc/fig_01.htm [Accessed 30.3.2019].

IODP, L. 2019b. *D/V Joides Resolution* [Online]. Internation ocean drilling program Available: http://www.odplegacy.org/operations/ship.html [Accessed 30.3.2019].

IPCC (2019):Summary for policy makers In: IPCC Special Report on the Ocean and Cryosphere in a Changing Climate. In [H.- O. Pörtner, D.C. Roberts, V. Masson-Delmotte, P. Zhai, M. Tignor, E. Poloczanska, K. Mintenbeck, M. Nicolai, A. Okem, J. Petzold, B. Rama, N. Weyer] (ed.) In Press.

Ivanova, E. M., et al. (1999) Living Neogloboquadrina pachyderma sin and its distribution in the sediments from Oman and Somalia upwelling areas. *Marine Micropaleontology,* 36 (2-3)**,** p. 91-107.

JAMSTEC. 2015. *Our coring toolkit* [Online]. Diane Hanano. Available: https://joidesresolution.org/our-coring-toolkit/ [Accessed 28.2 2019].

Jansen, E. & Sjøholm, J. (1991) Reconstruction of glaciation over the past 6 Myr from ice-borne deposits in the Norwegian Sea. *Nature,* 349 (6310)**,** p. 600-603.

Johnsen, S. J., et al. (2001) Oxygen isotope and palaeotemperature records from six Greenland ice-core stations: Camp Century, Dye-3, GRIP, GISP2, Renland and NorthGRIP. *Journal of Quaternary Science: Published for the Quaternary Research Association,* 16 (4)**,** p. 299-307.

Kaiser, J. & Lamy, F. (2010) Links between Patagonian Ice Sheet fluctuations and Antarctic dust variability during the last glacial period (MIS 4-2). *Quaternary Science Reviews,* 29 (11-12)**,** p. 1464-1471.

Kaiser, J., et al. (2007) Dynamics of the millennial-scale sea surface temperature and Patagonian Ice Sheet fluctuations in southern Chile during the last 70 kyr (ODP Site 1233). *Quaternary International,* 161 (1)**,** p. 77-89.

Kaiser, J., et al. (2005) A 70-kyr sea surface temperature record off southern Chile (Ocean Drilling Program Site 1233). *Paleoceanography,* 20 (4).

Kanfoush, S. L., et al. (2000) Millennial-scale instability of the Antarctic ice sheet during the last glaciation. *Science,* 288 (5472)**,** p. 1815-1819.

Kanner, L. C., et al. (2012) High-latitude forcing of the South American summer monsoon during the last glacial. *Science,* 335 (6068)**,** p. 570-573.

Kaplan, M., et al. (2008) Southern Patagonian glacial chronology for the Last Glacial period and implications for Southern Ocean climate. *Quaternary Science Reviews,* 27 (3-4)**,** p. 284-294.

Kellogg, T. B. (1976) Late Quaternary Climatic Changes: Evidence from Deep-Sea Cores of Norwegian and Greenland seas. *Investigation of Late Quaternary paleoceanography and paleoclimatology,* 145**,** p. 77-110.

Kerr, A. & Sugden, D. (1994) The sensitivity of the south Chilean snowline to climatic change. *Climatic Change,* 28 (3)**,** p. 255-272.

Kleiven, H. F., et al. (2002) Intensification of Northern Hemisphere glaciations in the circum Atlantic region (3.5–2.4 Ma)–ice-rafted detritus evidence. *Palaeogeography, Palaeoclimatology, Palaeoecology,* 184 (3-4)**,** p. 213-223.

Knorr, G. & Lohmann, G. (2003) Southern Ocean origin for the resumption of Atlantic thermohaline circulation during deglaciation. *Nature,* 424**,** p. 532-536.

Kohfeld, K., et al. (1996) Neogloboquadrina pachyderma (sinistral coiling) as paleoceanographic tracers in polar oceans: Evidence from Northeast Water Polynya plankton tows, sediment traps, and surface sediments. *Paleoceanography,* 11 (6)**,** p. 679-699.

Kohfeld, K., et al. (2013) Southern Hemisphere westerly wind changes during the Last Glacial Maximum: paleo-data synthesis. *Quaternary Science Reviews,* 68**,** p. 76-95.

Kucera, M. (2007) Planktonic foraminifera as tracers of past oceanic environments. *Developments in marine geology,* 1**,** p. 213-262.

Kucera, M., et al. (2005a) Multiproxy approach for the reconstruction of the glacial ocean surface (MARGO). *Quaternary Science Reviews,* 24 (7-9)**,** p. 813-819.

Kucera, M., et al. (2005b) Reconstruction of sea-surface temperatures from assemblages of planktonic foraminifera: multi-technique approach based on geographically constrained calibration data sets and its application to glacial Atlantic and Pacific Oceans. *Quaternary Science Reviews,* 24 (7-9)**,** p. 951-998.

Kuroyanagi, A. & Kawahata, H. (2004) Vertical distribution of living planktonic foraminifera in the seas around Japan. *Marine Micropaleontology,* 53 (1-2)**,** p. 173-196.

Lamy, F., et al. (2001) Holocene rainfall variability in southern Chile: a marine record of latitudinal shifts of the Southern Westerlies. *Earth and Planetary Science Letters,* 185 (3)**,** p. 369-382.

Lamy, F., et al. (1999) High-resolution marine record of climatic change in mid-latitude Chile during the last 28,000 years based on terrigenous sediment parameters. *Quaternary Research,* 51 (1)**,** p. 83-93.

Lamy, F. & Kaiser, J. (2009) Glacial to Holocene paleoceanographic and continental paleoclimate reconstructions based on ODP Site 1233/GeoB 3313 off southern Chile. *Past Climate Variability in South America and Surrounding Regions*. Springer, p. 129-156.

Lamy, F., et al. (2007) Modulation of the bipolar seesaw in the Southeast Pacific during Termination 1. *Earth and Planetary Science Letters,* 259 (3)**,** p. 400-413.

Lamy, F., et al. (2004) Antarctic timing of surface water changes off Chile and Patagonian ice sheet response. *Science,* 304 (5679)**,** p. 1959-1962.

Lamy, F., et al. (2010) Holocene changes in the position and intensity of the southern westerly wind belt. *Nature Geoscience,* 3 (10)**,** p. 695-699.

Lee, S. Y., et al. (2011) Southern Ocean wind response to North Atlantic cooling and the rise in atmospheric CO2: Modeling perspective and paleoceanographic implications. *Paleoceanography,* 26 (1).

Lisiecki, L. E. & Raymo, M. E. (2005) A Pliocene-Pleistocene stack of 57 globally distributed benthic δ18O records. *Paleoceanography,* 20 (1).

Little, M., et al. (1997a) Rapid palaeoceanographic changes in the Benguela Upwelling System for the last 160,000 years as indicated by abundances of planktonic foraminifera. *Palaeogeography, Palaeoclimatology, Palaeoecology,* 130 (1-4)**,** p. 135-161.

Little, M. G., et al. (1997b) Trade wind forcing of upwelling, seasonally, and Heinrich events as a response to sub-Milankovitch climate variability. *Paleoceanography,* 12 (4)**,** p. 568-576.

Liu, Z. & Alexander, M. (2007) Atmospheric bridge, oceanic tunnel, and global climatic teleconnections. *Reviews of Geophysics,* 45 (2).

Liu, Z., et al. (2002) Tropical cooling at the last glacial maximum and extratropical ocean ventilation1. *Geophysical Research Letters,* 29 (10)**,** p. 1409.

Locarnini, R. A., et al. (2013) *World ocean atlas Volume 1: Temperature,* Washington DC, National Oceanic and Atmospheric Administration (NOAA).

Loubere, P., et al. (2007) Variability in tropical thermocline nutrient chemistry on the glacial/interglacial timescale. *Deep Sea Research Part II: Topical Studies in Oceanography,* 54 (5-7)**,** p. 747-761.

Lund, S. P., et al. (2006) Late Quaternary paleomagnetic secular variation and chronostratigraphy from ODP Sites 1233 and 1234. *Proc. Ocean Drill. Program Sci. Results, in press*.

Marchant, M., et al. (2004) Seasonal and interannual variability in the flux of planktic foraminifera in the Humboldt Current System off central Chile (30 S). *Deep Sea Research Part II: Topical Studies in Oceanography,* 51 (20-21)**,** p. 2441-2455.

Marchant, M., et al. (1998) Seasonal flux patterns of planktic foraminifera in the Peru–Chile Current. *Deep Sea Research Part I: Oceanographic Research Papers,* 45 (7)**,** p. 1161-1185.

Markle, B. R., et al. (2017) Global atmospheric teleconnections during Dansgaard–Oeschger events. *Nature Geoscience,* 10 (1)**,** p. 36-40.

Marshall, J. & Speer, K. (2012) Closure of the meridional overturning circulation through Southern Ocean upwelling. *Nature Geoscience,* 5 (3)**,** p. 171-180.

Martinez, P., et al. (2006) Atypical δ15N variations at the southern boundary of the East Pacific oxygen minimum zone over the last 50 ka. *Quaternary Science Reviews,* 25 (21-22)**,** p. 3017-3028.

Martínez-Méndez, G., et al. (2013) Changes in the advection of Antarctic Intermediate Water to the northern Chilean coast during the last 970 kyr. *Paleoceanography,* 28 (4)**,** p. 607-618.

Matsumoto, K., et al. (2001) Similar glacial and Holocene southern ocean hydrography. *Paleoceanography and Paleoclimatology,* 16 (5)**,** p. 445-454.

McManus, J. F., et al. (2004) Collapse and rapid resumption of Atlantic meridional circulation linked to deglacial climate changes. *Nature,* 428 (6985)**,** p. 834-837.

Meier, M. & Post, A. (1987) Fast tidewater glaciers. *Journal of Geophysical Research: Solid Earth,* 92 (B9)**,** p. 9051-9058.

Melles, M., et al. (2012) 2.8 million years of Arctic climate change from Lake El'gygytgyn, NE Russia. *science,* 337 (6092)**,** p. 315-320.

Mix, A., et al. (2003) Southeast Pacific Paleoceanographic transect *Ocean Drilling Program. Proc. ODP, Initial Reports,* 202 (145).

Mix, A. C., et al. (1999) Foraminiferal faunal estimates of paleotemperature: Circumventing the no-analog problem yields cool ice age tropics. *Paleoceanography,* 14 (3)**,** p. 350-359.

Mohtadi, M. & Hebbeln, D. (2004) Mechanisms and variations of the paleoproductivity off northern Chile (24 S–33 S) during the last 40,000 years. *Paleoceanography,* 19 (2).

Mohtadi, M., et al. (2005) Upwelling and productivity along the Peru–Chile Current derived from faunal and isotopic compositions of planktic foraminifera in surface sediments. *Marine Geology,* 216 (3)**,** p. 107-126.

Mohtadi, M., et al. (2008) Deglacial pattern of circulation and marine productivity in the upwelling region off central-south Chile. *Earth and Planetary Science Letters,* 272 (1-2)**,** p. 221-230.

Mokeddem, Z., et al. (2014) Oceanographic dynamics and the end of the last interglacial in the subpolar North Atlantic. *Proceedings of the National Academy of Sciences,* 111 (31)**,** p. 11263-11268.

Moller, T., et al. (2013) The effect of sea surface properties on shell morphology and size of the planktonic foraminifer Neogloboquadrina pachyderma in the North Atlantic. *Palaeogeography, Palaeoclimatology, Palaeoecology,* 391**,** p. 34-48.

Montade, V., et al. (2015) Teleconnection between the Intertropical Convergence Zone and southern westerly winds throughout the last deglaciation. *Geology,* 43 (8)**,** p. 735-738.

Montade, V., et al. (2011) Pollen distribution in marine surface sediments from Chilean Patagonia. *Marine Geology,* 282 (3-4)**,** p. 161-168.

Moon, T., et al. (2018) Subsurface iceberg melt key to Greenland fjord freshwater budget. *Nature Geoscience,* 11 (1)**,** p. 49-54.

Moreno, P., et al. (2010) Covariability of the Southern Westerlies and atmospheric CO2 during the Holocene. *Geology,* 38 (8)**,** p. 727-730.

Moreno, P. I., et al. (2015) Radiocarbon chronology of the last glacial maximum and its termination in northwestern Patagonia. *Quaternary Science Reviews,* 122**,** p. 233-249.

Moreno, P. I., et al. (2001) Interhemispheric climate links revealed by a late-glacial cooling episode in southern Chile. *Nature,* 409 (6822)**,** p. 804-808.

Moreno, P. I., et al. (1999) Abrupt vegetation and climate changes during the last glacial maximumand last termination in the chilean lake district: a case study from canal de la puntilla (41° s). *Geografiska Annaler: Series A, Physical Geography,* 81 (2)**,** p. 285-311.

Morey, A. E., et al. (2005) Planktonic foraminiferal assemblages preserved in surface sediments correspond to multiple environment variables. *Quaternary Science Reviews,* 24 (7-9)**,** p. 925-950.

Morley, A., et al. (2017) Environmental Controls on Mg/Ca in Neogloboquadrina incompta: A Core-Top Study From the Subpolar North Atlantic. *Geochemistry, Geophysics, Geosystems,* 18 (12)**,** p. 4276-4298.

Mouginot, J. & Rignot, E. (2015) Ice motion of the Patagonian icefields of South America: 1984–2014. *Geophysical Research Letters,* 42 (5)**,** p. 1441-1449.

Moy, C. M., et al. (2008) Isotopic evidence for hydrologic change related to the westerlies in SW Patagonia, Chile, during the last millennium. *Quaternary Science Reviews,* 27 (13-14)**,** p. 1335-1349.

Muratli, J., et al. (2010) Increased glacial-age ventilation of the Chilean margin by Antarctic Intermediate Water. *Nature Geoscience,* 3 (1)**,** p. 23-26.

NASA. 2014. *West Antarctica Media Teleconference* [Online]. nasa.gov: NASA. Available: https://www.nasa.gov/jpl/earth/antarctica-telecon20140512/ [Accessed 31.8 2019].

Neshyba, S. (1979) On the southernmost extension of the Peru-Chile Undercurrent. *Deep Sea Research Part A. Oceanographic Research Papers,* 26 (12)**,** p. 1387-1393.

Niebler, H.-S. & Gersonde, R. (1998) A planktic foraminiferal transfer function for the southern South Atlantic Ocean. *Marine Micropaleontology,* 34 (3-4)**,** p. 213-234.

Ninnemann, U. S. & Charles, C. D. (1997) Regional differences in Quaternary Subantarctic nutrient cycling: Link to intermediate and deep water ventilation. *Paleoceanography,* 12 (4)**,** p. 560-567.

Orsi, A. J., et al. (2014) Magnitude and temporal evolution of Dansgaard–Oeschger event 8 abrupt temperature change inferred from nitrogen and argon isotopes in GISP2

ice using a new least-squares inversion. *Earth and Planetary Science Letters,* 395**,** p. 81-90.

Ortiz, J. D., et al. (1995) Environmental control of living symbiotic and asymbiotic foraminifera of the California Current. *Paleoceanography,* 10 (6)**,** p. 987-1009.

Pahnke, K., et al. (2003) 340,000-year centennial-scale marine record of Southern Hemisphere climatic oscillation. *Science,* 301 (5635)**,** p. 948-952.

Pantoja, S., et al. (2011) Oceanography of the Chilean Patagonia. *Continental shelf research,* 31 (3-4)**,** p. 149-153.

Pedro, J. B., et al. (2018) Beyond the bipolar seesaw: Toward a process understanding of interhemispheric coupling. *Quaternary Science Reviews,* 192**,** p. 27-46.

Pflaumann, U., et al. (1996) SIMMAX: A modern analog technique to deduce Atlantic sea surface temperatures from planktonic foraminifera in deep-sea sediments. *Paleoceanography,* 11 (1)**,** p. 15-35.

Philander, S. G. H. (1983) El Nino southern oscillation phenomena. *Nature,* 302 (5906)**,** p. 295-301.

Pickard, G. (1971) Some physical oceanographic features of inlets of Chile. *Journal of the Fisheries Board of Canada,* 28 (8)**,** p. 1077-1106.

Pinochet, A., et al. (2019) Seasonal Variability of Upwelling off Central-Southern Chile. *Remote Sensing,* 11 (15)**,** p. 1737.

Pisias, N., et al. (2001) Millennial scale climate variability of the northeast Pacific Ocean and northwest North America based on radiolaria and pollen. *Quaternary Science Reviews,* 20 (14)**,** p. 1561-1576.

Porter, S. C. (1981) Pleistocene glaciation in the southern Lake District of Chile. *Quaternary Research,* 16 (3)**,** p. 263-292.

Price, J. F., et al. (1987) Wind-driven ocean currents and Ekman transport. *Science,* 238 (4833)**,** p. 1534-1538.

Rasmussen, L., et al. (2007) Influence of upper air conditions on the Patagonia icefields. *Global and Planetary Change,* 59 (1-4)**,** p. 203-216.

Reynolds, L. A. & Thunell, R. C. (1986) Seasonal production and morphologic variation of Neogloboquadrina pachyderma (Ehrenberg) in the northeast Pacific. *Micropaleontology***,** p. 1-18.

Rignot, E., et al. (2003) Contribution of the Patagonia Icefields of South America to sea level rise. *Science,* 302 (5644)**,** p. 434-437.

Rintoul, S., et al. (1997) Seasonal evolution of upper ocean thermal structure between Tasmania and Antarctica. *Deep Sea Research Part I: Oceanographic Research Papers,* 44 (7)**,** p. 1185-1202.

Rintoul, S. R., et al. (2001) The antarctic circumpolar current system. *International Geophysics*. Elsevier, p. 271-302.

Rivera, A., et al. (2002) Use of remotely sensed and field data to estimate the contribution of Chilean glaciers to eustatic sea-level rise. *Annals of Glaciology,* 34**,** p. 367-372.

Rojas, M., et al. (2009) The Southern Westerlies during the last glacial maximum in PMIP2 simulations. *Climate Dynamics,* 32 (4)**,** p. 525-548.

Romero, O. E., et al. (2006) Paleoproductivity evolution off central Chile from the Last Glacial Maximum to the Early Holocene. *Quaternary Research,* 65 (3)**,** p. 519-525.

Ruddiman, W. F. (1977) Late Quaternary deposition of ice-rafted sand in the subpolar North Atlantic (lat 40 to 65 N). *Geological Society of America Bulletin,* 88 (12)**,** p. 1813-1827.

Rutherford, S., et al. (1999) Environmental controls on the geographic distribution of zooplankton diversity. *Nature,* 400 (6746)**,** p. 749 –753.

Sagredo, E., et al. (2011) Fluctuations of the Última Esperanza ice lobe (52 S), Chilean Patagonia, during the last glacial maximum and termination 1. *Geomorphology,* 125 (1)**,** p. 92-108.

Sarmiento, J. L., et al. (2004) High-latitude controls of thermocline nutrients and low latitude biological productivity. *Nature,* 427 (6969)**,** p. 56-60.

Schiebel, R. & Hemleben, C. (2000) Interannual variability of planktic foraminiferal populations and test flux in the eastern North Atlantic Ocean (JGOFS). *Deep Sea Research Part II: Topical Studies in Oceanography,* 47 (9-11)**,** p. 1809-1852.

Schiebel, R., et al. (2001) Planktic foraminiferal production stimulated by chlorophyll redistribution and entrainment of nutrients. *Deep Sea Research Part I: Oceanographic Research Papers,* 48 (3)**,** p. 721-740.

Schmidt, D. N., et al. (2003) Response of planktic foraminiferal size to late Quaternary climate change. *Paleoceanography,* 18 (2).

Schneider, C., et al. (2003) Weather observations across the southern Andes at 53 S. *Physical Geography,* 24 (2)**,** p. 97-119.

Schott, D. W. (1935) *Die Sedimente des aquatorialen atlantischen Ozeans I Lieferung. B. Die Foraminiferen in dem aquatorialen Teil des atlantischen Ozeans,* Berlin, Springer-Verlag.

Shaffer, G., et al. (1995) Currents in the deep ocean off Chile (30 S). *Deep Sea Research Part I: Oceanographic Research Papers,* 42 (4)**,** p. 425-436.

Shipboard Scientific Party (2003) Leg 202. In Mix, A.C., Tiedemann, R., Blum, P., et al., (ed.) *Proc ODP Init. Repts., 202:* . College Station TX (Ocean Srilling Program), p. 1-145.

Siddall, M., et al. (2008) Marine isotope stage 3 sea level fluctuations: Data synthesis and new outlook. *Reviews of Geophysics,* 46 (4).

Sijp, W. P. & England, M. H. (2009) Southern Hemisphere westerly wind control over the ocean's thermohaline circulation. *Journal of Climate,* 22 (5)**,** p. 1277-1286.

Sikes, E., et al. (2009) Southern Ocean seasonal temperature and Subtropical Front movement on the South Tasman Rise in the late Quaternary. *Paleoceanography and Paleoclimatology,* 24 (2).

Simstich, J., et al. (2003) Paired δ18O signals of Neogloboquadrina pachyderma (s) and Turborotalita quinqueloba show thermal stratification structure in Nordic Seas. *Marine Micropaleontology,* 48 (1-2)**,** p. 107-125.

Skinner, L., et al. (2010) Ventilation of the deep Southern Ocean and deglacial CO2 rise. *Science,* 328 (5982)**,** p. 1147-1151.

Sloyan, B. M. & Rintoul, S. R. (2001) Circulation, renewal, and modification of Antarctic Mode and Intermediate Water. *Journal of physical oceanography,* 31 (4)**,** p. 1005-1030.

Smedley, R., et al. (2016) Luminescence dating of glacial advances at Lago Buenos Aires (~ 46 S), Patagonia. *Quaternary Science Reviews,* 134**,** p. 59-73.

Soltvedt, N. V. 2014. *Centennial to decadal scale paleoclimatic reconstructions from ODP Site 1233 in the SE Pacific Ocean spanning Antarctic warming event 1*. Master Master, Department of Earth Science University of Bergen.

Southon, J., et al. (2012) A high-resolution record of atmospheric 14C based on Hulu Cave speleothem H82. *Quaternary Science Reviews,* 33**,** p. 32-41.

Spero, H. J. & Lea, D. W. (2002) The cause of carbon isotope minimum events on glacial terminations. *Science,* 296 (5567)**,** p. 522-525.

Stein, R. (1990) Organic carbon content/sedimentation rate relationship and its paleoenvironmental significance for marine sediments. *Geo-Marine Letters,* 10 (1), p. 37-44.

Stocker, T. F. & Johnsen, S. J. (2003) A minimum thermodynamic model for the bipolar seesaw. *Paleoceanography,* 18 (4).

Strub, P. T., J. M. Mesías, V. Montecino, J. Rutllant, and S. Salinas (1998) Coastal ocean circulation off western South America - Coastal segment (6,E). *The sea - the Global Coastal Ocean. Regional Studies and Syntheses,* 11, p. 273-315.

Swart, N. & Fyfe, J. C. (2012) Observed and simulated changes in the Southern Hemisphere surface westerly wind-stress. *Geophysical Research Letters,* 39 (16).

Talley, L. D. (1999) Some aspects of ocean heat transport by the shallow, intermediate and deep overturning circulations. *Geophys. Mono. Ser,* 112, p. 1-22.

Talley, L. D. (2011) *Descirptive Physical Oceanography - An introduction* New York, Elsevier.

Thomas, R. H., et al. (2000) Substantial thinning of a major east Greenland outlet glacier. *Geophysical Research Letters,* 27 (9), p. 1291-1294.

Thornburg, T. M. & Kulm, L. D. (1987) Sedimentation in the Chile Trench: Depositional morphologies, lithofacies, and stratigraphy. *Geological Society of America Bulletin,* 98 (1), p. 33-52.

Toggweiler, J. (2009) Shifting westerlies. *Science,* 323 (5920), p. 1434-1435.

Toggweiler, J., et al. (1991) The Peru upwelling and the ventilation of the South Pacific thermocline. *Journal of Geophysical Research: Oceans,* 96 (C11), p. 20467-20497.

Toggweiler, J. & Samuels, B. (1993) Is the magnitude of the deep outflow from the Atlantic Ocean actually governed by Southern Hemisphere winds? *The Global Carbon Cycle*. Springer, p. 303-331.

Toggweiler, J. R., et al. (2006) Midlatitude westerlies, atmospheric CO2, and climate change during the ice ages. *Paleoceanography,* 21 (2).

Trenberth, K. E. (1991) Storm tracks in the Southern Hemisphere. *Journal of the Atmospheric Sciences,* 48 (19), p. 2159-2178.

Vázquez Riveiros, N., et al. (2016) Mg/Ca thermometry in planktic foraminifera: Improving paleotemperature estimations for G. bulloides and N. pachyderma left. *Geochemistry, Geophysics, Geosystems,* 17 (4), p. 1249-1264.

Veit, H. (1996) Southern Westerlies during the Holocene deduced from geomorphological and pedological studies in the Norte Chico, Northern Chile (27–33 S). *Palaeogeography, Palaeoclimatology, Palaeoecology,* 123 (1-4), p. 107-119.

Voelker, A. H. (2002) Global distribution of centennial-scale records for Marine Isotope Stage (MIS) 3: a database. *Quaternary Science Reviews,* 21 (10), p. 1185-1212.

Voigt, I., et al. (2015) Holocene shifts of the southern westerlies across the South Atlantic. *Paleoceanography,* 30 (2), p. 39-51.

Volbers, A., et al. (2003) Palaeoceanographic Changes in the Northern Benguela Upwelling System over the last 245.000 Years as Derived from Planktic Foraminifera Assemblages. *The South Atlantic in the Late Quaternary*. Springer, p. 601-622.

Wagner, J. D., et al. (2010) Moisture variability in the southwestern United States linked to abrupt glacial climate change. *Nature Geoscience,* 3 (2), p. 110-113.

Wang, Y.-J., et al. (2001) A high-resolution absolute-dated late Pleistocene monsoon record from Hulu Cave, China. *science,* 294 (5550), p. 2345-2348.

Warren, C. & Aniya, M. (1999) The calving glaciers of southern South America. *Global and Planetary Change,* 22 (1-4), p. 59-77.

Warren, C. R. & Sugden, D. E. (1993) The Patagonian icefields: a glaciological review. *Arctic and Alpine Research,* 25 (4), p. 316-331.

Watson, A. J. & Naveira Garabato, A. C. (2006) The role of Southern Ocean mixing and upwelling in glacial-interglacial atmospheric CO2 change. *Tellus B: Chemical and Physical Meteorology,* 58 (1), p. 73-87.

Wenzens, G. (2006) Terminal moraines, outwash plains, and lake terraces in the vicinity of Lago Cardiel (49° S; Patagonia, Argentina)—evidence for Miocene Andean foreland glaciations. *Arctic, Antarctic, and Alpine Research,* 38 (2), p. 276-291.

Wijffels, S. E., et al. (2001) Revisiting the South Pacific subtropical circulation: A synthesis of World Ocean Circulation Experiment observations along 32 S. *Journal of Geophysical Research: Oceans,* 106 (C9), p. 19481-19513.

Wilson, K., et al. (2005) A one-million-year history of a north-south segment of the Subtropical Front, east of New Zealand. *Paleoceanography and Paleoclimatology,* 20 (2).

Wu, G. & Hillaire-Marcel, C. (1994) Oxygen isotope compositions of sinistral Neogloboquadrina pachyderma tests in surface sediments: North Atlantic Ocean. *Geochimica et Cosmochimica Acta,* 58 (4), p. 1303-1312.

Zachos, J. C., et al. (2001) Climate response to orbital forcing across the Oligocene-Miocene boundary. *Science,* 292 (5515)**,** p. 274-278.

Žarić, S., et al. (2005) Sensitivity of planktic foraminifera to sea surface temperature and export production as derived from sediment trap data. *Marine Micropaleontology,* 55 (1-2)**,** p. 75-105.

Zhang, X., et al. (2015) Spatial fingerprint and magnitude of changes in the Atlantic meridional overturning circulation during marine isotope stage 3. *Geophysical Research Letters,* 42 (6)**,** p. 1903-1911.

10. APPENDIX

Appendix A

The counts used to calculate the coiling ratios and relative abundances.

Core section	Depth (cm)	*N. pachyderma*	*N. incompta*	Other Plancitcs	Total Planctics	Benthics	IRD
ODP1233D							
7H3	52	33	9	94	136	93	13
7H3	60	35	9	248	292	537	12
7H3	68	75	42	312	429	538	0
7H3	76	0	0	21	21	1	1
7H3	84	2	3	58	63	121	2
7H3	92	28	4	216	248	347	3
7H3	100	7	2	31	40	49	1
7H3	108	1	0	33	34	24	1
7H3	116	301	46	657	1004	403	0
7H3	120	64	16	208	288	380	2
					0		
7H4	4	85	20	203	308	246	1
7H4	10	20	4	120	144	182	2
7H4	18	10	1	65	76	106	8
7H4	26	14	42	202	258	84	2
7H4	34	29	64	235	328	109	5
7H4	42	30	62	177	269	174	6
7H4	50	51	63	217	331	83	2

7H4	58	76	145	362	583	129	1
7H4	66	17	23	94	134	48	3
7H4	74	27	31	100	158	50	1
7H4	82	31	87	394	512	272	7
7H4	86	36	110	360	506	88	3
7H4	90	24	24	100	148	28	3
7H4	98	57	64	232	353	119	2
7H4	106	105	213	783	1101	277	5
7H4	114	86	114	398	598	83	4
7H4	122	95	126	369	590	157	2
7H4	130	55	70	224	349	110	0
7H4	138	67	83	146	296	115	0
7H4	146	36	142	234	412	89	2
					0		
7H5	4	31	85	164	280	99	2
7H5	12	40	139	213	392	137	16
7H5	20	91	163	260	514	107	1
7H5	28	26	66	150	242	132	1

7H5	36	13	14	33	60	22	1
7H5	44	3	1	7	11	20	5
7H5	52	24	69	198	291	374	2
7H5	60	61	82	72	215	123	2
7H5	68	27	35	68	130	106	2
7H5	76	94	76	148	318	1641	50
7H5	84	5	2	21	28	532	7
7H5	92	3	3	21	27	45	17
7H5	100	12	14	82	108	583	4
7H5	108	55	94	91	240	770	7
7H5	116	94	105	99	298	156	5
7H5	124	58	79	123	260	111	6
7H5	132	118	205	277	600	485	5
7H5	140	85	70	96	251	137	5
					0		
7H6	2	51	55	121	127	141	11
7H6	6	168	158	227	553	474	17
7H6	10	147	175	368	690	349	18

7H6	18	92	101	206	399	100	1
7H6	26	93	81	188	362	248	0
7H6	34	81	88	265	434	128	2
7H6	42	38	72	113	223	177	0
7H6	50	52	59	269	380	347	0
7H6	58	18	15	55	88	119	0
7H6	66	6	3	29	38	22	20
7H6	74	144	31	218	393	352	3
7H6	82	64	49	130	243	166	6
7H6	90	69	40	186	295	179	0
7H6	98	102	81	262	445	180	0
7H6	104	64	54	199	317	122	9
7H6	110	98	114	242	454	107	1
7H6	118	87	64	274	425	245	3
7H6	122	167	142	323	632	68	
7H7	10	37	53	245	335	214	1
7H7	22	52	74	245	371	159	0
					0		

ODP1233C							
7H3	40	6	7	14	27	18	16
7H3	44	14	9	19	42	46	18
7H3	48	202	46	167	415	314	0
7H3	56	84	57	146	287	125	0
7H3	60	29	17	81	127	93	1
7H3	64	130	110	269	509	353	1
7H3	72	60	52	173	285	106	0
7H3	80	68	56	169	293	151	3
7H3	88	110	101	147	358	85	2
7H3	96	44	51	193	288	111	3
7H3	104	69	56	122	247	656	22
7H3	112	82	86	201	369	347	6
7H3	120	84	124	127	335	95	5
7H3	128	40	31	68	139	57	13
7H3	136	64	33	170	267	288	0
7H3	144	48	30	102	180	121	12
7H3	148	31	28	44	103	81	7

7H4	2	62	58	90	210	149	11
7H4	10	113	185	198	496	268	1
7H4	18	52	23	53	128	259	1
7H4	26	79	31	159	269	161	3
7H4	34	29	29	94	152	153	1
7H4	42	11	9	36	56	37	1
7H4	50	5	0	9	14	23	2
7H4	58	123	149	292	564	307	1
7H4	66	54	47	122	223	300	2
7H4	74	24	21	108	153	136	0
7H4	82	14	4	22	40	35	2
7H4	90	103	52	220	375	538	2
7H4	98	110	86	246	442	215	2
7H4	106	4	0	2	6	47	0
7H4	114	70	126	159	355	78	0
7H4	122	19	13	32	64	125	0
7H4	130	77	37	240	354	336	0
7H4	138	86	34	225	345	112	0

7H4	146	55	58	209	322	135	0
7H5	4	51	99	258	408	357	0
7H5	12	42	42	263	347	275	0
7H5	20	60	29	196	285	289	0
7H5	28	21	8	83	112	346	0
7H5	36	1	2	19	22	283	1
7H5	44	7	4	24	35	80	0
7H5	52	5	0	19	24	24	0
7H5	60	21	69	119	209	214	0
7H5	68	30	41	171	242	260	0
7H5	76	23	46	174	243	219	0
7H5	84	24	35	128	187	228	0
7H5	92	58	104	281	443	487	6
7H5	100	13	36	109	158	279	0
7H5	108	9	8	41	58	94	0
7H5	116	72	85	222	379	271	0
7H5	124	31	43	213	287	301	0
7H5	132	42	73	200	315	219	0

7H5	140	48	33	196	277	127	2

Appendix B

Foraminiferal and lithic Counts, calculated based on Equation 1,2,3 and 4, given in the method chapter.

Core section	Depth (cm)	Nps+incompta	Total number of grains	Nps coiling ratio (%)	*N.pachyderma* %	*N. incompta* %	% IRD
ODP 1233							
7H3	52	42	242,00	78,57	24,26	6,62	5,37
7H3	60	44	841,00	79,55	11,99	3,08	1,43
7H3	68	117	967,00	64,10	17,48	9,79	0,00
7H3	76	0	23,00	0,00	0,00	0,00	4,35
7H3	84	5	186,00	40,00	3,17	4,76	1,08
7H3	92	32	598,00	87,50	11,29	1,61	0,50
7H3	100	9	90,00	77,78	17,50	5,00	1,11
7H3	108	1	59,00	100,00	2,94	0,00	1,69
7H3	116	347	1407,00	86,74	29,98	4,58	0,00
7H3	120	80	670,00	80,00	22,22	5,56	0,30
7H4	4	105	555,00	80,95	27,60	6,49	0,18
7H4	10	24	328,00	83,33	13,89	2,78	0,61
7H4	18	11	190,00	90,91	13,16	1,32	4,21
7H4	26	56	344,00	25,00	5,43	16,28	0,58
7H4	34	93	442,00	31,18	8,84	19,51	1,13
7H4	42	92	449,00	32,61	11,15	23,05	1,34
7H4	50	114	416,00	44,74	15,41	19,03	0,48

7H4	58	221	728,00	34,39	12,71	24,25	0,14
7H4	66	40	185,00	42,50	12,69	17,16	1,62
7H4	74	58	209,00	46,55	17,09	19,62	0,48
7H4	82	118	791,00	26,27	6,05	16,99	0,88
7H4	86	146	597,00	24,66	7,11	21,74	0,50
7H4	90	48	179,00	50,00	16,22	16,22	1,68
7H4	98	121	474,00	47,11	16,15	18,13	0,42
7H4	106	318	1383,00	33,02	9,54	19,35	0,36
7H4	114	200	685,00	43,00	14,38	19,06	0,58
7H4	122	221	749,00	42,99	16,10	21,36	0,27
7H4	130	125	459,00	44,00	15,76	20,06	0,00
7H4	138	150	411,00	44,67	22,64	28,04	0,00
7H4	146	178	501,00	20,22	8,74	34,47	0,00
			0,00				
7H5	4	116	381,00	26,72	11,07	30,36	0,52
7H5	12	179	545,00	22,35	10,20	35,46	2,94
7H5	20	254	622,00	35,83	17,70	31,71	0,16
7H5	28	92	375,00	28,26	10,74	27,27	0,27

7H5	36	27	83,00	48,15	21,67	23,33	1,20
7H5	44	4	36,00	75,00	27,27	9,09	13,89
7H5	52	93	667,00	25,81	8,25	23,71	0,30
7H5	60	143	340,00	42,66	28,37	38,14	0,59
7H5	68	62	238,00	43,55	20,77	26,92	0,84
7H5	76	170	2009,00	55,29	29,56	23,90	2,49
7H5	84	7	567,00	71,43	17,86	7,14	1,23
7H5	92	6	89,00	50,00	11,11	11,11	19,10
7H5	100	26	695,00	46,15	11,11	12,96	0,58
7H5	108	149	1017,00	36,91	22,92	39,17	0,69
7H5	116	199	459,00	47,24	31,54	35,23	1,09
7H5	124	137	377,00	42,34	22,31	30,38	1,59
7H5	132	323	1090,00	36,53	19,67	34,17	0,46
7H5	140	155	393,00	54,84	33,86	27,89	1,27
7H6	2	106	279,00	48,11	40,16	43,31	3,94
7H6	6	326	1044,00	51,53	30,38	28,57	1,63
7H6	10	322	1057,00	45,65	21,30	25,36	1,70
7H6	18	193	500,00	47,67	23,06	25,31	0,20

7H6	26	174	610,00	53,45	25,69	22,38	0,00
7H6	34	169	564,00	47,93	18,66	20,28	0,35
7H6	42	110	400,00	34,55	17,04	32,29	0,00
7H6	50	111	727,00	46,85	13,68	15,53	0,00
7H6	58	33	207,00	54,55	20,45	17,05	0,00
7H6	66	9	80,00	66,67	15,79	7,89	25,00
7H6	74	175	748,00	82,29	36,64	7,89	0,40
7H6	82	113	415,00	56,64	26,34	20,16	1,45
7H6	90	109	474,00	63,30	23,39	13,56	0,00
7H6	98	183	625,00	55,74	22,92	18,20	0,00
7H6	104	118	448,00	54,24	20,19	17,03	2,01
7H6	110	212	562,00	46,23	21,59	25,11	0,18
7H6	118	151	673,00	57,62	20,47	15,06	0,45
7H6	122	309	700,00	54,05	26,42	22,47	0,00
7H7	10	90	550,00	41,11	11,04	15,82	0,18
7H7	22	126	530,00	41,27	14,02	19,95	0,00
ODP 1233C							

7H3	40	13	61,00	46,15	22,22	25,93	26,23
7H3	44	23	106,00	60,87	33,33	21,43	16,98
7H3	48	248	729,00	81,45	48,67	11,08	0,00
7H3	56	141	412,00	59,57	29,27	19,86	0,00
7H3	60	46	221,00	63,04	22,83	13,39	0,45
7H3	64	240	863,00	54,17	25,54	21,61	0,12
7H3	72	112	391,00	53,57	21,05	18,25	0,00
7H3	80	124	447,00	54,84	23,21	19,11	0,67
7H3	88	211	445,00	52,13	30,73	28,21	0,45
7H3	96	95	402,00	46,32	15,28	17,71	0,75
7H3	104	125	925,00	55,20	27,94	22,67	2,38
7H3	112	168	722,00	48,81	22,22	23,31	0,83
7H3	120	208	435,00	40,38	25,07	37,01	1,15
7H3	128	71	209,00	56,34	28,78	22,30	6,22
7H3	136	97	555,00	65,98	23,97	12,36	0,00
7H3	144	78	313,00	61,54	26,67	16,67	3,83
7H3	148	59	191,00	52,54	30,10	27,18	3,66
7H4	2	120	370,00	51,67	29,52	27,62	2,97

7H4	10	298	765,00	37,92	22,78	37,30	0,13
7H4	18	75	388,00	69,33	40,63	17,97	0,26
7H4	26	110	433,00	71,82	29,37	11,52	0,69
7H4	34	58	306,00	50,00	19,08	19,08	0,33
7H4	42	20	94,00	55,00	19,64	16,07	1,06
7H4	50	5	39,00	100,00	35,71	0,00	5,13
7H4	58	272	872,00	45,22	21,81	26,42	0,11
7H4	66	101	525,00	53,47	24,22	21,08	0,38
7H4	74	45	289,00	53,33	15,69	13,73	0,00
7H4	82	18	77,00	77,78	35,00	10,00	2,60
7H4	90	155	915,00	66,45	27,47	13,87	0,22
7H4	98	196	659,00	56,12	24,89	19,46	0,30
7H4	106	4	53,00	100,00	66,67	0,00	0,00
7H4	114	196	433,00	35,71	19,72	35,49	0,00
7H4	122	32	189,00	59,38	29,69	20,31	0,00
7H4	130	114	690,00	67,54	21,75	10,45	0,00
7H4	138	120	457,00	71,67	24,93	9,86	0,00
7H4	146	113	457,00	48,67	17,08	18,01	0,00

7H5	4	150	765,00	34,00	12,50	24,26	0,00
7H5	12	84	622,00	50,00	12,10	12,10	0,00
7H5	20	89	574,00	67,42	21,05	10,18	0,00
7H5	28	29	458,00	72,41	18,75	7,14	0,00
7H5	36	3	306,00	33,33	4,55	9,09	0,33
7H5	44	11	115,00	63,64	20,00	11,43	0,00
7H5	52	5	48,00	100,00	20,83	0,00	0,00
7H5	60	90	423,00	23,33	10,05	33,01	0,00
7H5	68	71	502,00	42,25	12,40	16,94	0,00
7H5	76	69	462,00	33,33	9,47	18,93	0,00
7H5	84	59	415,00	40,68	12,83	18,72	0,00
7H5	92	162	936,00	35,80	13,09	23,48	0,64
7H5	100	49	437,00	26,53	8,23	22,78	0,00
7H5	108	17	152,00	52,94	15,52	13,79	0,00
7H5	116	157	650,00	45,86	19,00	22,43	0,00
7H5	124	74	588,00	41,89	10,80	14,98	0,00
7H5	132	115	534,00	36,52	13,33	23,17	0,00
7H5	140	81	406,00	59,26	17,33	11,91	0,49